Fundamental study on seismic behavior of hinge types of precast arch culverts in culvert longitudinal direction

2019

Yusuke MIYAZAKI

Abstract

In the Great East Japan Earthquake, many hinge types of precast arch culverts suffered seismic damage which spoiled their serviceability. Initially, hinged arch culverts must undergo a seismic inspection on their arch members. This is because these culverts are beyond the applicable range of the conventional types of culverts that do not require a seismic inspection. Although the seismic damage to hinged arch culverts seems to be correlated with the inertial force in the culvert longitudinal direction, there is currently no method of seismic inspection in the longitudinal direction, and thus, no requirement for one either. Therefore, the clarification of the damage mechanism due to the Great East Japan Earthquake and the seismic reinforcement of existing structures are now viewed as urgent issues to be addressed.

In the present study, in order to clarify the seismic behavior of precast arch culverts in the culvert longitudinal direction and to develop a method for evaluating the seismic behavior in the longitudinal direction, a series of studies using dynamic centrifuge model tests and numerical analyses was conducted. The dynamic centrifuge tests were carried out to clarify the seismic effect of the design method for hinged arch culverts, including the longitudinal structural connectivity and the embankment shape. Then, a new numerical method to simulate the 3-dimensional dynamic behavior of hinged arch culverts was developed based on the experimental observations of the seismic effect of the longitudinal structural connectivity and the embankment shape.

In terms of the longitudinal structural connectivity of the culverts, it was found in the dynamic centrifuge model tests that separating the culverts allowed each culvert to behave independently in the embankment. This unrestrained behavior resulted in an aperture at each interconnecting section of the culverts. Connecting the culverts was seen to cause all the culverts to behave integrally during an earthquake. Moreover, the initial stress situation of the culverts differed due to the connection of the culverts. In this experiment, connecting the culverts was seen to be advantageous in the seismic resistant design from the viewpoint of preventing apertures in the culverts and reducing the embankment deformation and the internal forces of the arch culverts.

In terms of the embankment shape of three-hinged arch culverts in the longitudinal direction, it was found in the dynamic centrifuge model tests that the seismic behavior of culverts in the longitudinal direction is closely related to the degree of overburden. A shallow soil cover, such as 1.0 m, allowed the response acceleration of the culverts to be amplified and to exceed that of the surrounding soil at the mouth. Conversely, a deep soil cover of more than 4.0 m caused the culverts to respond as an integrated body with the surrounding soil. However, the magnitude of the embankment deformation was seen to increase proportionally to the degree of overburden.

Based on the above experimental results, a numerical method that can simulate the 3-dimensional seismic behavior in the culvert longitudinal direction was developed. The analysis was based on an elasto-plastic 3D FEM. In the analysis, the interface of the arch members was modeled with nonlinear spring elements for the longitudinal structural connectivity. From the 2D and 3D dynamic FEM analyses, with non-linear spring elements applied for structural connectivity in the dynamic analysis, the apertures of the culverts due to the deformation of the embankment could be expressed. Additionally, the independent behavior of the culverts, as well as the united behavior of the culverts, and the various stress states of the arch members due to the structural connectivity and the embankment shape were evaluated.

Finally, through the dynamic centrifuge tests and the 3D dynamic FEM analysis, the seismic

damage done to the three-hinged arch culverts in the Great East Japan earthquake was discussed. From the results, the damage observed at the arch members, such as the edge defect of and the cracks in the arch crown and the arch feet, could be explained by the combination of the weak structural connectivity of the culverts and the torsional deformation of the arch members. Considering the seismic damage incurred by the old type of three-hinged arch culverts, it was found that the weak structural connectivity due to the absence of concrete beams at the arch crown induced the critical damage to the arch members.

Acknowledgements

Table of contents

List of tables and figures

List of tables

List of figures

Chapter 1 Introduction

A culvert is an open-cut tunnel that allows water to flow beneath a road, railroad, embankment or ground. Culverts which satisfy the specific conditions of the concrete material and the size of the culvert cross section are classified as conventional types of culverts (Figure 1.1). According to Culvert Construction Guidelines (Japan Road Association, 2014), conventional culverts generally take the design load into consideration, except for the seismic load. The seismic effect has not commonly been addressed in the design criteria because conventional types of culverts have experienced almost no clear damage in past earthquakes. However, opportunities to construct culverts using precast concrete members instead of cast-in-place concrete, which are beyond the applicable range of the conventional types of culverts, have been increasing.

Some advantages that can be expected through the use of precast concrete members include the saving of labor, a shortening of the construction period, and high quality control of the concrete members. The hinge types of precast arch culverts (hinge types of arch culverts) represent these precast-style culverts. Currently, the two-hinge type of precast arch culvert (two-hinged arch culvert) (Association of Modularch Construction Method, 2017) and the three-hinge type of precast arch culvert (three-hinged arch culvert) (Investigative Committee of Manual for the Design and Construction of Techspan Construction Method, 1998) are mainly used (Figure 1.2). More than 200 sets of these precast arch culverts have been constructed along arterial roads in Japan (Abe and Nakamura, 2014), composing an important network of road embankments.

The hinge types of arch culverts are stabilized by positively inducing the subgrade reaction from the surrounding ground by allowing for the deformation of the arch members due to the hinge structure attached at the boundary of the arch members. Hence, the subgrade reaction is converted to axial force acting on the arch, which enables a reduction in the thickness of the members compared to rigid box culverts and arch culverts constructed with larger overburdens and cross sections. On the other hand, the hinge structure in the hinge types of arch culverts does not satisfy the applicable conditions of conventional types of culverts. The hinge types of arch culverts exceed the applicable range of conventional types of culverts regardless of the dimensions of the overburden or the cross section; thus the hinge types of arch culverts require an inspection to confirm the seismic effect.

In order to discuss the seismic performance of culverts, the seismic behavior in the culvert transverse direction and that in the culvert longitudinal direction are generally classified along with the behavior in the direction of the culvert and the input wave (refer to Figure 1.2). So far, considering the stress inspection of the RC members, the seismic performance of the precast arch culverts in the transverse direction has mainly been studied through shaking table tests (e.g., Toyota and Takagai, 1999 and Sawamura et al., 2016) and numerical analyses (Byrne, et al. 2000 and Wood and Jenkins, 2000). As a result, the high seismic performance of both the two- and the three-hinged arch culverts was proven by the large shaking table tests and the reproduction of the numerical analyses (Sawamura et al., 2016, 2017).

However, the study of the seismic performance in the culvert longitudinal direction has remained
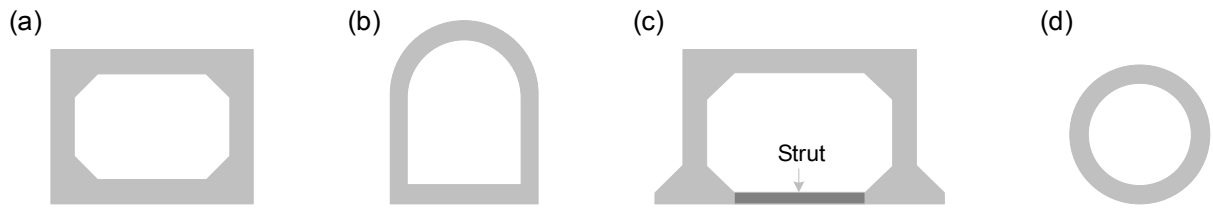
Figure 1.1: Representative structures of conventional types of culverts: (a) box culvert, (b) arch culvert, (c) portal type of culvert, and (d) pipe culvert (Japan Road Association, 2010).
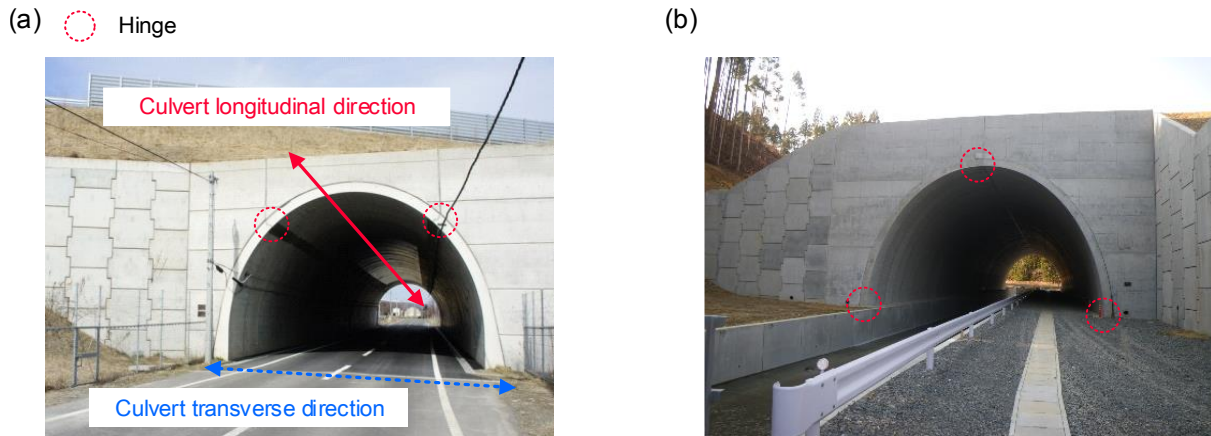
Figure 1.2: Hinge types of precast arch culverts: (a) two-hinged arch culvert and (b) three-hinged arch culvert.
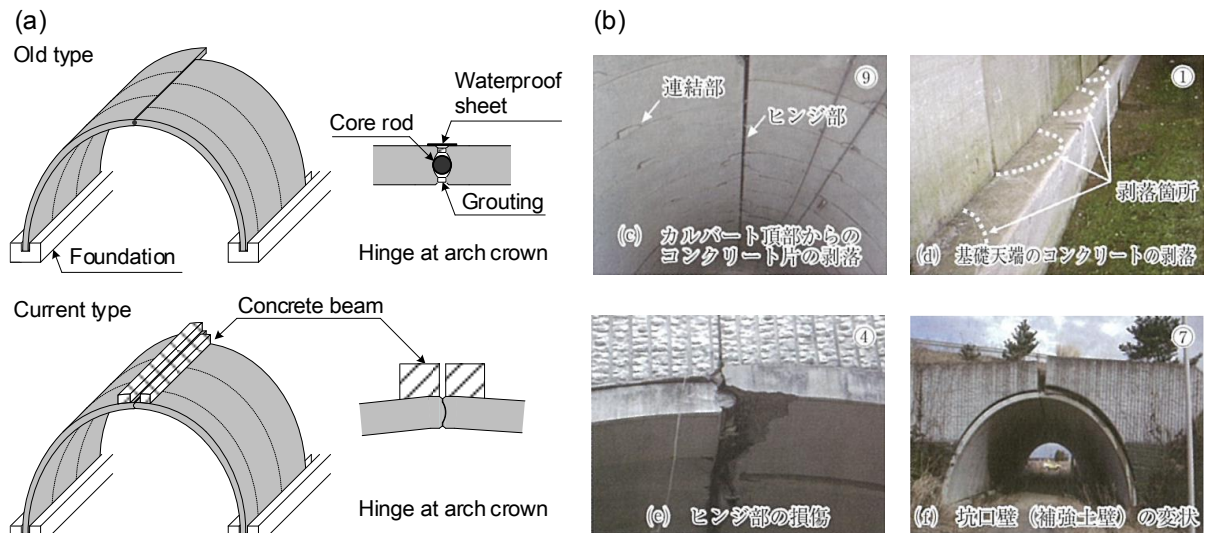
Figure 1.3: (a) Schematic drawings of old and current types of three-hinged arch culverts and (b) damage to old type of three-hinged arch culvert due to Great East Japan Earthquake (cited from report by Abe and Nakamura, 2014).

at a relatively fundamental level in terms of understanding the dynamic behavior (e.g., Kumada et al., 1995 and Toyota and Ito, 2000) compared to that in the culvert transverse direction. Moreover, in the Great East Japan Earthquake (March 11, 2011), nine old-type three-hinged arch culverts (Figure 1.3) suffered damage related to seismic waves in the culvert longitudinal direction, namely, the edge defect of and cracks in the arch members and the concrete foundation, the displacement of the hinge at the arch crown, and the deformation of the mouth wall, as reported by Abe and Nakamura (2014). In particular,

the old type of three-hinged arch culverts had no concrete beams at the arch crown, which are thought to prevent the slipping of the arch members due to the longitudinal slope of the foundation and uneven settlement (Investigative Committee of Manual for the Design and Construction of Techspan Construction Method, 1998).

More than 200 precast arch culverts have been constructed without an inspection of the seismic performance in the culvert longitudinal direction, which emphasizes the possibility for severe seismic damage to these precast arch culverts due to longitudinal inertial force. However, there is currently no evaluation method for the seismic performance in the culvert longitudinal direction and there are few literature reviews on the mechanism of the seismic damage caused by the Great East Japan Earthquake. Accordingly, effective reinforcing countermeasures for the existing precast arch culverts cannot be conducted.

Therefore, the motivation of the present study is to establish an evaluation method for the seismic performance of the hinge types of precast arch culverts in the culvert longitudinal direction in order to contribute to the reasonable design and the antiseismic reinforcement of these culverts. To achieve the development of this new evaluation method, the various seismic behaviors are investigated in the culvert longitudinal direction up to the design conditions. As for the design conditions, dynamic centrifuge tests are conducted on the longitudinal structural connectivity and the embankment shape of the hinge types of precast arch culverts; they are the critical factors controlling the longitudinal displacements and stiffness of the culverts. These two conditions seem to be deeply correlated with the characteristic damage incurred by the old type of three-hinged arch culverts in the Great East Japan Earthquake. Additionally, based on the dynamic centrifuge tests, a new 3D numerical method is developed in order to establish an evaluation method for the longitudinal seismic performance. The method can reveal the seismic effect of both the structural connectivity and the embankment shape. Finally, with the developed numerical method, the damage mechanism of the old type of three-hinged arch culverts in the Great East Japan Earthquake is discussed.

References

Abe, T. and Nakamura, M. (2014): *The use of and the caution in the application of the culvert constructed by large precast element in the expressway construction*, *The Foundation Engineering & Equipment, Monthly,* Vol. 42, No. 4, pp. 8-11 (in Japanese).

Association of Modularch Construction Method (2017): *Engineering Manual for Modularch*, *Geo-Research Institute* (in Japanese).

Byrne, P. M., Anderson, D. L. and Jitno, H. (1994): Seismic Analysis of Large Buried Culvert Structures, *Transportation Research Record*, Vol. 1541, pp. 133-139.

Irie, N., Ito, A., Takahashi, O., and Kusakabe, O. (2002): Dynamic behavior of three-hinged tunnel in a centrifuge, *Proceedings of the Japan National Conference on Geotechnical Engineering*, *The Thirty-seventh Japan National Conference on Geotechnical Engineering*, pp. 1779-1780 (in Japanese).

Investigative Committee of Manual for the Design and Construction of Techspan Construction Method (1998): *Manual for the Design and Construction of Techspan Construction Method (Draft)*,

Advanced Construction Technology Center (in Japanese).

Japan Road Association (2010): *Road Earthwork Guidelines - Guidelines for Culvert Work* (in Japanese).

Kumada, T., Takahashi, Y., Kitabayashi, T., Hotta, M., Ohi, J., and Koizumi, A. (1995): *Shaking table test on a tunnel of Techspan construction method (No. 1); outline of Techspan construction method and shaking table test, the Proceedings of the JSCE Annual Meeting*, Vol. 65, III-556, pp. 1112-1113 (in Japanese).

Sawamura, Y., Ishihara, H., Kishida, K., and Kimura, M. (2016): Experimental Study on Damage Morphology and Critical State of Three-hinge Precast Arch Culvert through Shaking Table Tests, *Procedia Engineering, Advances in Transportation Geotechnics III*, Vol. 143, pp. 522-529.

Sawamura, Y., Matsushita, R., Kishida, K., and Kimura, M. (2017): Evaluation of mechanical behavior of two-hinge precast arch culvert in construction process and its seismic damage morphology through strong earthquake response experiments, *Japanese Geotechnical Journal*, Vol. 15, No. 4, pp. 385-396 (in Japanese). doi.org/10.3208/jgs.12.385

Technological Examination Committee of Techspan Construction Method (2014): *Comparison Outline of Revised Items in Manual for the Design and Construction of Techspan Construction Method (Draft)*, *Advanced Construction Technology Center* (in Japanese).

Toyota, H., and Takagai, M. (1999): Dynamic behavior of 3-hinge arch in terre armee foundation, Journal of JSCE, No. 624/III-47, pp. 255-266 (in Japanese).
dx.doi.org/10.2208/jscej.1999.624_255

Toyota, H., and Ito, T. (2000): Effects of shaking conditions and material properties on dynamic behavior of terre armee foundation and 3-hinge arch, *Journal of JSCE*, No. 666/III-53, pp. 279-289 (in Japanese).
dx.doi.org/10.2208/jscej.2000.666_279

Wood, J. H. and Jenkins, D. A. (2000): Seismic analysis of buried arch structures, *Proc. of the 12th World Conference of Earthquake Engineering*, No. 0768.

Chapter 2 Literature review of seismic performance of hinge types of precast arch culverts

2.1 Introduction

In this chapter, an outline of the structures of the conventional types of culverts and the hinge types of culverts is given, and a past seismic disaster that affected these culverts will be introduced. Then, the seismic performance of the hinge types of arch culverts is described through literature reviews. Finally, the tasks to be solved in the present study are summarized based on the reviews and the reported seismic disaster.

2.2 Outline of culvert structures

A culvert is an open-cut tunnel that allows water to flow beneath a road, railroad, embankment or ground. Many mountainous regions exist in Japan; this inevitably brings about the need for the construction of many embankments. Thus, culverts have the important role of saving communities from being split geologically by the construction of road networks. Most conventionally constructed culverts can be classified as one of three types, namely, rigid box culvert, rigid pipe culvert or flexible pipe culvert (Figure 2.1).

2.2.1 Application of and design method for conventional types of culverts

According to the Culvert Construction Guidelines (Japan Road Association, 2014), the conventional types of culverts (refer to Figure 2.1) have a commonly used design and construction. Based on this design, certain types of culverts satisfy the applicable range shown in Table 2.1 and are believed capable of maintaining the required level of structural performance. Accordingly, conventional culverts generally take the design load into consideration, except for the seismic load. The seismic effect has not commonly been addressed in the design criteria because conventional types of culverts have experienced almost no clear damage in past earthquakes. Therefore, the inspection for the seismic load can be omitted for all conventional types of box culverts, except for the portal type of culvert. On the other hand, the design guidelines require that the culverts satisfy a predetermined design condition in terms of the overburden and the dimensions of the cross section as well as the following items:

1. Sand shall be used for the filling material.
2. A gradient of less than 10% of the longitudinal slope of the culvert shall be maintained.
3. No hinges shall be attached to the cross section of the culvert.
4. The culvert is to be established individually.
5. The culvert is to be supported by a spread foundation.
6. The culvert shall not be a multiple structure constructed with a central pier.
7. A thickness of 50 cm is to be maintained for the overburden

Conventional type of culvert
- Classification by material
  - Reinforced concrete
  - Prestressed concrete
  - Corrugated metal
  - Rigid polyvinyl chloride
  - Fiber-reinforced plastic material (FRPM)
  - High-density polyethylene
- Classification by structure
  - Rigid box culvert
    - (a) Box culvert made by
      - Cast-in-place
      - Precast member
    - (b) Arch culvert made by
      - Cast-in-place
      - Precast member
    - (c) Portal type of culvert
  - (d) Pipe culvert
    - Rigid pipe culvert made by
      - Centrifugal reinforced concrete
      - Prestressed concrete
    - Flexible pipe culvert made by
      - Corrugated metal
      - Rigid polyvinyl chloride
      - Fiber reinforced plastic material
      - High pressure-resistant polyethylene
- Classification by purpose of use
  - As a road
  - As a water channel

(a)   (b)   (c)   (d)

Strut

Figure 2.1: Classification of conventional types of culverts: (a) box culvert, (b) arch culvert, (c) portal type of culvert, and (d) pipe culvert (Japan Road Association, 2010).

2.2.2 Representative hinge types of precast arch culverts

Recently, many culverts have been constructed beyond the design guidelines for the conventional types of culverts (Table 2.1). Moreover, opportunities to construct culverts using precast concrete members instead of cast-in-place concrete have been increasing. Some advantages that can be expected through the use of precast concrete members include the saving of labor, a shortening of the construction period, and high quality control of the concrete members. The hinge types of precast arch culverts (hinge types of arch culverts) represent these precast-style culverts.

The hinge types of arch culverts are stabilized by positively inducing the subgrade reaction from

Table 2.1: Scope of applications for conventional types of culverts (Japan Road Association, 2010).

Type of culvert			Applicable overburden [m] *	Cross-sectional size B = Inner width [m] H = Inner height [m] D = Diameter [m]
Rigid box culvert	Box culvert	Made of cast-in-place concrete	$0.5 \sim 20$	*B*: within 6.5 *H*: within 5.0
		Made of precast members	$0.5 \sim 6.0$ **	*B*: within 5.0 *H*: within 2.5
	Portal type of culvert		$0.5 \sim 10$	*B*: within 8.0
	Arch culvert	Made of cast-in-place concrete	More than 10	*B*: within 8.0
		Made of precast members	$0.5 \sim 14$ **	*B*: within 3.0 *H*: within 3.2
Rigid pipe culvert	Made of centrifugally reinforced concrete		$0.5 \sim 20$ **	*D*: within 3
	Made of prestressed concrete		$0.5 \sim 31$ **	*D*: within 3.0
Flexible pipe Culvert	Made by corrugated metal		Pavement thickness +0.3 or $0.6 \sim 60$ **	*D*: within 4.0
	Made of rigid polyvinyl chloride (In case of a circular shape [VU]) ***		Pavement thickness +0.3 or $0.6 \sim 7$ **	*D*: within 0.7
	Made of fiber-reinforced plastic material		Pavement thickness +0.3 or $0.6 \sim 10$ **	*D*: within 3.0
	Made of high pressure-resistant polyethylene		Pavement thickness +0.3 or $0.6 \sim 26$ **	*D*: within 2.4

*The thickness of the applicable overburden differs depending on the cross-sectional size.

** The overburden is the maximum overburden for industrial products.

*** Rigid polyvinyl pipe culverts include circular-shaped pipe culverts (VU, VP, and VM) and those with ribs (PRP). Mainly, the VU-type is used.

the surrounding ground by allowing for the deformation of the arch members due to the hinge structure attached at the boundary of the arch members. Hence, the subgrade reaction is converted to axial force acting on the arch, which enables a reduction in the thickness of the members compared to rigid box culverts and arch culverts constructed with larger overburdens and cross sections. On the other hand, the hinge structure in the hinge types of arch culverts does not satisfy the applicable range of conventional types of culverts discussed in 2.2.1. The hinge types of arch culverts exceed the applicable range of conventional types of culverts regardless of the dimensions of the overburden or the cross section; the hinge types of arch culverts require an inspection to confirm the seismic effect.

Currently, the two-hinge type of precast arch culvert (two-hinged arch culvert) (Association of Modularch Construction Method, 2017) and the three-hinge type of precast arch culvert (three-hinged arch culvert) (Investigative Committee of Manual for the Design and Construction of Techspan Construction Method, 1998) are mainly used. More than 200 sets of these precast arch culverts have
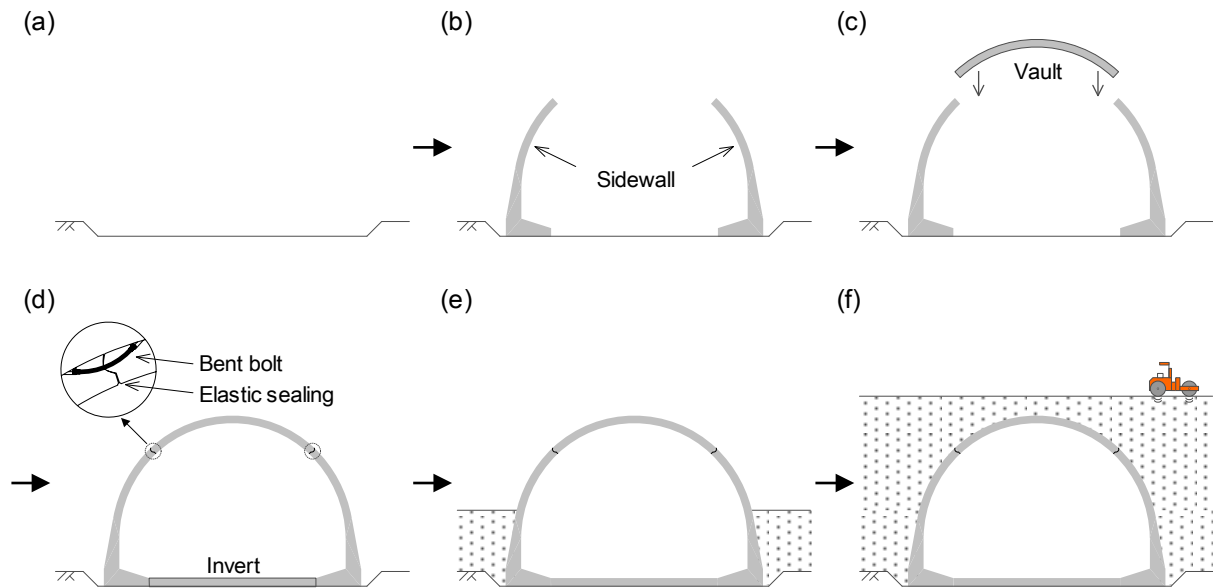
Figure 2.2: Construction procedure for two-hinged type of precast arch culvert: (a) construction of foundation ground, (b) setting of sidewalls, (c) setting of bolts, (d) casting in place of invert foundation, (e) filling in sides of culvert, and (f) filling in whole embankment.

been constructed along arterial roads in Japan (Abe and Nakamura, 2014), composing an important network of road embankments.

Two-hinged arch culverts are separated at both arch shoulders with the hinge structure being connected by bent bolts to prevent the slipping of the members. Figure 2.2 shows the procedure for the construction of the two-hinged arch culverts. In constructing these culverts with an invert type of foundation, after the construction of the foundation, the sidewalls of the arch culverts are set, the bolts are attached to the sidewalls, and the casting in place of the concrete for the invert foundation is carried out. The two-hinged arch culverts require the filling of the whole embankment by compaction using a rolling machine after the setting of the arch culverts.

On the other hand, three-hinged arch culverts are composed of two half-arch members of precast concrete and the foundation. The statically determinate structure is due to the three hinges located at the arch crown and arch feet. Figure 2.3 shows a schematic drawing of the structure. Three-hinged arch culverts are constructed as follows. Firstly, the casting in place of the concrete foundation, called the 'keyway', is conducted. Then, the two half-arch members are combined so as to bend toward each other and the foundation. Next, to satisfy the staggered arrangement, grouting is performed at the arch feet of the hinge. Finally, the culverts are filled.

From the above introductions, it is seen that while reasonable construction is required for the hinge types of arch culverts, a seismic inspection must be conducted due to the dissatisfaction of the applicable range of conventional types of culverts. The hinge types of arch culverts are stabilized by the specified ground conditions (a value of more than 30 N for the SPT in the foundation ground and no excessive or asymmetrical overburden on the culverts). Moreover, an inspection of the stress in the arch's cross section basically requires the 2-dimensional response displacement method. However, close attention must be paid to the seismic effect in order that the stability of the hinge types of arch culverts not be spoiled.
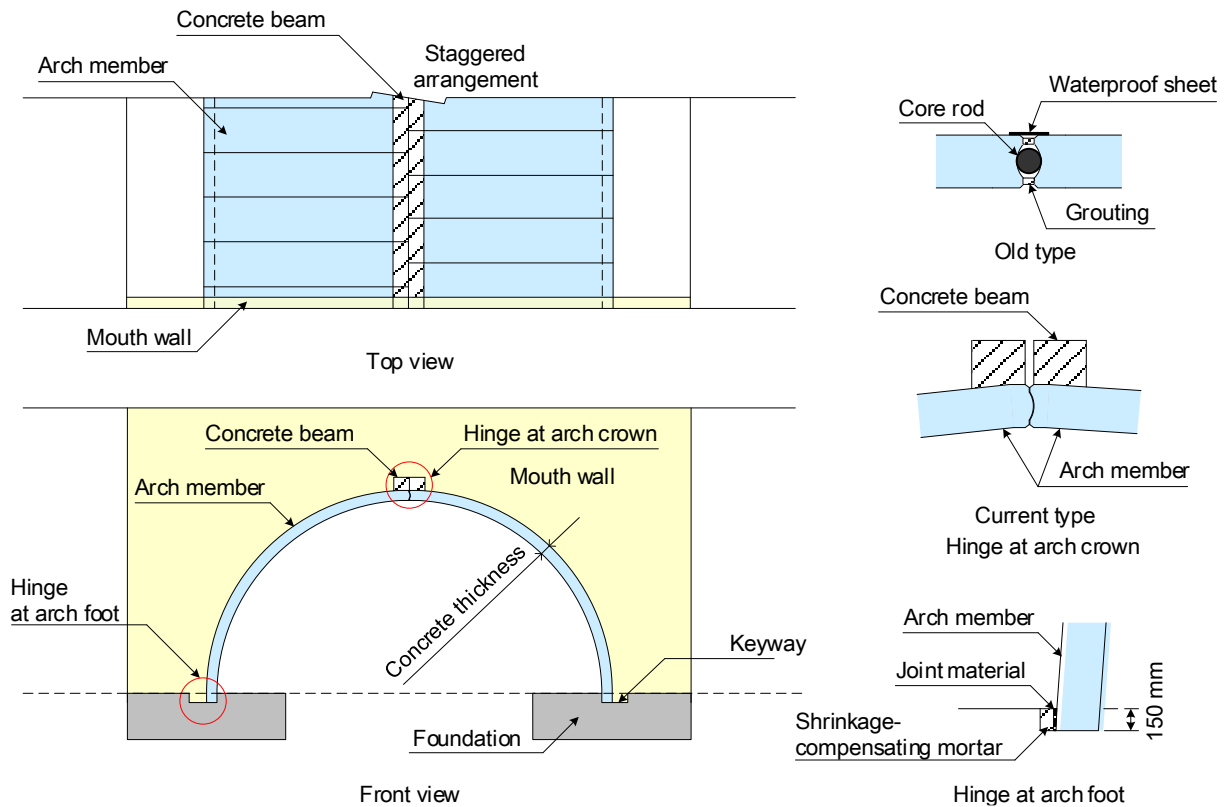
Figure 2.3: Schematic drawings of structural components of three-hinged type of precast arch culvert (based on drawing by Seto and Ootani, 2014).

2.3 Seismic disaster to hinged arch culverts and related consideration of design and construction

In this chapter, a past seismic disaster experienced by the hinge types of arch culverts is introduced. The critical design and construction method of these culverts are mentioned.

2.3.1 Seismic disaster incurred by hinge types of precast arch culverts due to Great East Japan Earthquake

During the Great East Japan Earthquake (March 11, 2001), many hinge types of arch culverts suffered damage related to seismic waves in the culvert longitudinal direction. In the two-hinged arch culverts, small fragments of the arch members broke off, sand infiltration occurred, and cracks appeared in the pavement due to apertures in the culverts, as shown in Figure 2.4. On the other hand, nine old-type three-hinged arch culverts (refer to Figure 2.3) also experienced the disaster (Abe and Nakamura, 2014). Figure 2.5 shows the damage situation, which includes the edge defect of and the cracks on the arch members and the concrete foundation, the water infiltration due to the damage to the waterproof sheet for the culverts, the displacement of the hinge of the arch crown, and the deformation of the mouth wall. In particular, these old-type three-hinged arch culverts (refer to Figure 2.3) had no concrete beams at the arch crown, which are thought to prevent the slipping of the arch members due to the longitudinal slope of the foundation (Investigative Committee of Manual for the Design and Construction of Techspan Construction Method, 1998).

Figure 2.4: Damage to two-hinged arch culvert due to Great East Japan Earthquake: (a) outflow of filling material in apertures of culvert and (b) crack running along pavement.
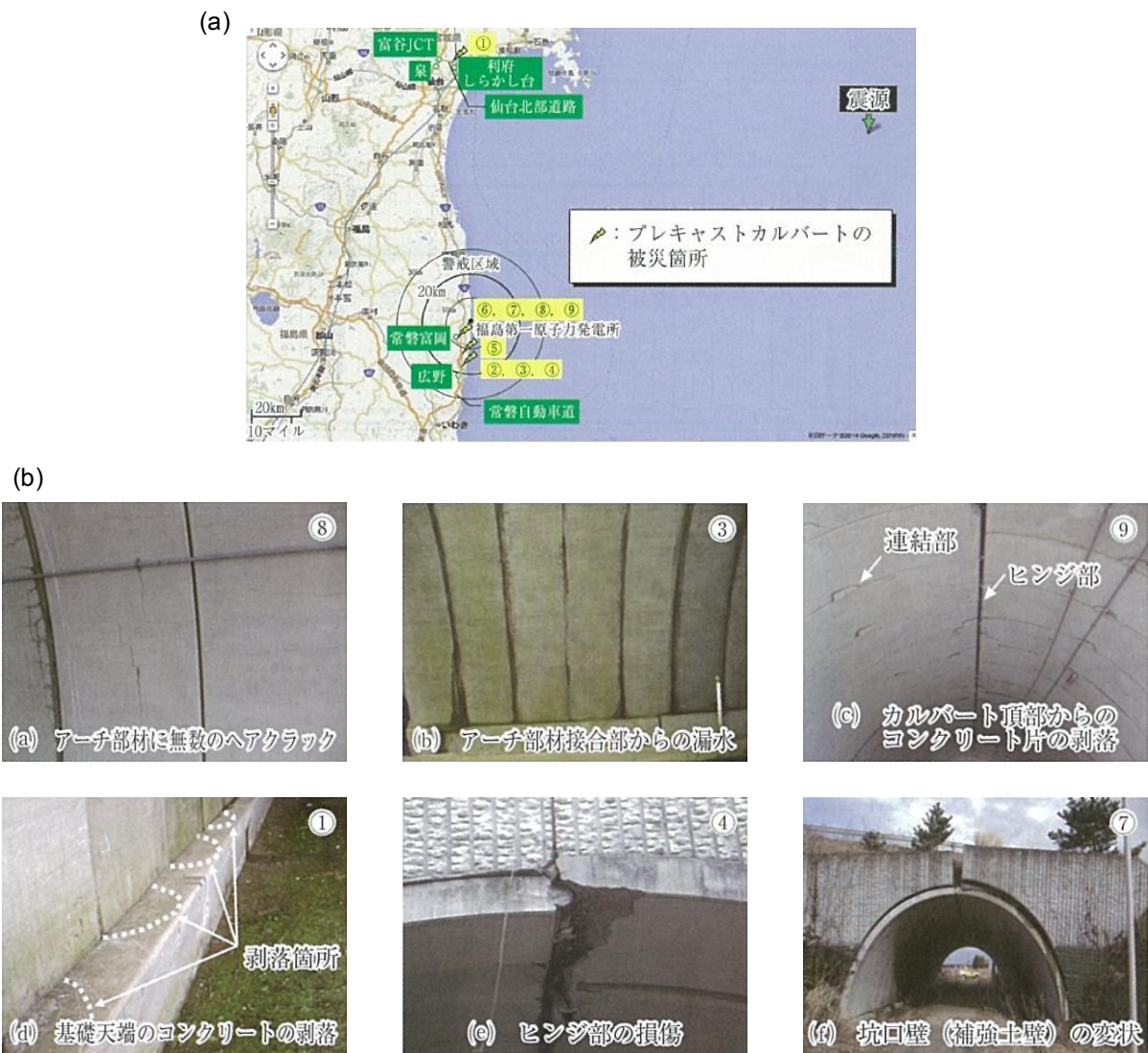
Figure 2.5: Damage to three-hinged arch culvert due to Great East Japan Earthquake (cited from report by Abe and Nakamura, 2014): (a) locations of damaged culverts and (b) states of damage.

Table 2.2 shows the profiles for the three-hinged arch culverts damaged in the Great East Japan Earthquake, cited from a report by Abe and Nakamura (2014). It is seen that the culverts suffered various

Table 2.2: Construction profile of three-hinged arch culverts damaged in Great East Japan Earthquake (cited from report by Abe and Nakamura, 2014).

No.	Expressway section	L [m]	f [m]	D [m]	t [m]	Filling	Overburden [m] Max.	Min.	Oblique angle (degree)	Gradient (%)	Type of foundation	Damage level	Completion date
①	SENDAI-HOKUBU ROAD From RIFU-SHIRAKASHI IC to TOMIYA ICT	13.2	7.3	62.4	0.35	Temp.	13.6	1.0	90.0	1.15	Continuous	Severe	2005.1
②		5.4	2.9	64.9	0.25	Temp.	9.7	1.0	81.0	1.40	Independent	Minor	2001.3
③		9.7	5.6	39.1	0.25	Temp.	4.9	1.0	87.0	1.34	Independent	Severe	2001.4
④		9.9	5.2	46.6	0.25	Temp.	3.7	1.0	60.5	1.23	Independent	Severe	2001.4
⑤	Joban Expressway From HIRONO IC to JOBAN-TOMIOKA IC	10.2	5.3	45.9	0.25	Temp.	5.7	1.4	74.5	1.57	Independent	Small	2001.12
⑥		8.8	5.3	28.3	0.25	Temp.	3.2	1.0	70.0	1.20	Continuous	Severe	2002.2
⑦		7.8	4.7	30.1	0.25	Temp.	4.1	1.0	70.0	1.90	Continuous	Medium	2002.1
⑧		8.2	4.7	33.4	0.25	Comp.	2.9	1.0	90.0	2.20	Independent	Severe	2002.5
⑨		9.0	5.3	42.8	0.25	Comp.	2.9	1.0	90.0	0.73	Continuous	Severe	2002.9

Definition of dimension
L : Inner width of arch culvert.
f : Inner height of arch culvert.
D: Longitudinal distance of arch culvert.
t : Thickness of RC arch member.

Definition of damage level
Severe : Most arch members have cracking and peeling.
Medium : A few parts of the arch members have cracking and peeling.
Small : A few parts of the arch members have cracking.
Minor : Arch members have slight cracking.

types of damage related to their construction and design. Here, the characteristics of the damage are explained by separating the damage into No. 1 and Nos. 2-9 according to the location of the culverts.

In Nos. 2-9, severe damage occurred in culverts with more than 8.0 m of inner width which is the limit for conventional types of culverts. Moreover, Figure 2.6 shows the damage situation of No. 9 described from the inside of the culvert by Abe and Nakamura (2014). From the figure, it can be seen that the edge defect of the arch members at the arch crown occurred overall along the culvert longitudinal direction, although tensile cracks appeared on the arch members located from the mouth of the culvert to the area with a small overburden.

Therefore, to classify the relation between the degree of damage and the overburden, the relation between the maximum overburden ratio and the degree of damage is summarized in Table 2.3. Here, the maximum overburden ratio is defined as H_{max}/D; H is the maximum overburden and D is the inner width of the culverts. It is seen from the table that when the maximum overburden ratio is less than 0.53, the degree of damage increases. This implies that the insufficient overburden of culverts of a certain size tends to cause heavier damage to the culverts. In short, the shape of an embankment, including the overburden depth, is likely to be the reason for some damage to the culverts.

On the other hand, the maximum overburden ratio for No. 1 was 1.03, but the damage to the culverts was critical. However, as shown in Table 2.2, the three-hinged arch culverts of No. 1 had an inner width of 13.2 m, an inner height of 7.3 m, and a maximum overburden of 13.6 m. The extra-large arch culvert and overburden were totally different from the structural characteristics of Nos. 2-9, which may have induced the different damage mechanisms of the culverts.

Moreover, the point of caution is an oblique angle. An oblique angle is defined as the crossing angle given by the direction of the culvert and the road embankment (Culvert Construction Guidelines). When a culvert is placed at a certain oblique angle to the road embankment, an uneven overburden will
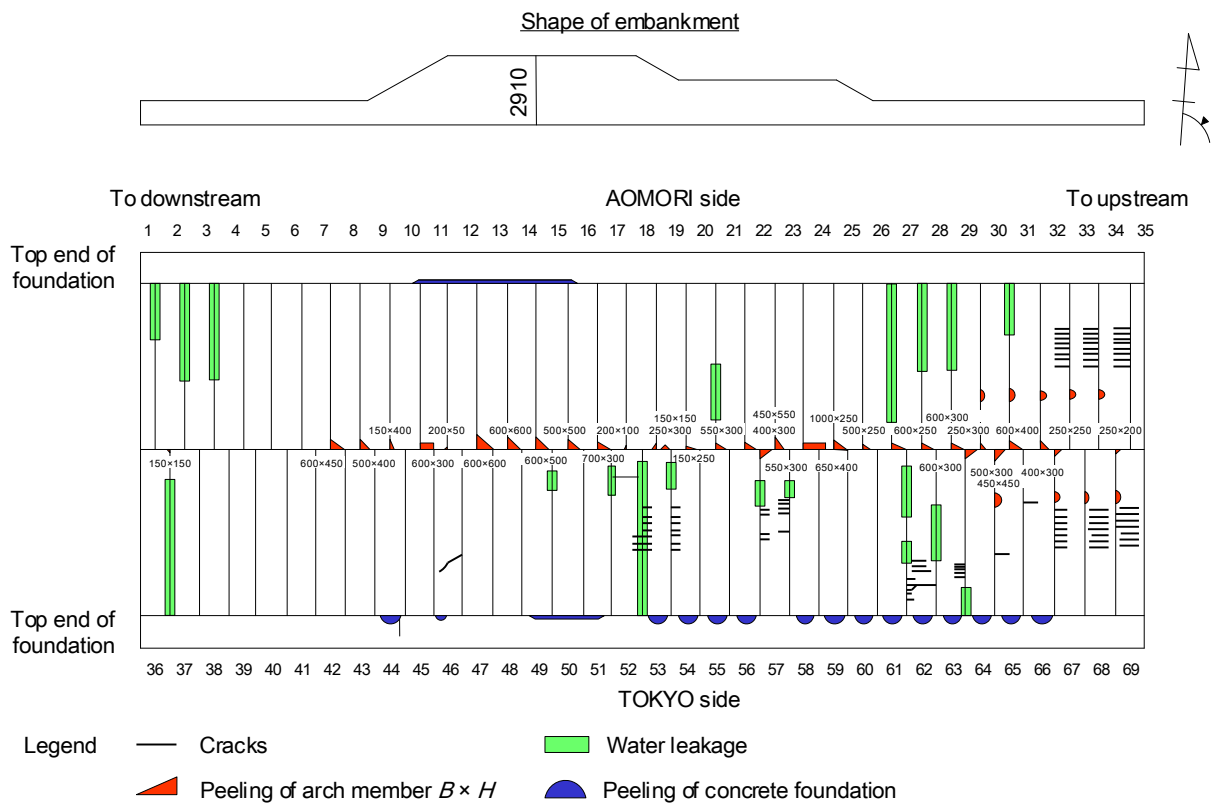
Figure 2.6: Schematic drawing of No. 9 (cited from report by Abe and Nakamura, 2014).

Table 2.3: Relation between maximum overburden ratio and degree of damage to culverts.

No.	②	⑤	⑦	③	④	⑥	⑧	⑨
H_{max}/D	1.80	0.56	0.53	0.51	0.37	0.36	0.35	0.32
Damage level	Minor	Small	Medium	Severe	Severe	Severe	Severe	Severe

H_{max}/D: High ⟵⟶ Small

H_{max} is transferred from the *Max overburden* shown in Table 2.4.

Definition of H_{max}/D
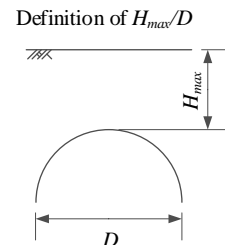
be loaded onto the arch culvert near the mouth of the culvert. This may cause instability at the mouth of the culvert due to the unexpected load. In reality, the oblique angle of 60.5º of No. 4 and the oblique angle of 70.0º of No. 7 showed displacement of the arch crown and asymmetrical deformation of the mouth wall, respectively, as shown in Figure 2.5. That is why a certain degree of oblique angle is one of the important triggers to check when examining the seismic effect on the hinge types of arch culverts.

As written above, a discussion on the damage to culverts was given based on a report by Abe and Nakamura (2014) with new viewpoints regarding the maximum overburden ratio and the oblique angle. In the culverts of No. 4 and No. 9, after removing the backfill temporally to observe the damage to the arch crowns, a pattern with regularity was found in the damaged conditions. For example, damage to the arch crowns continuously occurred along the culvert longitudinal direction on one side of the arch crowns of most arch members. And, damage to the concrete foundation continuously occurred along the culvert longitudinal direction on one side of the edge of the arch feet in each of the arch members.
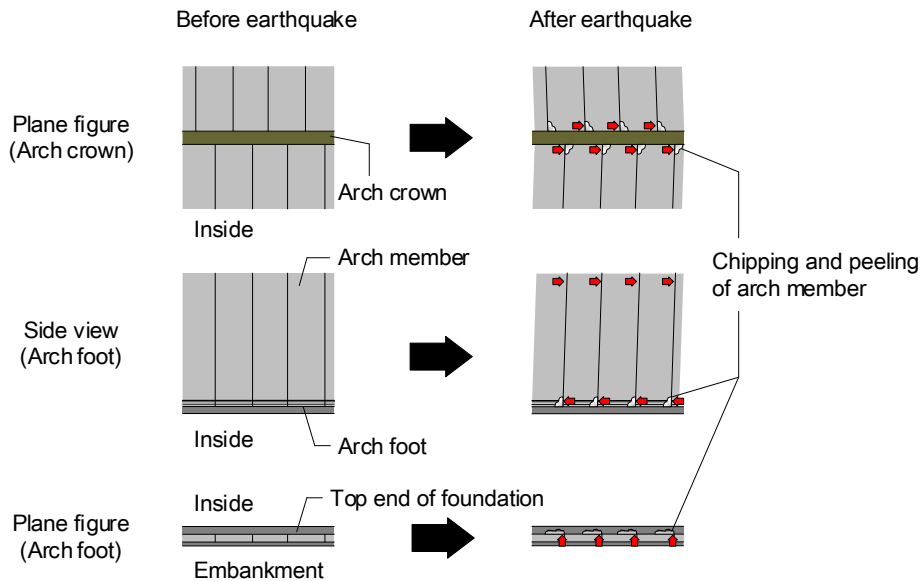
Figure 2.7: Damage mechanism of arch members due to Great East Japan Earthquake (assumed by Abe and Nakamura, 2014).

Therefore, Abe and Nakamura summarized the damage mechanism, as shown in Figure 2.7. According to the figure, torsion of the arch members occurred due to the earthquake, knocking the arch members against each other. This caused the pattern of damage to the arch members.

The characteristics of these disasters were brought about by various factors, namely, the dimensions of the cross section, the filling construction, and the foundation construction or the positional relation between the location of the culvert and the seismic center.

However, one clear discovery related to these seismic disasters is that no consideration was given to the seismic design of the culvert longitudinal direction. Moreover, the classification by the maximum overburden ratio illuminates a certain trend in relation to the degree of damage, which emphasizes that the small overburden was a trigger to the larger degree of damage to the culvert.

2.3.2 Structural connection in hinge types of precast arch culverts

Both types of hinged arch culverts are constructed by continuously setting the precast RC members, 1~2 m in length, in the culvert longitudinal direction. Additionally, when a hinged arch culvert is installed in an embankment, a perpendicular mouth wall is normally constructed for the culvert based on the reinforced soil wall (Modurach, Techspan). Accordingly, considering the possible disaster related to the seismic behavior in the culvert longitudinal direction (Figure 2.5), the longitudinal shear stiffness of the hinge types of arch culverts seems to be critical. Currently, however, the design concept for the culvert longitudinal direction only considers the prevention of the slipping of the arch members due to the longitudinal gradient of the foundation ground and the uneven settlement. In the following, the design concepts for the longitudinal structural connection and the mouth wall are explained. The concepts control the shear resistance in the culvert longitudinal direction of hinged arch culverts.
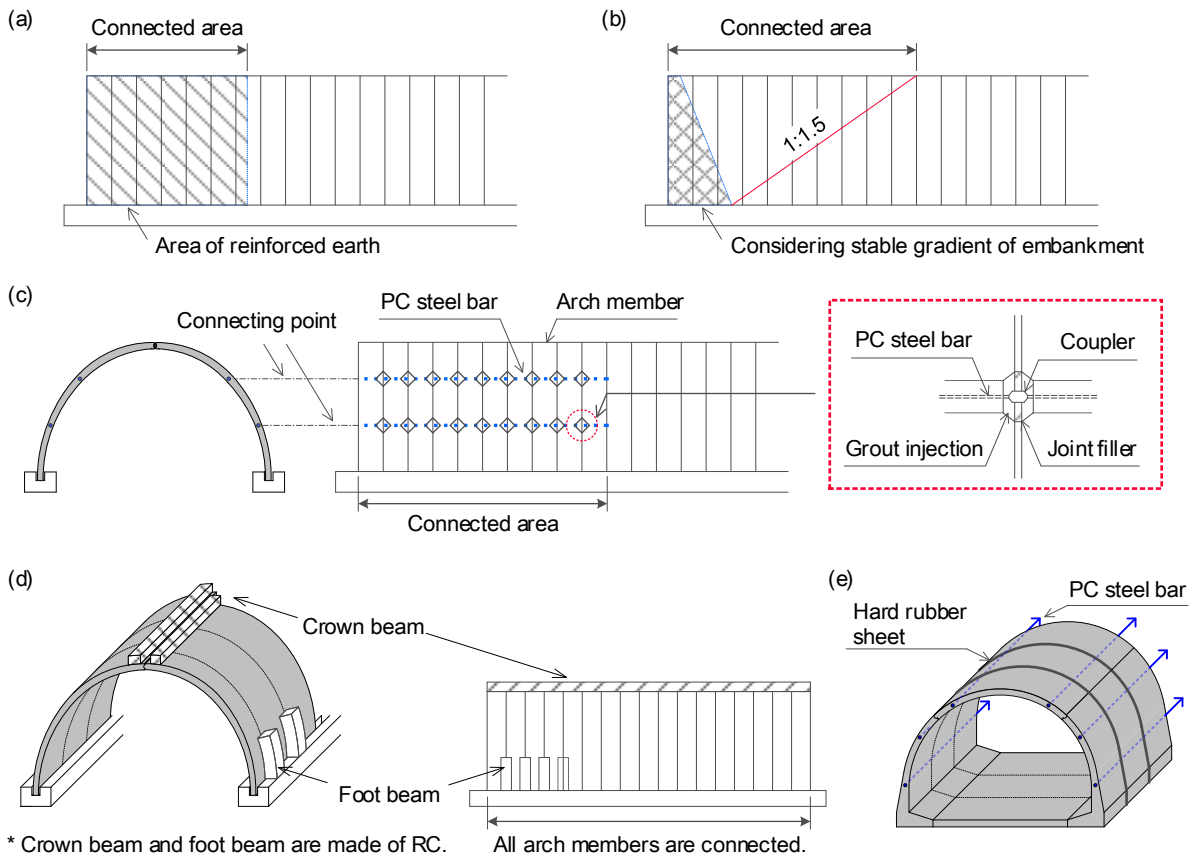
Figure 2.8: The longitudinal connection of the arch members depends on the type of hinged arch culvert. In the old type of three-hinged arch culvert, the arch members are (a) connected with the construction of a reinforced earth wall or (b) connected without the construction of a reinforced earth wall, and (c) connected longitudinally by PC steel bars. In (d), the longitudinal connection in the current type of three-hinged arch culvert, after the revision of the design manual in 2014, is seen. In (e), the two-hinged arch culvert is seen.

(1) Longitudinal structural connectivity of hinged arch culverts

Figure 2.8 shows schematic drawings of the structural connection in the two-hinged and three-hinged arch culverts. In addition, Table 2.4 summarizes the construction method for the structural connectivity in the culvert longitudinal direction. In the three-hinged arch culvert, the arch members are connected to each other at a certain distance in the longitudinal direction (e.g., the equivalent distance to the reinforcing member attached to the mouth wall of the culvert) (Figure 2.8 (a)). After the revision of the design manual in 2014, concrete beams must now be attached to the arch crowns to increase the stiffness of the longitudinal structural connection (Figure 2.8 (d)).

In the two-hinged arch culvert, on the other hand, considering the unclear seismic effect on the seismic behavior in the culvert longitudinal direction, all the arch members are connected to each other in the longitudinal direction by PC steel bars (Figure 2.8 (e)).

Considering these different concepts of the longitudinal structural connectivity in the hinged arch culverts, the characteristic damage to the arch members of the old type of three-hinged arch culverts (refer to Figure 2.6) are likely to be given by unexpected displacements of the specific arch members without the longitudinal connection.

Table 2.4: Longitudinal structural connectivity in two-hinged and three-hinged arch culverts.

	Longitudinal connections of arch members	Connection with mouth wall
Three-hinge culvert	■ The length of the longitudinal connections is based on the type of mouth wall. For example, in a reinforced earth wall, the length is equivalent to the reinforcing area (Refer to Figure 2.8(a)). ■ Since the revision of the design manual in 2014, all arch members must now be connected to crown beams made of RC. The foot beam is attached to the arch members based on the dimensions of the arch culvert and the longitudinal gradient (Refer to Figure 2.8 (d)).	■ The mouth wall of the culvert shall be independent of the arch members in order to prevent any harmful force from acting on the arch members near the mouth. ■ The arch members and the mouth wall shall be separated by the joint material.
Two-hinge culvert	■ Two-hinge arch rings connect the arch members to PC steel bars via hard rubber sheets (Refer to Figure 2.8 (e)).	■ There is no mention of this connection in the design manual.
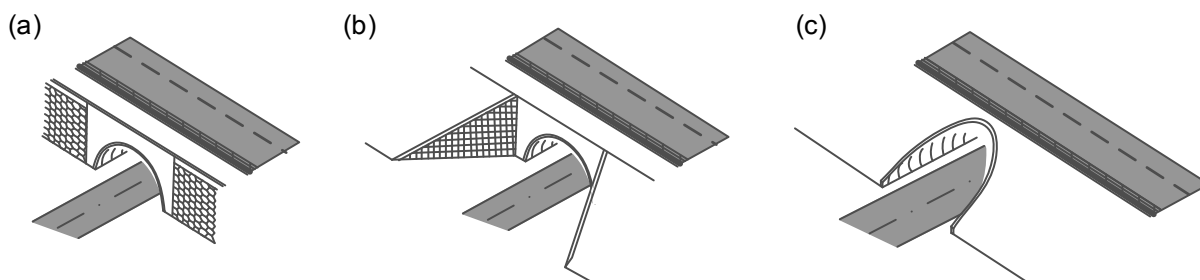
Figure 2.9: Representative mouth structures of culverts in hinge types of arch culverts: (a) portal type, (b) wing type, and (c) bamboo split type.

(2) Mouth wall of hinged arch culverts

Figure 2.9 summarizes the various types of mouth walls. The mouth wall of hinged arch culverts is mainly constructed as a perpendicular wall composed of reinforced earth or RC (a wing wall). However, in cases where the embankment has an oblique angle, or for the purpose of creating a pleasing appearance, a bamboo split type of mouth wall with an inclined wall is applied.

According to the design criteria for reinforced earth walls (Public Works Research Center, 2014), in the case of underground structures, such as culverts, considerations must be given so that an irregular wall panel is not used, based on an advance investigation of the arrangement of wall panels and the location of the underground structure, and that harmful influences to the wall structure are avoided due to the joint of the interface between the wall panel and the underground structure when it is suspected that there is settlement of the reinforced earth wall. Therefore, in the case of hinged arch culverts, the mouth wall and the culvert should generally be separated from each other in order to avoid any harmful interaction (Association of Modularch Construction Method, 2017 and Investigative Committee of Manual for the Design and Construction of Techspan Construction Method, 1998).

2.4 Literature reviews on seismic performance of precast arch culverts

The seismic performance of precast arch culverts is closely related to the stability of the hinges, which may cause the collapse of the arch structures themselves. In addition, in order to determine the required performance of the RC members, an examination of the stress condition of the arch's cross section is required. Therefore, the seismic behavior in the culvert transverse direction has been the main interest in the seismic performance of the hinged arch culverts. That is why the literature reviews of the seismic behavior in the culvert longitudinal direction are still insufficient. In this section, literature reviews of

the seismic performance in the culvert transverse direction and the culvert longitudinal direction, respectively, are introduced.

2.4.1 Seismic behavior in culvert transverse direction

Byrne, et al. (2000) aimed to verify the application of a semi-static analysis to three-hinged arch culverts and conducted a comparison with a dynamic analysis using FLUSH. As a result, they reported that the axial force acting on the arch members was largely influenced by the effect of the vertical acceleration and that the bending moment acting on the arch members was affected by the horizontal acceleration.

Wood and Jenkins (2000) conducted a static analysis with a horizontal load equivalent to 0.2 G of inertial force and a dynamic analysis with horizontal acceleration based on the response spectrum method for three-hinged arch culverts with overburdens of 3 m and 15 m, respectively. They reported that through a sensitivity analysis of the parameters of the soil, the effect of the soil stiffness was critical for the magnitude of the bending moment and the shear force acting on the arch members.

Irie et al. (2005) conducted dynamic centrifuge tests on the seismic behavior in the culvert transverse direction and the vertical direction, respectively, of three-hinged arch culverts to verify the effect on the stability of the arch feet. As a result, the function of the hinge structure in the three-hinged arch culverts was found to be advantageous for the seismic resistance in the culvert transverse direction. However, with excitation in the vertical direction, especially with a large overburden, it was found that the hinge structure was unlikely to function at the arch feet.

Sawamura et al. (2014a) conducted dynamic centrifuge tests on the seismic behavior of a box culvert, a rigid arch culvert, and a two-hinged arch culvert to clarify the seismic effect due to the various structural types and overburdens of culverts. From the experiments, as characteristics of the two-hinged arch culvert, the increase in the bending moment during excitation due to the overburden was found to be relatively constant compared to the box culvert; this is structurally advantageous for a larger overburden. However, a larger overburden suppresses the function of the hinge structure. That is why a careful inspection of the hinge structure is required according to the height of the embankment.

Sawamura et al. (2016, 2017) aimed to clarify the damage morphology and the ultimate state of the three-hinged and the two-hinged arch culverts through large shaking table tests on a 1/5 model of the prototype scale. As a result, it was found that the deviation in the hinge is unlikely to occur in advance of the failure of the arch members even after the occurrence of a strong earthquake which has caused more than 7% shear strain of the ground in the three-hinged arch culvert and 6% of that in the two-hinged arch culvert. Moreover, the damage pattern for the arch members was reproduced through dynamic and static analyses, respectively, with a 2D elasto-plastic FEM. Hence, they reported that the 2-dimensional response displacement method is applicable as a method for evaluating the seismic performance of the hinge types of arch culverts in the culvert transverse direction.

2.4.2 Seismic behavior in culvert longitudinal direction

As mentioned above, the literature reviews on the seismic performance of the transverse direction are sufficient for clarification of the damage morphology and the ultimate state of the hinge types of arch culverts. On the other hand, although the seismic damage to road embankments has mainly occurred in

the culvert longitudinal direction (Tokida et al., 2007), the seismic behavior of culverts in the longitudinal direction has not been studied well. In the following literature reviews, the fundamental knowledge of the seismic behavior in the longitudinal direction is reported, which is still insufficient for gaining a clear understanding of the disaster reported after the Great East Japan Earthquake.

Kumada et al. (1995) conducted 1-G shaking table tests on the three-hinged arch culvert in the culvert transverse and culvert longitudinal directions. As a result, the response behavior of the three-hinged arch culvert followed the behavior of the surrounding ground in the case of shaking in the culvert transverse direction. In short, the amplification of the response acceleration was closer to that of the surrounding ground. On the other hand, in the case of shaking in the culvert longitudinal direction, the culvert showed independent behavior and the amplification of the response acceleration was smaller than that of the surrounding ground. This is because the culvert seemed to have higher stiffness in the culvert longitudinal direction than in the culvert transverse direction.

Toyota and Takagai (1999) and Toyota and Ito (2000) conducted shaking table tests and a 2D finite element analysis on the 1/20 scaled down model of three-hinged arch culverts with a reinforcing earth wall model and observed the seismic behavior in the culvert transverse and culvert longitudinal directions (Figure 2.10). They concluded that the amplification of the bending moment due to the seismic wave was not largely affected by the longitudinal excitation, but by the transverse direction. Sawamura et al. (2014b) conducted dynamic centrifuge tests on two-hinged arch culverts to clarify the seismic effect due to the structural connection of the culverts and the design condition at the mouth of the culverts (Figure 2.11). They modeled each side of the mouth wall of the culvert with an embankment. The sides of the mouth wall were connected with aluminum connections, as shown in the figure. As a result, the tensile force acting on the culverts changed largely due to the structural connection of the culverts. Moreover, they reported that connecting the culverts caused excessive cross-sectional force on the culverts.

2.5 Scope and structure

In this chapter, an outline of culvert structures and a past disaster, as well as an investigation of the seismic performance of the hinge types of precast arch culverts, have been presented. The current issues to be solved in terms of the seismic behavior of the hinge types of precast arch culverts are summarized as follows:

1) As for the seismic behavior in the culvert transverse direction, the failure mechanism of the hinge types of precast arch culverts - damage morphology and the ultimate state - was investigated by Sawamura et al. (2016, 2017). Through their research, the applicability of a static analysis with the response displacement method was verified through a reproduction of the observed damage pattern of the arch members by experiments. However, damage occurred to the overall culverts and the embankment in the Great Japan Earthquake of 2011. This implies that the design method, which was only directed at the arch's cross section, was insufficient for evaluating the whole aspect and mechanism of the disaster.

2) On the other hand, past research works on the behavior in the culvert longitudinal direction
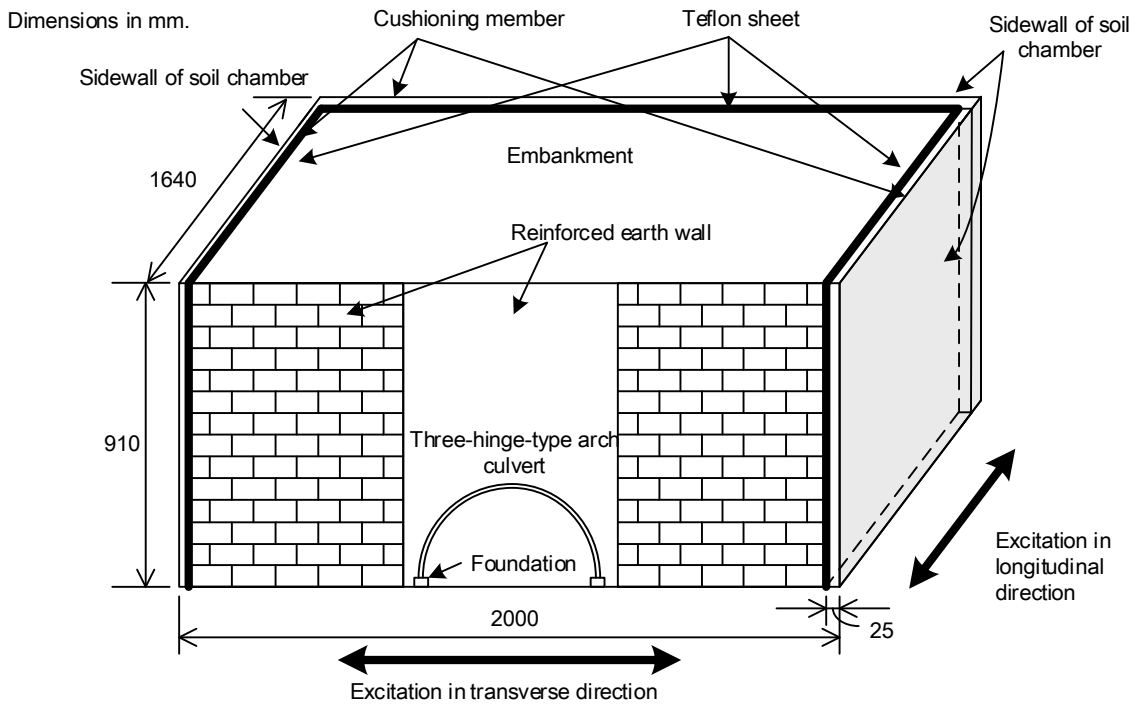
Figure 2.10: Schematic drawing of shaking table tests on three-hinged arch culvert with mouth wall of reinforcing earth wall (Toyota and Takagai, 1999; Toyota and Ito, 2000).
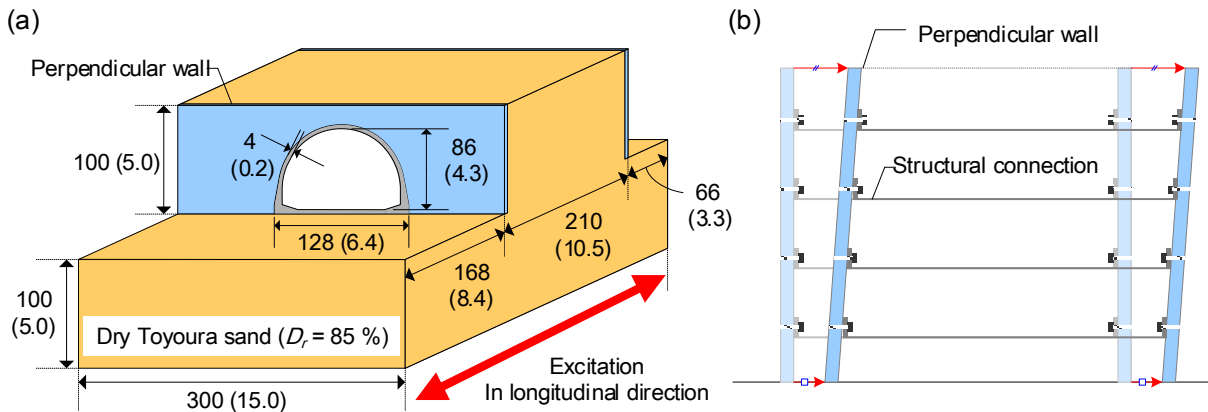
Dimensions in mm, model scale (m, prototype scale)

Figure 2.11: Schematic drawing of dynamic centrifuge test on longitudinal seismic behavior of culvert with embankment (Sawamura et al., 2014b): (a) experimental model and (b) structure of wall panel.

focused on the design method of the culvert longitudinal direction, but these attempts only discussed the stress state of the arch members and contained insufficient explanations of the seismic mode of the culverts. No clear interpretations for the actual damage mechanism related to the inertial force in the culvert longitudinal direction were given.

3) Additionally, the Great East Japan Earthquake motivated civil engineers to include earthquake resistance in the established precast arch culverts; there are currently more than 200 such established precast arch culverts. However, due to the lack of an accurate evaluation method for the seismic performance of precast arch culverts, no effective countermeasures to earthquakes have been developed.

```
┌─────────────────────────────────────────────────────────────────┐
│ Chapter 2                                                        │
│ Literature review of seismic performance of hinge types of       │
│ precast arch culverts                                            │
└─────────────────────────────────────────────────────────────────┘
                              ↓
┌─────────────────────────────────────────────────────────────────┐
│ Chapter 3                                                        │
│ Outline of centrifuge tests and numerical analyses               │
└─────────────────────────────────────────────────────────────────┘
              ↓                                ↓
┌──────────────────────────────┐  ┌──────────────────────────────┐
│ Chapter 4                    │  │ Chapter 5                    │
│ Dynamic centrifuge tests on  │  │ Dynamic centrifuge tests on  │
│ longitudinal structural      │  │ patterns of embankment shape │
│ connectivity                 │  │                              │
└──────────────────────────────┘  └──────────────────────────────┘
                              ↓
┌─────────────────────────────────────────────────────────────────┐
│ Chapter 6                                                        │
│ Numerical analysis of seismic behavior in culvert longitudinal   │
│ direction                                                        │
└─────────────────────────────────────────────────────────────────┘
                              ↓
┌─────────────────────────────────────────────────────────────────┐
│ Chapter 7                                                        │
│ Discussion of damage mechanism of three-hinged arch culverts     │
│ during the Great East Japan Earthquake                           │
└─────────────────────────────────────────────────────────────────┘

┌─────────────────────────────────────────────────────────────────┐
│ Chapter 8                                                        │
│ Conclusions and future studies                                   │
└─────────────────────────────────────────────────────────────────┘
```

Figure 2.12: Structure of thesis.

In order to solve the above issues, a series of research studies, shown in Figure 2.12, is provided in this thesis. To solve these issues, the clarification of the seismic mode in the culvert longitudinal direction and the establishment of a reproducible analytical method are required. Accordingly, one of the solutions is the observation of the various seismic modes in the culvert longitudinal direction due to the structural connection of the culvert (Chapter 4), the shape of the embankment (Chapter 5), and the development of a new evaluation method for these seismic modes (Chapter 6). Therefore, the aim of the present study is to classify the disaster mechanisms and to develop an evaluation method for the seismic performance of the hinge types of precast arch culverts. Then, dynamic centrifuge tests and the elasto-plastic finite element method for the longitudinal seismic behavior of culverts, considering the structural connectivity of the culverts and the embankment shape, are conducted.

In both hinge types of precast arch culverts, the various seismic effects brought about by the structural connectivity and the embankment shape should be investigated. The structural connectivity of the two-hinged arch culvert was studied due to its simple structural connection (Figure 2.8), and the shape of the embankment of the three-hinged arch culvert was studied considering the actual damage due to the earthquake. The dynamic centrifuge tests on the structural connectivity basically followed the modeling by Sawamura et al. (2016, 2017) with more actual construction conditions, namely, the compaction of unsaturated soil for the ground model and the making of the reinforced earth wall for the mouth wall of the culverts. Through dynamic centrifuge tests on the embankment shape, the dynamic

soil-culvert interaction in the culvert longitudinal direction could be observed with various patterns of overburden for the culvert.

To develop a new evaluation method for precast arch culverts, an elasto-plastic FEM analysis was conducted for the seismic behavior in the culvert longitudinal direction based on the experimental results of the dynamic soil-culvert interaction due to the structural connectivity and the embankment shape. In the analysis, firstly, the applicability of the analytical method was verified through a simple 2D analysis, and secondly, the analytical method was applied through a 3D analysis.

Finally, the damage morphology due to the input wave direction, structural connectivity, and embankment shape is classified with the above evaluation method (Chapter 7). It approaches an interpretation of the damage mechanism of the old type of three-hinged arch culverts.

References

Abe, T. and Nakamura, M. (2014): *The use of and the caution in the application of the culvert constructed by large precast element in the expressway construction*, *The Foundation Engineering & Equipment, Monthly,* Vol. 42, No. 4, pp. 8-11 (in Japanese).

Association of Modularch Construction Method (2017): *Engineering Manual for Modularch*, *Geo-Research Institute* (in Japanese).

Byrne, P. M., Anderson, D. L. and Jitno, H. (1994): Seismic Analysis of Large Buried Culvert Structures, *Transportation Research Record*, Vol. 1541, pp. 133-139.

Irie, N., Ito, A., Takahashi, O., and Kusakabe, O. (2002): Dynamic behavior of three-hinged tunnel in a centrifuge, *Proceedings of the Japan National Conference on Geotechnical Engineering*, *The Thirty-seventh Japan National Conference on Geotechnical Engineering*, pp. 1779-1780 (in Japanese).

Investigative Committee of Manual for the Design and Construction of Techspan Construction Method (1998): *Manual for the Design and Construction of Techspan Construction Method (Draft)*, *Advanced Construction Technology Center* (in Japanese).

Japan Road Association (2010): *Road Earthwork Guidelines - Guidelines for Culvert Work* (in Japanese).

Kumada, T., Takahashi, Y., Kitabayashi, T., Hotta, M., Ohi, J., and Koizumi, A. (1995): *Shaking table test on a tunnel of Techspan construction method (No. 1); outline of Techspan construction method and shaking table test*, *the Proceedings of the JSCE Annual Meeting*, Vol. 65, III-556, pp. 1112-1113 (in Japanese).

Public Works Research Center (2014): *Manual for the Design and Construction of Reinforced Earth Wall, 4th Revised Edition* (in Japanese).

Sawamura, Y., Kishida, K. and Kimura, M. (2014a): Evaluation of dynamic behavior of culverts and embankments through centrifuge model tests and a numerical analysis, *Proc. of the 14th International Conference of the International Association for Computer Methods and Recent Advances in Geomechanics*, pp. 743-748, Kyoto.

Sawamura, Y., Arai, T., Kishida, K., and Kimura, M. (2014b): Centrifuge model test on the earthquake performance of culvert longitudinal direction in arch culvert embankment with perpendicular wall, *Japanese Geotechnical Journal*, Vol. 9(1), pp. 41-57 (in Japanese). dx.doi.org/10.3208/jgs.9.41

Sawamura, Y., Ishihara, H., Kishida, K., and Kimura, M. (2016): Experimental Study on Damage Morphology and Critical State of Three-hinge Precast Arch Culvert through Shaking Table Tests, *Procedia Engineering, Advances in Transportation Geotechnics III*, Vol. 143, pp. 522-529.

Sawamura, Y., Matsushita, R., Kishida, K., and Kimura, M. (2017): Evaluation of mechanical behavior of two-hinge precast arch culvert in construction process and its seismic damage morphology through strong earthquake response experiments, *Japanese Geotechnical Journal*, Vol. 15, No. 4, pp. 385-396 (in Japanese). doi.org/10.3208/jgs.12.385

Seto, H., and Ootani, Y. (2014): *Outline of and construction example of Techspan construction method, The Foundation Engineering & Equipment, Monthly,* Vol. 42, No. 4, pp. 8-11(in Japanese).

Technological Examination Committee of Techspan Construction Method (2014): *Comparison Outline of Revised Items in Manual for the Design and Construction of Techspan Construction Method (Draft)*, *Advanced Construction Technology Center* (in Japanese).

Tokida, K., Oda, K., Nabeshima, Y., and Egawa, Y. (2007): Damage level of road infrastructure and road traffic performance in the mid Niigata prefecture earthquake of 2004, *Structural Eng./ Earthquake Eng., JSCE*, Vol. 24, No. 1, pp. 51-61. doi.org/10.2208/jsceseee.24.51s

Toyota, H., and Takagai, M. (1999): Dynamic behavior of 3-hinge arch in terre armee foundation, Journal of JSCE, No. 624/III-47, pp. 255-266 (in Japanese).
dx.doi.org/10.2208/jscej.1999.624_255

Toyota, H., and Ito, T. (2000): Effects of shaking conditions and material properties on dynamic behavior of terre armee foundation and 3-hinge arch, *Journal of JSCE*, No. 666/III-53, pp. 279-289 (in Japanese).
dx.doi.org/10.2208/jscej.2000.666_279

Wood, J. H. and Jenkins, D. A. (2000): Seismic analysis of buried arch structures, *Proc. of the 12th World Conference of Earthquake Engineering*, No. 0768.

Chapter 3 Outline of centrifuge tests and numerical analyses

3.1 Introduction

The present study aims to clarify the seismic behavior of the hinge types of precast arch culverts. Dynamic centrifuge tests and finite element analyses were conducted for this purpose. In Chapter 4 and Chapter 5, the dynamic centrifuge tests will be carried out considering the longitudinal structural connectivity and the embankment shape of the culverts, respectively. In Chapter 6 and Chapter 7, based on the aforementioned experiments, dynamic analyses by FEM will be carried out considering the observed seismic effects of the structural connection and the embankment shape. In this chapter, an outline of the experiments and the analyses will be given.

3.2 Geotechnical centrifuge

3.2.1 Outline of centrifuge model test

The centrifuge test is one type of physical modeling which loads a geometrically $1/N$ scaled-down model N times as the acceleration of gravity through the centrifugal loading device to evaluate the mechanical behavior. Generally speaking, except for the prototype-scaled test, the scale law between the scaled-down model and the prototype cannot be satisfied. In particular, the effects of the self-weight of the ground and the structure cannot be considered, which makes it difficult to quantitatively evaluate and directly apply the obtained data to actual designs and construction through the scaled-down model test under 1 G.

The centrifuge test can reproduce the self-weight situation of the prototype with the $1/N$ scaled-down model by loading N G of centrifugal acceleration. Accordingly, the centrifugal loading device can satisfy the geometrical and mechanical scale laws simultaneously between the prototype and the model. Table 3.1 shows the main scale law between the model and the prototype under N G of acceleration gravity (Scofield, 1980). In the field of geotechnical engineering, the centrifuge test called 'geotechnical centrifuge' is used to evaluate and verify the actual investigation, design, and construction of civil engineering structures.

On the other hand, the amount of sand material used for the ground model under N G of centrifugal acceleration is converted to N times that of the original particle size. However, regulating the $1/N$ scaled-down particle size is difficult. Accordingly, the scale effect of the particle is one of the defects of the geotechnical centrifuge.

3.2.2 Devices of dynamic centrifuge test

In the centrifuge test of this study, the centrifugal loading device of DPRI (Disaster Prevention Research Institute, Kyoto University) was used. Figure 3.1 shows a schematic drawing of the centrifugal loading device. The rotation of the arm for the centrifugal loading is controlled by converting the vertical rotation by the motor located under the main pit into the horizontal rotation by the bevel gear. The tip of the arm is connected to the platform by a hinge. With an increase in the rotational velocity of the arm, the platform rises with the scaled down model by obtaining an increase in the centrifugal load.

Table 3.1: Scaling law of centrifuge modeling.

Physical quantity	Prototype/ Model (N G)
Displacement/length	N
Area	N^2
Volume	N^3
Pressure	1
Strain	1
Force	N^2
Time (consolidation)	N^2
Time (dynamic)	N

Table 3.2: Specifications of centrifugal apparatus.

Items	Specifications
Effective radius	2.5 [m]
Maximum capacity of loading	24 [G×ton]
Maximum centrifugal acceleration	100 [G]: Static test
	50 [G]: Dynamic test

Control room

① PC for measurement　　　　　⑤ Air conditioner　　　　⑨ Motor for loading
② PC for control of shaking table　⑥ Platform　　　　　　　⑩ Bevel gear
③ Slip ring　　　　　　　　　　⑦ Arm　　　　　　　　　⑪ Instrumentation for dynamic strain
④ Rotary joint　　　　　　　　　⑧ Pressure oil tank　　　　⑫ Laptop for control of shaking table
　　　　　　　　　　　　　　　　　　　　　　　　　　⑬ Wireless LAN
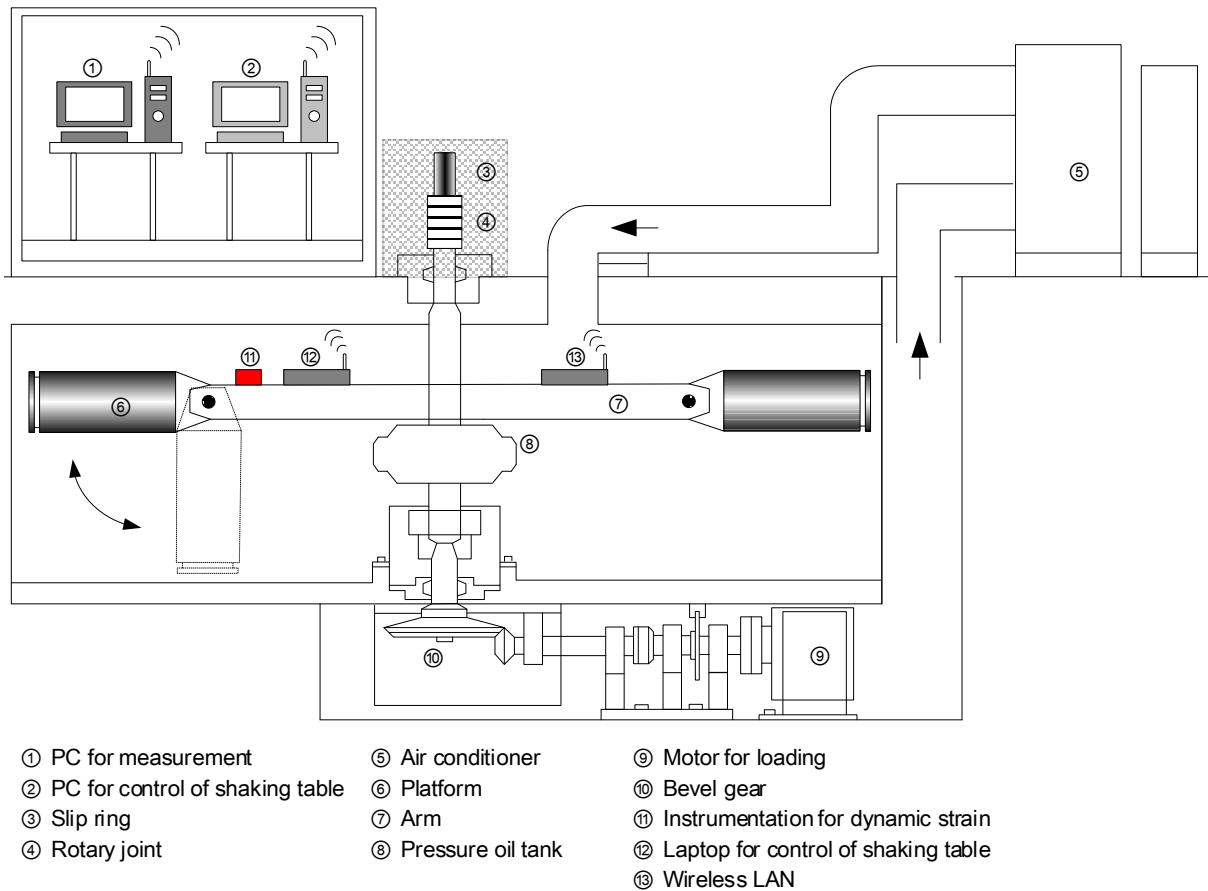
Figure 3.1: Schematic drawing of the centrifugal loading device of DPRI: (a) mouth wall with reinforcing members, (b) reinforcing member, and (c) attachment of reinforcing member with mouth wall.

Table 3.2 shows the specifications of the centrifugal device of DPRI. The effective radius between the rotational axis of the arm and the center of the model is 2.50 m. The maximum centrifugal acceleration is 100 G under static loading and 50 G under dynamic loading by the shaking table. The maximum capacity of the gross weight is 24 G • ton. Additionally, the camera below the arm can observe the experimental situation visually.

Dimensions in mm
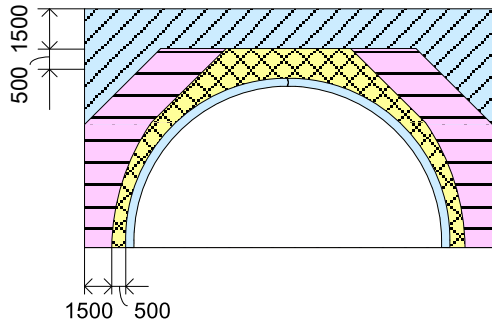
Area	Legend	Material	Type of compactor
1		C-40	Plate
2		C-40	Small roller
3		-	Middle roller

* The other area follows the road embankment guideline.

Figure 3.2: Standard of filling in three-hinged arch culverts (Technological Examination Committee of Techspan Construction Method, 2014).

A simulation of the seismic behavior under a certain centrifugal acceleration is conducted by the shaking table. The shaking table is attached to the platform and controlled by an electro-hydraulic type of actuator. The hydraulic servo control system is used to regulate the horizontal displacement of the shaking table to realize the large displacement and force with the small shaking table and to easily regulate the frequency of the excitation. Currently, this system is mostly applied in general centrifugal loading devices.

3.2.3 Filling material and buffer material for ground model

Hinge types of precast arch culverts will be affected by the deformation of the surrounding ground due to the hinge structure in the arch's cross section. Accordingly, certain standards in the compaction or the stiffness of the foundation ground and the embankment are required for stabilizing the arch structure. The design criteria for the two-hinged arch culverts (Association of Modularch Construction Method, 2017) require a stiffer foundation ground with more than 15 N values of SPT. Additionally, as shown in Figure 3.2, the filling should be compacted to Dc of more than 92%. The design criteria for the three-hinged arch culverts (Technological Examination Committee of Techspan Construction Method, 2014) require that the filling near the arch culverts be compacted to Dc of more than 90%. Thus, the hinge types of arch culverts require a well-graded foundation ground and embankment. In this study, therefore, *Edosaki* sand was chosen to satisfy the requirement that the sand have well-distributed particles suitable for compaction. Figure 3.3 shows the compaction curve and particle size distribution curve of *Edosaki* sand. Accordingly, in the experiments that will be described in Chapter 4 and Chapter 5, the ground model is made of *Edosaki* sand to satisfy the Dc of 92% in order to meet the required standards of compaction for precast arch culverts.

The dynamic centrifuge tests in the present study were conducted using a rigid chamber, 450 × 340 × 300 in mm (W × H × D), as shown in Figure 3.4. However, a rigid chamber will cause reflected waves from the side wall of the chamber during excitation. Therefore, a gel sheet was used to reduce the effect of the reflected waves by referring to a past literature review (Kiyota et al., 2010). To select a suitable gel sheet for the experiments, a preliminary experiment was conducted, as seen in the schematic drawing of the experiment given in Figure 3.5. In the experiment, three types of gel sheets with different levels of compressive stiffness were used, and the response accelerations of the ground were measured
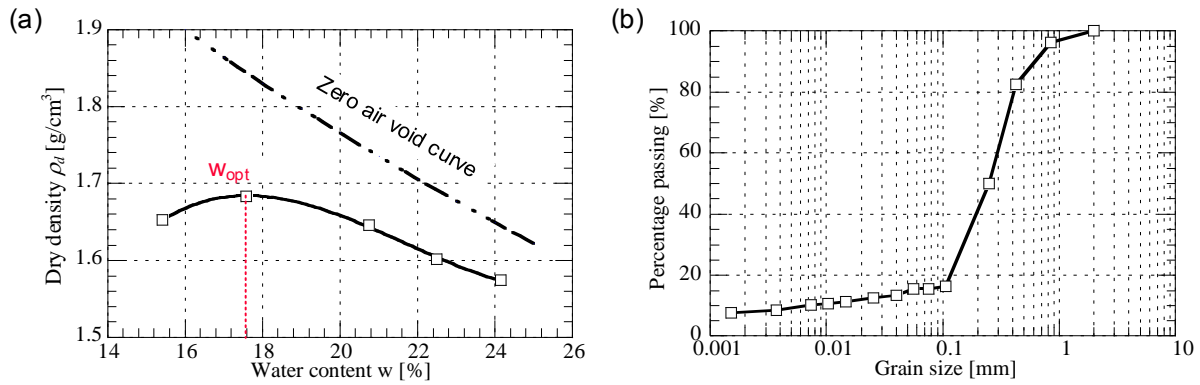
Figure 3.3: Characteristics of *Edosaki* sand in (a) compaction curve and (b) particle size distribution curve.
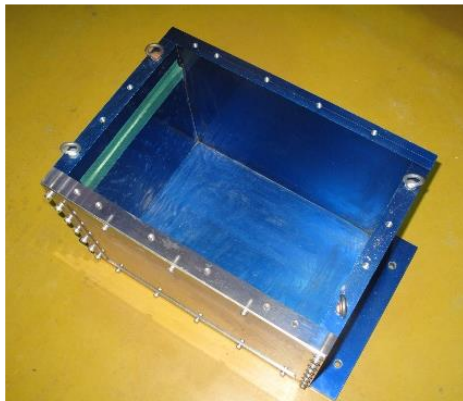
Figure 3.4: Rigid chamber.
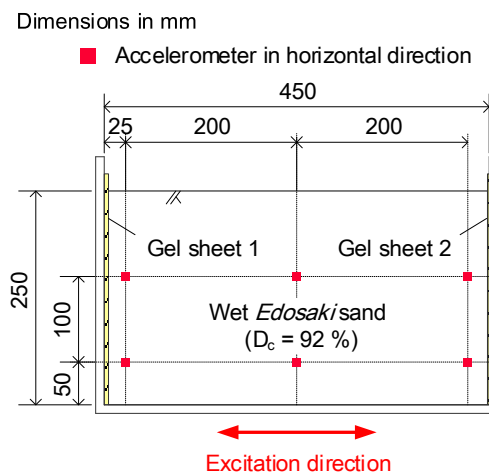
Figure 3.5: Preliminary experiment for selecting suitable gel sheet.

during the excitation of a sin wave with 1 Hz in the prototype scale and two cycles. The frequency of the input wave equaled the input wave that will be employed in Chapter 4 and Chapter 5. As a result, when the gel sheet was 2 mm in thickness and 0.07 N/mm^2 in compressive stiffness at 10% compression, the smallest difference in response acceleration between the ground near the side wall of the chamber and the central ground was obtained. From this result, the following experiments used the above gel sheet as cushion material for the side wall of the rigid chamber.

3.2.4 Modeling mouth wall of precast arch culverts

The mouth wall of the hinge types of precast arch culverts is mainly constructed as a perpendicular wall composed of reinforced earth (Investigative Committee of Manual for the Design and Construction of Techspan Construction Method, 1998). In the geotechnical centrifuge for the reinforcing soil wall, the wall structure was modeled in various ways based on the experimental conditions (e.g., Ichikawa, 2006). The present study modeled the reinforcing earth wall (Public Works Research Center, 2014) by referring to Figure 3.6 and Figure 3.7. As shown in the figures, the standard type of concrete skin for the reinforcing earth wall is a cruciform plate, 1.5 m × 1.5 m in size. The back side of each piece of concrete
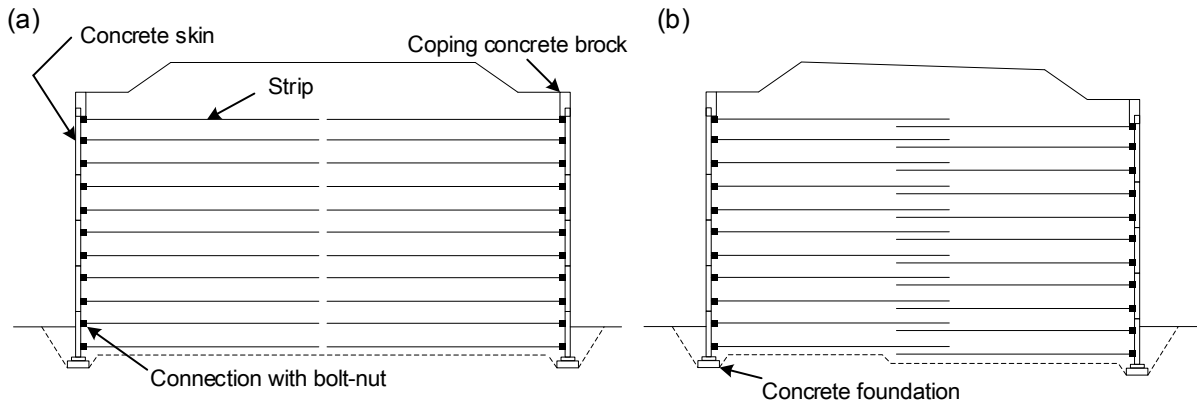
Figure 3.6: Embankment with reinforcing earth wall on both sides of embankment (Public Works Research Center, 2014): (a) connected type and (b) fitting type of wall.
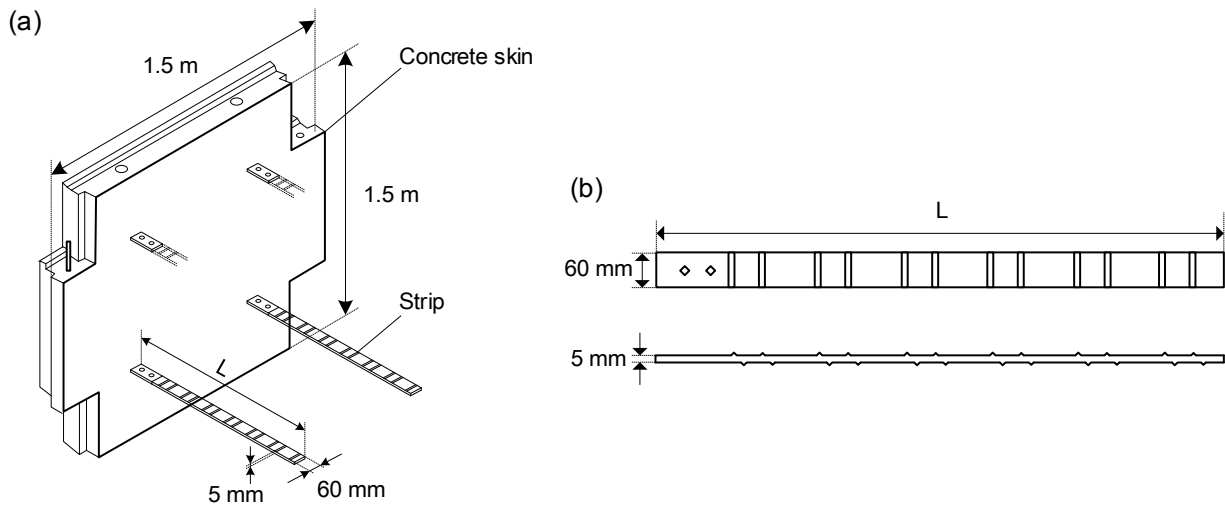
Figure 3.7: Shapes of (a) concrete skin and (b) strip in reinforcing earth wall (Public Works Research Center, 2014).

skin has four metal strips, 60 mm in width and 5 mm in thickness, as shown in Figure 3.7. If the actual plate is minimized in model scale, the concrete skin is 30 mm × 30 mm and the width of the strip is 1.2 mm under 50 G of centrifugal acceleration. Producing a model with such minimized dimensions is not realistic. In this experiment, therefore, considering only the dynamic similarity of the reinforcing member, the wall plate was made of an acryl plate, 5 mm of thickness, and the strips were made of aluminum plates, 0.1 mm in thickness and 10 mm in width.

The wall model that will be used in Chapter 4 is shown in Figure 3.8 as an example of the model of the wall structure. The surfaces of the strips were coated with dry *Edosaki* sand to increase the friction between the reinforcing member and the filling. From direct shear tests between the reinforcing member and the *Edosaki* sand, regulated to the optimum moisture ratio, the internal friction angle was 28.2º and the cohesion was 10.8 kN/m². Tatsuoka (1991) classified the structural resistance of the wall structure into the five types shown in Figure 3.9. According to this classification, the experimental model corresponds to the type of wall structure described in Figure 3.9 (d).

Here, the density of the reinforcing members is defined as the width of a strip divided by the area
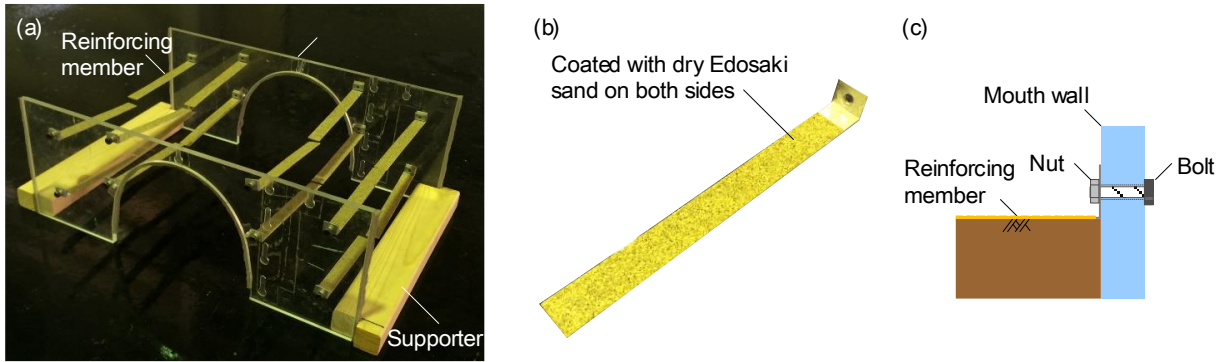
Figure 3.8: Example of modeling of reinforcing earth wall in dynamic centrifuge tests described in **Chapter 4**: (a) mouth wall with reinforcing members, (b) reinforcing member, and (c) attachment of reinforcing member to mouth wall.

Type of wall	(a)	(b)	(c)	(d)	(e)
Local stiffness	✕	◯	◯	◯	◯
Whole shear stiffness	✕	✕	◯	◯	◯
Whole bending stiffness	✕	✕	✕	◯	◯
Shearing resistance due to self-weight	✕	✕	✕	✕	◯
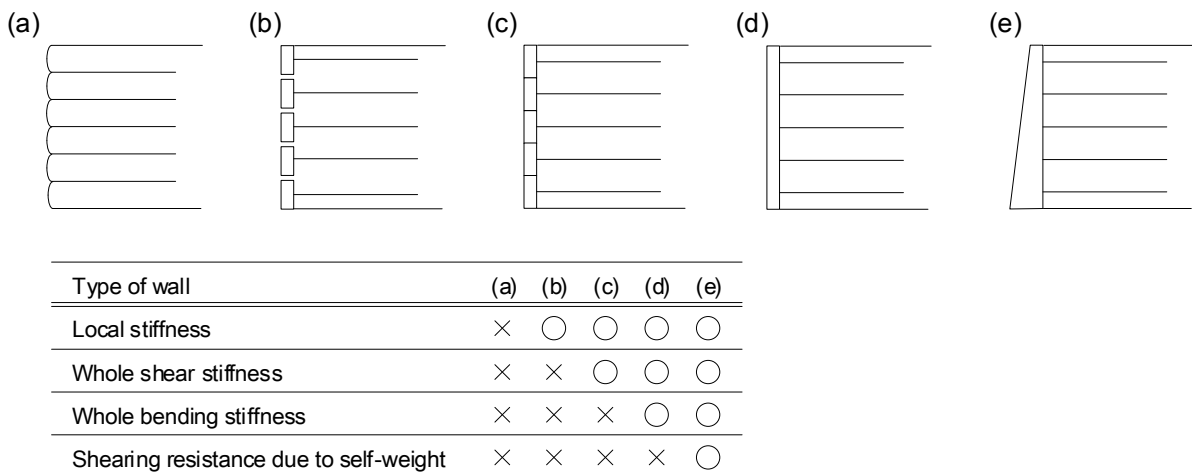
Figure 3.9: Classification due to mechanical role of wall structure: (a) soft wall structure, (b) rigid wall without mechanical interaction between wall panels, (c) rigid wall simply constructed by accumulating wall panels, (d) rigid wall, and (e) retaining wall (Tatsuoka, 1991).

of the wall panel. In an actual structure, the prototype density of the reinforcing members is 60 mm × 4 / (1.5 m × 1.5 m) = 107 mm/m^2. On the other hand, the model density of the reinforcing members is 500 mm × 10 / (15 m × 15 m) = 67 mm/m^2, which is an insufficient arrangement of the reinforcing members compared to the actual construction. However, a wall model with a smaller density of the reinforcing members was made of one acrylic plate which is stiffer in the shear stiffness of the wall than that in the prototype structure.

3.3 Numerical analysis

3.3.1 Outline of numerical analysis

Numerical analyses were conducted in the present study for the seismic behavior in the culvert longitudinal direction of the three-hinged arch culverts, as will be described in **Chapter 6** and **Chapter 7**. To analyze the seismic behavior in the culvert longitudinal direction, the nonlinear deformation of the embankment due to seismic waves needs to be modeled. Additionally, the precast arch culverts are

composed of the mouth wall of the culvert (reinforcing earth wall), the arch members, and the embankment, which requires 3-dimensional modeling. That is why the 3D elasto-plastic finite element analysis operated in DBLEAVES (Ye et al., 2007) was conducted. DBLEAVES is an analytical code improved by Ye et al. (2007) based on DGPILE3D, a 3D FEM analysis code developed by Kimura and Zhang (2000), which can consider large deformation through a finite deformation analysis. The applicability of DBLEAVES for ground deformation problems has been verified through various analyses for pile foundations (e.g., Dannno et al., 2007, Dannno et al., 2009, and Jin et al., 2010), tunnels (Cui et al., 2010), and underground structures (Zhang et al., 2007).

3.3.2 Modeling of cyclic mobility

The present study used the cyclic mobility model proposed by Zhang et al. (2007) for the constitutive model of soil. This proposed model was newly developed to describe the cyclic mobility of soil by systematically combining the evolution equations for the development of stress-induced anisotropy and the changes in the over-consolidation of soils. As an important advantage, the proposed model can express the behavior of soils under cyclic loading with different drained conditions and by uniformly considering the density, the over-consolidation ratio, the naturally accumulated structure of the soil, and the stress-induced anisotropy of the soil. The yielding surface and the consistency equation in the cyclic mobility model are explained as follows.

Zhang et al. (2007) proposed a new yielding surface, described in **Figure 3.10**, based on the concepts of the subloading and the superloading surfaces by Hashiguchi et al. (1989) and Asaoka et al. (1998). The yielding surfaces of this model, shown in the figure, stand on the idea of the constant gradient of C.S.L. proved by the research works of Hyodo et al. (1994) and Kato et al. (2001). In the proposed model, the increase in the stress-induced anisotropy promotes the increase in the eccentric ratio of the ellipses of the yielding surface to consider their dependency.

Here, based on the research work by Asaoka et al. (2002), the similarity ratio of the superloading surface to normal yield surface R^* and the similarity ratio of the superloading surface to subloading surface R are the same, namely,

$$R^* = \frac{\tilde{p}}{\bar{p}} = \frac{\tilde{q}}{\bar{q}}, \;\; 0 < R^* \leq 1 \tag{3.1}$$

$$R = \frac{p}{\bar{p}} = \frac{q}{\bar{q}}, \;\; 0 < R \leq 1, \;\; R = \frac{1}{OCR} \tag{3.2}$$

$$\frac{\bar{q}}{\bar{p}} = \frac{\tilde{q}}{\tilde{p}} = \frac{q}{p} \tag{3.3}$$

where (p', q), $(\tilde{p}', \tilde{q})$, and $(\bar{p}', \bar{q})$ represent the present stress state, the corresponding normally consolidated state, and the structured stress state at the p-q plane, respectively.

Therefore, according to **Figure 3.10**, normal yield surface R^* is given in the following equations as:
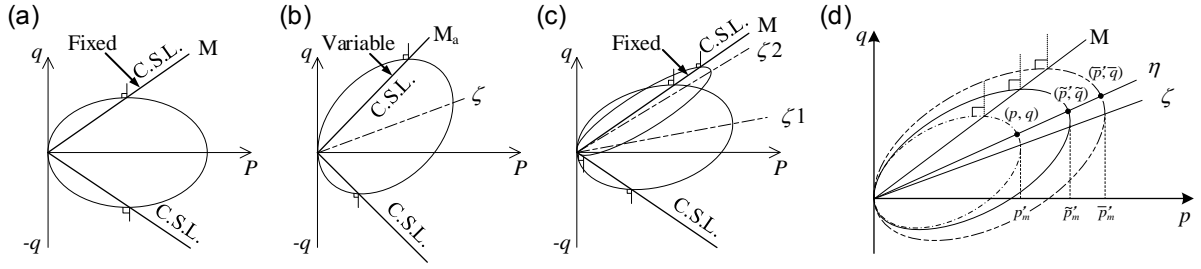
Figure 3.10: Concept of yielding surfaces in cyclic mobility model (Zhang et al., 2007): changes in subloading yielding surfaces at different anisotropy ζ in (a) modified Cam-clay model (Schofield and Wroth, 1968), (b) SYS Cam-clay model (Asaoka et al., 2002), (c) cyclic mobility model, and (d) subloading, normal, and superloading yield surfaces in p-q plane adopted in cyclic mobility model.

$$f = \ln \frac{\tilde{p}}{p} + \ln \frac{M^2 - \varsigma^2 + \eta^{*2}}{M^2 - \varsigma^2} - \frac{\varepsilon_v^p}{C_p} = 0 \tag{3.4}$$

$$\eta^* = \sqrt{\frac{3}{2}\hat{\eta}_{ij}\hat{\eta}_{ij}}\ ,\ \ \hat{\eta}_{ij} = \eta_{ij} - \beta_{ij}\ ,\ \ \eta_{ij} = \frac{S_{ij}}{p}\ ,\ \ S_{ij} = \sigma_{ij} - p \cdot \delta_{ij}\ ,\ \ p = \frac{\sigma_{ij}}{3} \tag{3.5}$$

$$\eta = \sqrt{\frac{3}{2}\eta_{ij}\eta_{ij}}\ ,\ \ \varsigma = \sqrt{\frac{3}{2}\beta_{ij}\beta_{ij}} \tag{3.6}$$

$$C_p = \frac{\lambda - \kappa}{1 + e_0} \tag{3.7}$$

where S_{ij} is the deviatoric stress tensor and β_{ij} is the anisotropic stress tensor. From the definitions for the subloading and the superloading surfaces shown in Eqs. (3.1) to (3.3), the first member of Eq. (3.4) is given in the following form:

$$\ln \frac{\tilde{p}}{\tilde{p}_0} = \ln \frac{\tilde{p}}{p} - \ln \frac{p}{\tilde{p}} + \ln \frac{p}{\tilde{p}_0} = \ln R^* - \ln R + \ln \frac{p}{\tilde{p}_0} \tag{3.8}$$

With Eq. (3.8), the subloading surface is given as a more general expression as

$$f = \ln \frac{p}{\tilde{p}_0} + \ln \frac{M^2 - \varsigma^2 + \eta^{*2}}{M^2 - \varsigma^2} + \ln R^* - \ln R - \frac{\varepsilon_v^p}{C_p} = 0 \tag{3.9}$$

Here, ς, the second member of Eq. (3.9), denotes the magnitude of the stress-induced anisotropy, and the evolution of ς expresses the change in the eccentric ratio of the ellipses of the yielding surface. Focusing on the partial differentiations of Eq. (3.9),

$$\frac{\partial f}{\partial p} = \frac{M^2 - \eta^2}{(M^2 - \varsigma^2 + \eta^{*2})p} \tag{3.10}$$

$$\frac{\partial f}{\partial S_{ij}} = \frac{3\hat{\eta}_{ij}}{(M^2 - \varsigma^2 + \eta^{*2})p} \tag{3.11}$$

$$\frac{\partial f}{\partial \sigma_{ij}} = \frac{3\hat{\eta}_{ij}}{(M^2 - \zeta^2 + \eta^{*2})p} + \frac{M^2 - \zeta^2}{(M^2 - \zeta^2 + \eta^{*2})p} \cdot \frac{\delta_{ij}}{3} \qquad (3.12)$$

$$\frac{\partial f}{\partial \beta_{ij}} = \frac{3(-M^2\hat{\eta}_{ij} + \eta^{*2}\beta_{ij} + \zeta^2\hat{\eta}_{ij})}{(M^2 - \zeta^2 + \eta^{*2})(M^2 - \zeta^2)} \qquad (3.13)$$

when $\partial f / \partial p = 0$, the C.S.L. defined by the above conditions always satisfies $\eta = M$, which proves that constant C.S.L. is independent of the evolution of the stress-induced anisotropy. On the other hand, the plastic volumetric strain is given in the following equation and definitions:

$$\varepsilon_v^p = -\int_0^t Jtr\mathbf{D}^p d\tau \qquad (3.14)$$

$$J = \det \mathbf{F} = \frac{v}{v_0} = \frac{1+e}{1+e_0} \qquad (3.15)$$

$$D = \frac{\tilde{\lambda} - \tilde{\kappa}}{M(1+e_0)} = \frac{\tilde{\lambda} - \tilde{\kappa}}{Mv_0} \qquad (3.16)$$

J is the Jacobian determination of deformation gradient tensor $\mathbf{F}$. $\mathbf{D}^p$ is the plastic component of stretching D which can be expressed by $\tilde{\lambda}$ and $\tilde{\kappa}$, the compression and swelling indexes, respectively.

Finally, from Eq. (3.9), the consistency equation is given as

$$df = 0 \implies \frac{\partial f}{\partial \sigma_{ij}} d\sigma_{ij} + \frac{\partial f}{\partial \beta_{ij}} d\beta_{ij} + \frac{1}{R^*} dR^* - \frac{1}{R} dR - \frac{1}{C_p} \varepsilon_v^p = 0 \qquad (3.17)$$

3.3.3 Paramters of cyclic mobility model

In the numerical analysis, the mechanical properties of the soil were based on the *Edosaki* sand used in the experiment, and the dynamic properties of *Edosaki* sand were modeled by the cyclic mobility model (Zhang et al., 2007).

The cyclic mobility model requires eight parameters; five of the eight parameters are equivalent to those of Cam-clay model (Rcs, λ, κ, N, v_e), which can be determind by triaxial compression tests. The other three parameters (a, m, b_r) require trial and error of the fitting of the results obtained from the triaxial tests. The respective physical meanings of the parameters are clear, as follows:

R_{cs} : Principal stress ratio at failure under triaxial compression condition given in

$$R_{cs} = \left(\frac{\sigma_1}{\sigma_3}\right)_{CS(comp.)}$$

λ : Compression index.
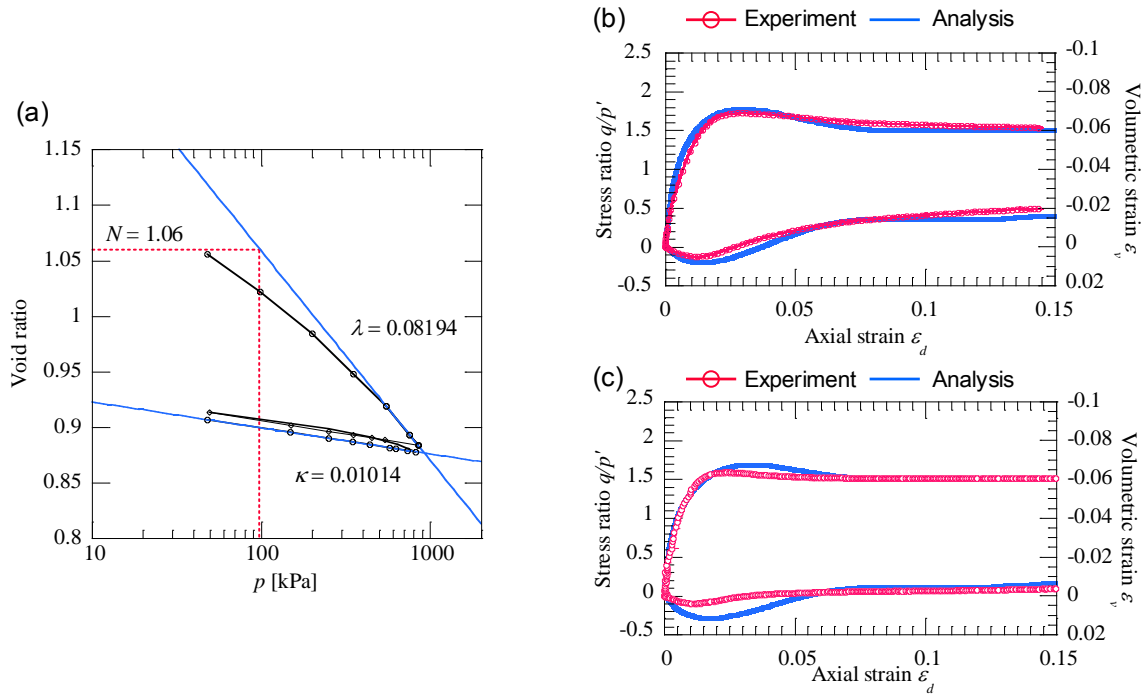
Figure 3.11: Results of (a) isotropic consolidation tests and triaxial compression tests and their simulations in (b) 50 kPa of and (c) 100 kPa of confining stress for *Edosaki* sand (Sawamura et al., 2016).

> The parameter is determined by isotropic consolidation and an unloading test; the gradient is e-ln$p$' in the loading process of the normal consolidation.

κ : Swelling index.

> The parameter is determined by isotropic consolidation and an unloading test; the gradient is e-ln$p$' in the loading process of the overconsloidation.

N : Void ratio at air pressure (p' = 98 kPa, q = 0 kPa).

ν_e : Poisson's ratio.

a : Degradation parameter of structure.

m : Degradation parameter of overconsolidation state.

b_r : Evolution parameter of anisotropy.

The parameters were determined by triaxial tests and isotropic consolidation tests on *Edosaki* sand. The results of the tests and their simulations are shown in Figure 3.11. The effect of the confining stress was adjusted by changing the state variable of $R*_0$ related to the initial structure of the soil. Although the simulation showed a tendency for an increase in volumetric strain in the small axial strain, the simulation can reproduce all the experimental results relatively well. Based on the simulation results, the parameters for the cyclic mobility model and the state variables of R^*_0 and ζ_0 were determined as shown in Table 3.3.

Table 3.3 : Parameters for Cyclic mobility model.

Principal stress ratio at critical state $R_{CS} = (\sigma_1/\sigma_3)_{CS(comp.)}$	4.0
Compression index λ	0.082
Swelling index κ	0.101
$N = e_{NC}$ at $p = 98$ kPa & $q = 0$ kPa	1.06
Poisson's ratio ν_e	0.276
Degradation parameter of overconsolidation state m	0.020
Degradation parameter of structure a	0.65
Evolution parameter of anisotropy b_r	0.4
Wet unit weight (kN/m^3) γ_t	17.738
Initial degree of structure R^*_0	0.1491 ~ 0.1584
Initial anisotropy ζ_0	0.5

References

Asaoka, A., Nakano, M. and Noda, T. (1998): Super loading yield surface concept for the saturated structured soils, *Proc. of the Fourth European Conference on Numerical Methods in Geotechnical Engineering-NUMGE98*, pp. 232-242. dx.doi.org/10.1007/978-3-7091-2512-0_22

Asaoka, A., Neda, T., Yamada, E., Kaneda, K, and Nakano, M. (2002): An elasto-plastic description of two distinct volume change mechanisms of soils, *Soils and Foundations*, Vol. 42 No. 5, pp. 47-57. dx.doi.org/10.3208/sandf.42.5_47

Association of Modularch Construction Method (2017): *Engineering Manual for Modularch*, *Geo-Research Institute* (in Japanese).

Cui, Y. Kishida, K. and Kimura, M (2010): Analytical study on the control of ground subsidence arising from the phenomenon of accompanied settlement using footing reinforcement pile. *Geotechnical Special Publication, Deep and Underground Excavation,* ASCE, pp. 307-312. dx.doi.org/10.1061/9780784411070

Danno, K., Kimura, M. and Suzuki, Y. (2007): Prediction of long-term displacements of pile foundation with soil-water coupling elasto-plastic FEM, *Journal of Japan Society of Civil Engineers (Geosphere Engineering C)*, Vol. 63, No. 4, pp. 1041-1053 (in Japanese). dx.doi.org/10.2208/jscejc.63.1041

Danno, K. and Kimura, M. (2009): Evaluation of long-term displacements of pile foundation using coupled FEM and centrifuge model test, *Soils and Foundations*, Vol. 49, No. 6, pp. 941-958. dx.doi.org/10.3208/sandf.49.941

Hashiguchi, K. (1989): Subloading surface model in unconventional plasticity, *International Journal of Solids and Structures*, Vol. 25, No. 8, pp. 917-945. dx. doi.org/10.1016/0020-7683(89)90038-3

Hyodo, M., Tanimizu, H., Yasufuku, N. and Murata, H. (1994): Undrained cyclic and monotonic triaxial behavior of saturated loose sand, *Soils and Foundations*, Vol. 34, No. 1, pp. 19-32. dx. doi.org/10.3208/sandf1972.34.19

Ichikawa, S., Suemasa, T., Katada, T., Toyosawa, Y., and Shimada, S. (2006): Dynamic centrifuge model tests on two types of retaining walls reinforced with anchors diddering in wall rigidity, *Journal of Japan Society of Civil Engineers (Geosphere Engineering C)*, Vol. 62, No. 4, pp. 767-779 (in Japanese). dx.doi.org/10.2208/jscejc.62.767

Investigative Committee of Manual for the Design and Construction of Techspan Construction Method

(1998): *Manual for the Design and Construction of Techspan Construction Method (Draft)*, *Advanced Construction Technology Center* (in Japanese).

Japan Road Association (2012): *Specifications for Highway Bridges Vol. V: Seismic Design* (in Japanese).

Jin, Y., Bao, X., Kondo, Y. and Zhang, F. (2010): Soil-water coupling analysis of real-scale field test for 9-pile foundation subjected to cyclic horizontal loading, *Geotechnical Special Publication, Deep Foundation and Geotechnical In Situ Test,* ASCE, Vol. 205, pp. 111-118. dx.doi.org/10.1061/41106(379)13

Kato, S., Ishihara, K. and Towhata, I. (2001): Undrained shear characteristics of saturated sand under anisotropic consolidation, *Soils and Foundations*, Vol. 41, No. 1, pp. 1-11. dx. doi.org/10.3208/sandf.41.1

Kimura, M. and Zhang, F. (2000): Seismic evaluations of pile foundations with three different methods based on three-dimensional elasto-plastic finite element analysis, *Soils and Foundations*, Vol. 40, No. 5, pp. 113-132. dx.doi.org/10.3208/sandf.40.5_113

Public Works Research Center (2014): *Manual for the Design and Construction of Reinforced Earth Wall, 4th Revised Edition* (in Japanese).

Sakamoto, H., Kojima, K., Yonezawa, T., Morino, T., Maruyama, S., and Suzuki, Y. (2010): *Shaking table test on the pile slab track embankment; Selection of buffer, Japan Society of Civil Engineers 2010 Annual Meeting*, pp. 727-728 (in Japanese).

Sawamura, Y., Ishihara, H., Kishida, K., and Kimura, M. (2016): Experimental Study on Damage Morphology and Critical State of Three-hinge Precast Arch Culvert through Shaking Table Tests, *Procedia Engineering, Advances in Transportation Geotechnics III*, Vol. 143, pp. 522-529.

Schofield, A. N. and Wroth, C. P. (1968): Critical State Soil Mechanics, McGraw-Hill, London.

Scofield, A. N. (1980): Cambridge geotechnical centrifuge operations, *Geotechnique*, Vol. 30, No. 3, pp. 227-268, 1980.

dx.doi.org/10.1680/geot.1980.30.3.227

Tatsuoka, F. (1991): *The present, the past and the future of reinforced earth retaining wall: theoretical thought on its mechanism, The Foundation Engineering & Equipment*, No. 11, pp. 8-18 (in Japanese).

Technological Examination Committee of Techspan Construction Method (2014): *Comparison Outline of Revised Items in Manual for the Design and Construction of Techspan Construction Method (Draft)*, *Advanced Construction Technology Center* (in Japanese).

Xia, Z. F., Ye, G. L., Wang, J. H., Ye, B and Zhang, F. (2010): Numerical analysis on the influence of thickness of liquefiable soil on seismic response of underground structure, *Journal of Shanghai Jiaotong University*, Vol. 15, No. 3, pp. 279-284.

Ye, B., Ye, G. L., Zhang, F. and Yashima, A. (2007): Experiment and numerical simulation of repeated liquefaction-consolidation of sand, *Soils and Foundations*, Vol. 47, No. 3, pp. 547-558. dx.doi.org/10.3208/sandf.47.547

Zhang, F., Ye, B., Noda, T., Nakano, M. and Nakai, K. (2007): Explanation of cyclic mobility of soils, Approach by stress-induced anisotropy, Soil and Foundations, Vol. 47, No. 4, pp. 635-648. dx.

Chapter 4 Dynamic centrifuge tests on longitudinal structural connectivity

4.1 Introduction

Precast arch culverts are constructed by continuously placing and connecting each segment. This longitudinal connecting condition of the arch members is clearly correlated with the longitudinal shear stiffness of the culverts. That is why the dynamic behavior of precast arch culverts is believed to depend heavily on the method in which the culverts are connected. Accordingly, the aim in this chapter is to evaluate how the longitudinal structural connection of precast arch culverts influences the dynamic behavior in the culvert longitudinal direction by conducting dynamic centrifuge tests.

4.2 Experimental setup

The dynamic centrifuge tests were conducted with the centrifugal acceleration of 50 G in order to clarify the seismic behavior of precast arch culverts due to the structural connectivity. Figure 4.1 shows schematic drawings of the experimental model, with a soil chamber of 340 mm × 450 mm × 300 mm, and the culvert model.

The precast arch culvert installed in the embankment was composed of three parts, as shown in Figure 4.1 (a), namely, the precast arch culvert, the embankment, and the reinforcing wall. The modeling methods for these three parts are explained in the following.

4.2.1 Precast arch culvert model

The precast arch culvert consists of several pieces and a hinged precast reinforced concrete arch. As introduced in Chapter 2, there are two main types of precast arch culverts depending on the location of the hinge structure (Figure 4.2). In comparing the arch member arrangement between the two-hinged arch culvert and the three-hinged arch culvert, the three-hinge type is constructed with a staggered disposition, while the two-hinge type is not. Considering the aim of this study, the two-hinged arch culvert was chosen for the centrifuge tests with the simple arrangement of the precast concrete arch members.

The precast arch culverts installed in the embankment were modeled with mortar. Table 4.1 shows the physical properties of the mortar model. The arch culvert model was rigid and did not model the hinge structure of the precast arch culvert. However, in the actual construction method, a coupler (bent bolt) is installed in the hinge structure to prevent the precast members from slipping, as shown in Figure 4.2 (a). Therefore, it is believed that the hinge structure has little influence on the seismic behavior in the culvert longitudinal direction.

The culvert model was prepared under two types of connecting conditions, the connected condition and the separated condition, as shown in Figure 4.3. In the connected condition, the five arch culvert models were connected by an adhesive, used as the concrete material. Then, the intersections of the models were covered with masking tape to protect them. In the separated condition, the intersections of the separated arch culvert models were covered with polypropylene sheets. The role of these polypropylene sheets was not to connect the arch culvert models, but to prevent sand infiltration.
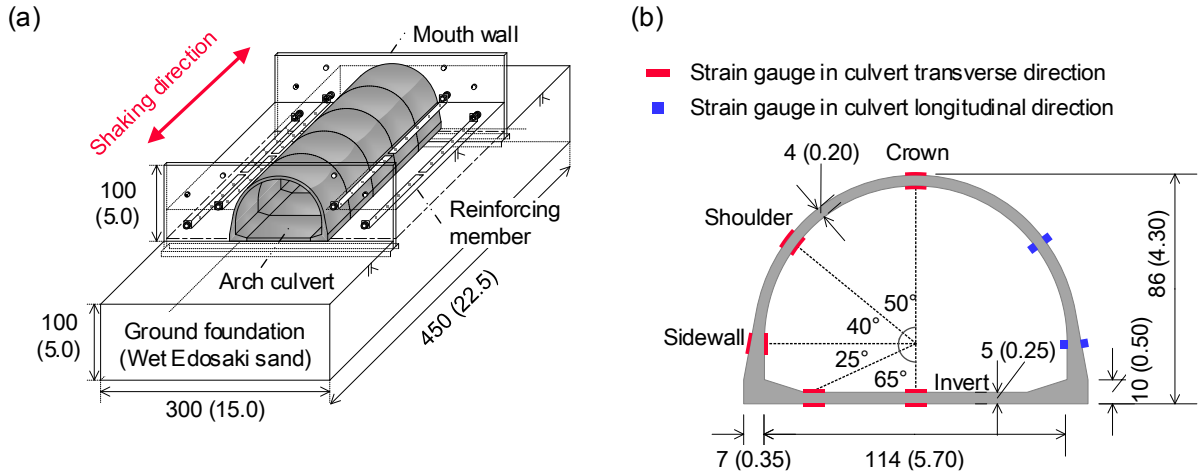
Figure 4.1: Schematic drawings of (a) embankment model with culvert and (b) arch culvert with strain gauges.
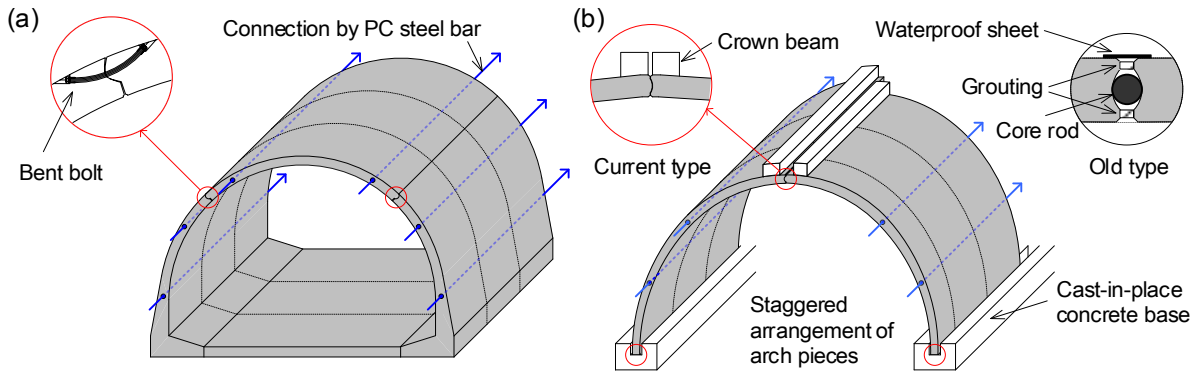
Figure 4.2: Structural connectivity of culvert longitudinal direction in precast arch culvert in (a) two-hinged arch culvert and (b) three-hinged arch culvert (Association of Modularch Construction Method, 2017 and Advanced Construction Technology Center, 2014).

Table 4.1: Properties of mortar culvert model.

Young's modulus	E	[kN/m^2]	2.07×10^7
Unit weight	γ	[kN/m^3]	19.35
Compressive strength	f_c	[kN/m^2]	4.92×10^4
Bending strength	f_b	[kN/m^2]	1.17×10^4
Tensile strength	f_t	[kN/m^2]	5.76×10^3
Poisson's ratio	ν	—	0.18

4.2.2 Mouth wall model

Figure 4.4 shows the structure of the reinforcing earth wall of the culvert model. A reinforcing earth wall (Public Works Research Center, 2014) is generally constructed for the wall face of the embankment of precast arch culverts (Association of Modularch Construction Method, 2017). The wall face used in the centrifuge tests was made by combining an acrylic plate and an aluminum band both sides of which were coated with dry *Edosaki* sand, as shown in Figure 4.4 (b) (Refer to the discussion on the actual density of the reinforcing member in the reinforcing earth wall in 3.2.4.).
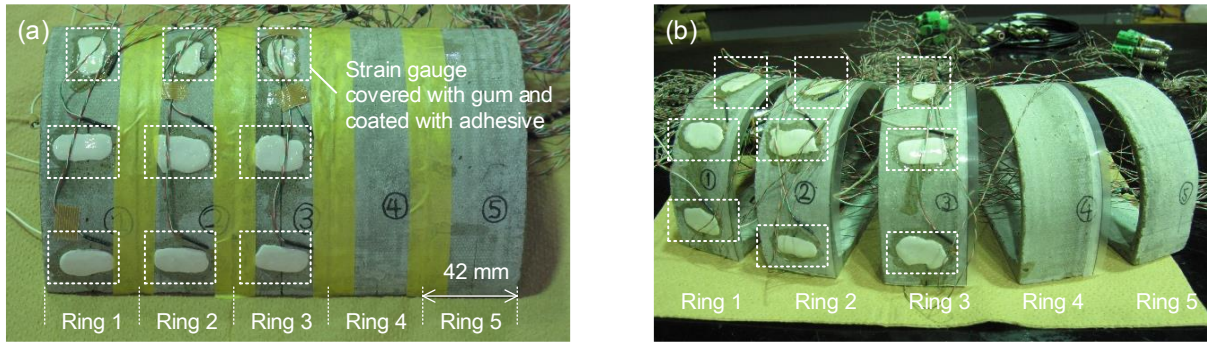
Figure 4.3: Arch culvert model due to two structural conditions: (a) connected condition by adhesive for concrete and (b) separated condition. In the connected condition, the joint of the arch culverts was protected with masking tape. In the separated condition, a polypropylene sheet was used to cover the joint sections of the culverts to prevent soil infiltration.
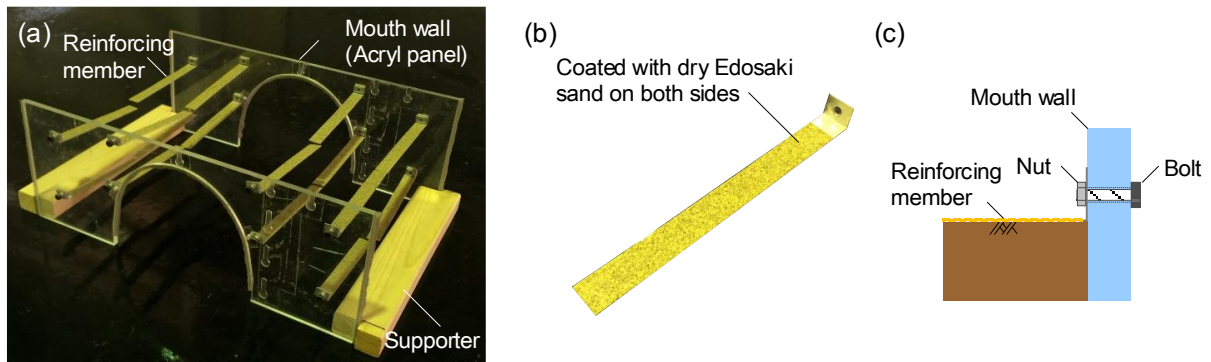
Figure 4.4: Modeling reinforcing earth wall: (a) mouth wall with reinforcing members, (b) reinforcing member, and (c) attachment of reinforcing member with mouth wall.
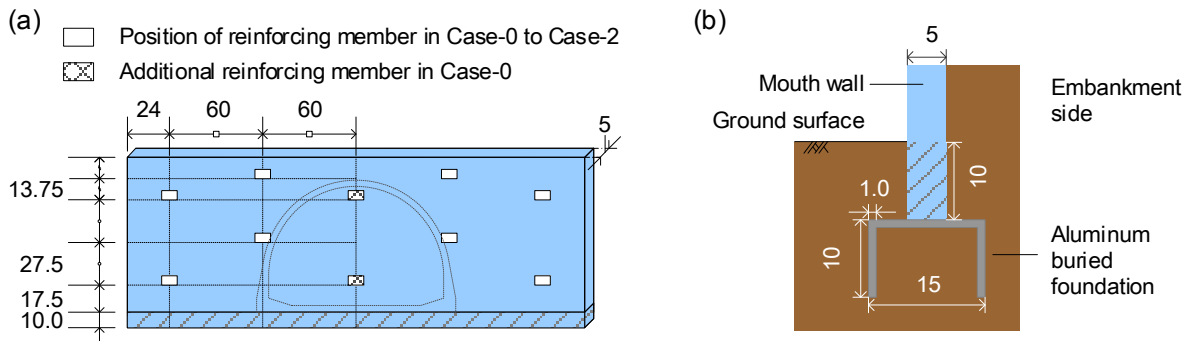
Dimensions in mm, model scale

Figure 4.5: Schematic drawings of (a) arrangement of reinforcing members and (b) embedment section of mouth wall.

Figure 4.5 shows the arrangements of the reinforcing members and the foundation of the mouth wall. The wall structure was embedded to a depth of 10 mm in the foundation ground. Additionally, a foundation made of an aluminum, C-type channel was set for supporting the wall model.

4.2.3 Procedure for making the ground model

Edosaki sand, whose average particle size was adjusted to 0.2 mm for use in the centrifuge tests, is a
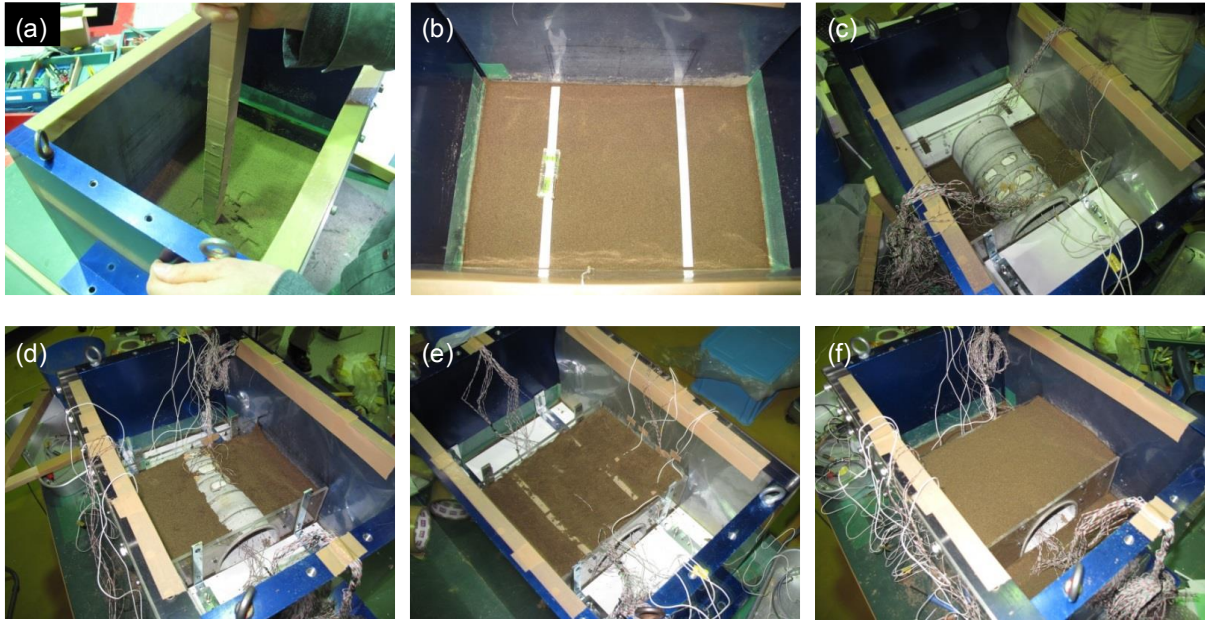
Figure 4.6: Procedure for making embankment model with culvert: (a) compaction of foundation ground with wooden rectangular tamper, (b) setting foundations for wall model, (c) setting culvert model and mouth wall, (d) backfilling around culvert model, (e) attachment of reinforcing members, and (f) completion of embankment model with culvert and mouth wall.

fine, wet sand (Refer to 3.2.3.). The foundation ground and the embankment portion were made by regulating the *Edosaki* sand to Dc = 92% and w = 15.8% (= w_{opt} of *Edosaki* sand). As a rigid chamber was used, a 2-mm-wide gel sheet was set on the side wall of the chamber in the vertical direction against the shaking direction in order to decrease the influence of response waves during the shaking (Refer to the material properties of the gel sheet in 3.2.3.).

Figure 4.6 shows the procedure for constructing the model embankment. Two rectangular wooden tampers were used for the soil compaction. One rectangular tamper, 30×30 mm^2 with 0.25 kg, was used for the foundation ground and the other, 15×15 mm^2 with 0.08 kg, was used for the embankment near the culverts. Thus, the influence of the compaction to the culverts was decreased by using different sizes of rectangular wooden tampers.

4.2.4 Test instrumentation

The experimental cases are shown in Figure 4.7, namely, the embankment model (Case-0), the connected culverts (Case-1), and the separated culverts (Case-2). The wave was input by shaking in steps in order to focus on the transition of the embankment deformation. Figure 4.8 shows the arrangement of the test instrumentation in Case-1 and Case-2. Definitions of the positive direction in the response acceleration and the wall displacement are also shown in the figure. The positive direction of the response acceleration is the right-hand side of the figure, and that of the horizontal wall displacement at the mouth walls is the direction from the backfill to the front of the mouth walls. The measuring items are summarized as follows:
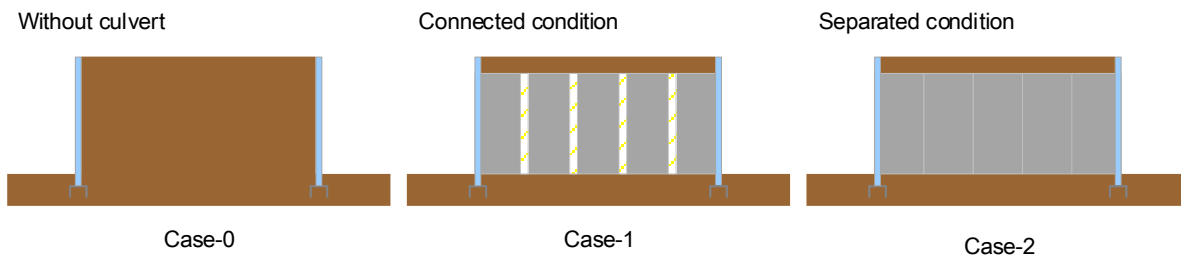
Figure 4.7: Experimental cases: condition of no culvert in Case-0, condition of connected culverts in Case-1, and condition of separated culverts in Case-2.
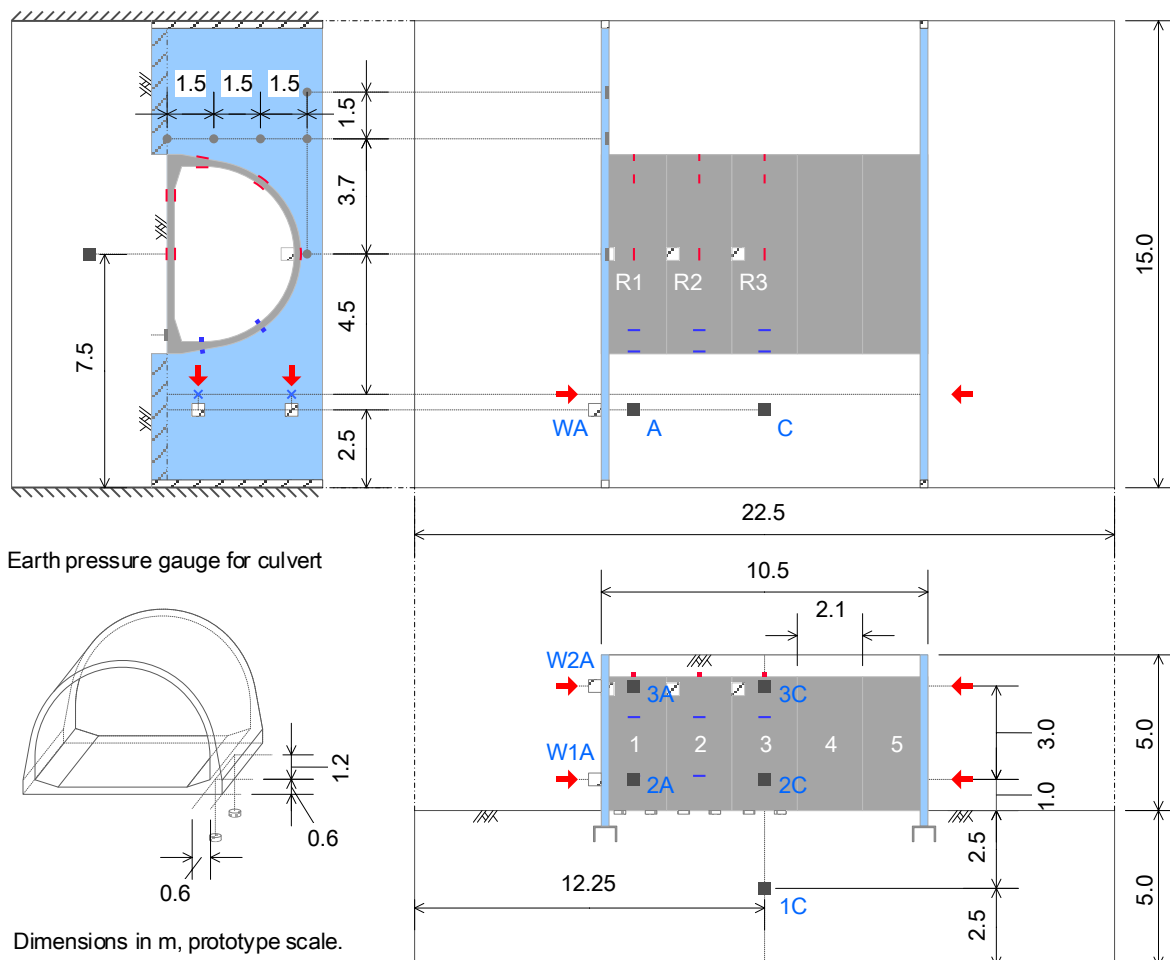
Figure 4.8: Test instrumentation for Case-1 and Case-2. In Case-0, the test instrumentation is the same as that used for Case-1 and Case-2, except for the sections with connected or separated culverts, as there are no culverts in Case-0.
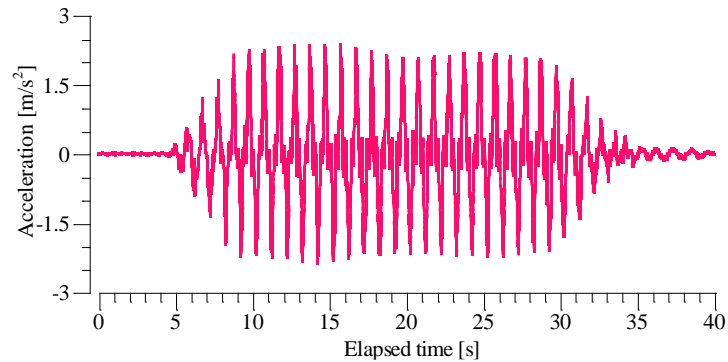
Figure 4.9: Input wave: continuous sin wave with taper at 1 Hz and 30 cycles.

1) Response acceleration of arch culvert, mouth wall, and embankment
2) Horizontal displacement of mouth wall
3) Earth pressure on mouth wall
4) Strain on culvert in culvert longitudinal direction and transverse direction
5) Vertical earth pressure on bottom slab of culvert

Great attention should be paid so that the contact pressure is measured accurately. For example, to decrease the bumping of the pressure gauge, it is a common practice to cut a furrow into the model and to fit the gauge snugly into it to keep the gauge horizontal on the surface of the slab in order to obtain accurate measurements. In this case, however, the thickness of the model, 5 mm, was too thin to enable the cutting of a furrow into the model. That is why, in this study, the pressure gauge was set directly onto the bottom slab of the arch culvert. Additionally, keeping the surface of the foundation ground as horizontal as possible and scraping the surface of the ground slightly allowed the pressure gauge to make uniform contact with the ground.

4.2.5 Input wave

In this experiment, ten steps of excitation were applied to observe the gradual deformation of the embankment. The initial step, STEP 0, was defined as the time it took to reach 50 G of centrifugal acceleration. A continuous wave with 30 cycles of sine waves was applied with a taper of the prototype at 1 Hz. It was input ten times, from STEPS 1 to 10, with an increase of 0.5 m/s^2 per step to observe the gradual deformation of the embankment. Figure 4.9 shows the input wave of the shaking table at STEP 5 in which the maximum target acceleration is 2.5 m/s^2. The wave was input by controlling the displacement of the shaking table. The frequency of the input wave, 1 Hz, was determined based on the earthquake data taken at Takatori Station of the West Japan Railway Co. due to the Kobe Earthquake (1995). The predominant period of the earthquake was about 0.9 seconds (Japan Road Association, 2012).

4.3 Results and discussions

The test results were discussed by considering the residual deformation of the embankment by the
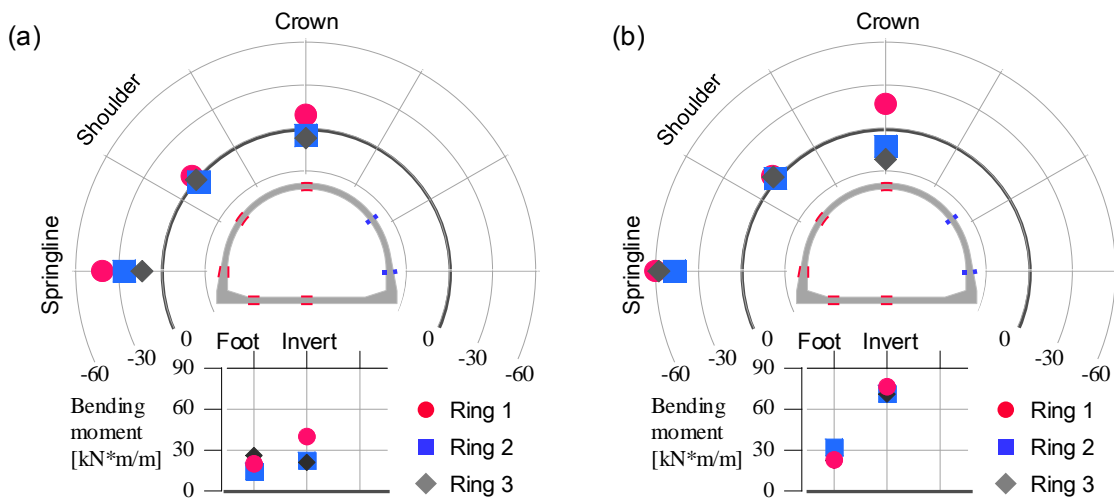
Figure 4.10: Initial condition of bending moment acting on arch culverts in (a) Case-1 and (b) Case-2.

repeated excitations. This is because an attempt is made to investigate the accumulation of the stress state on the culverts and the embankment deformation throughout all the excitation steps. The values of the results were converted to the prototype scale.

4.3.1 Initial condition of stress state

The initial state of the bending moment working on the arch culverts before the excitations is shown in Figure 4.10. In Case-1, the bending moment working on the bottom slab yields higher values in order of Rings 1, 2, and 3 from the mouth of the culverts to the center of the embankment. In Case-2, on the other hand, with the separated culverts, no clear difference in the bending moment for Rings 1-3 working on the bottom slab can be observed. In comparing Case-1 and Case-2, the bending moment working on each measurement portion of the arch culverts beomes higher in Case-2 than in Case-1.

In order to discuss the reason why the stress state of the arch culverts changes due to the connecting condition, the distribution of vertical earth pressure working on the bottom slab of the arch culverts is shown in Figure 4.11. The vertical earth pressure is measured at the feet of the arch culverts, as shown in Figure 4.8.

In Case-1, the vertical earth pressure is different for each measurement position. Considering the bending moment of the arch culverts, however, the bending force increases at both ends of the five arch culverts. In short, the connected arch culverts seem to deform into arched shapes and to support the vertical load.

In Case-2, on the other hand, the vertical earth pressure is almost homogeneous for each measurement position. In addition, a satisfactory correlation is found between the bending moment and the vertical earth pressure in Case-2, and there is little difference in the values for each arch culvert. This is because each arch culvert of the separated culverts supports the vertical pressure itself.

4.3.2 Deformation after excitation

From the above discussions, the initial stress state of the culverts due to the centrifugal load was seen to
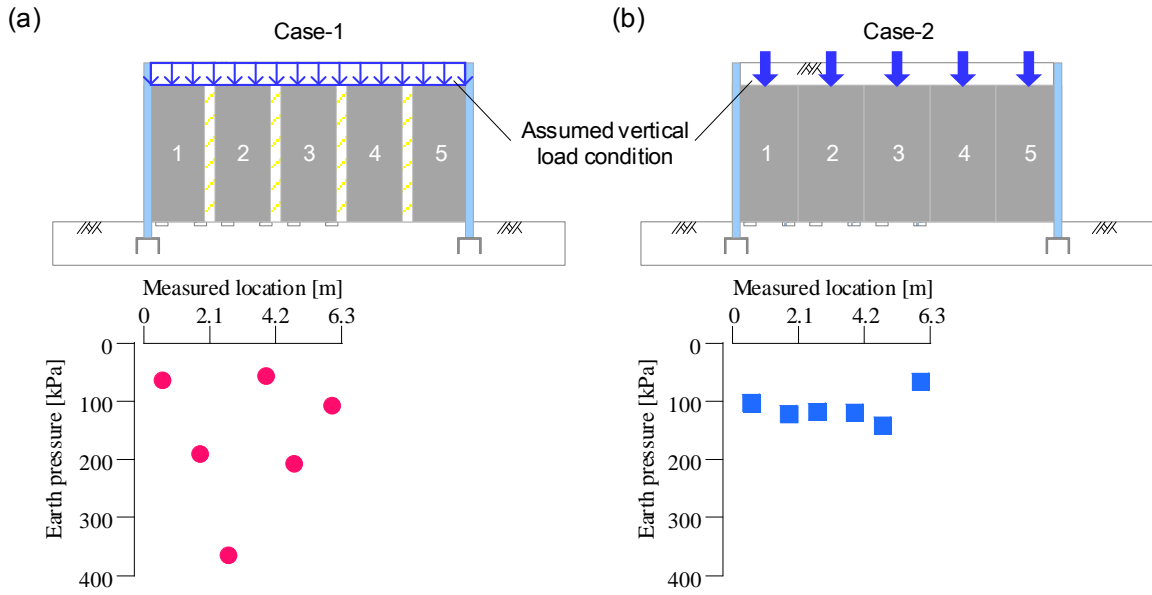
Figure 4.11: Initial vertical stress measured on bottom slab of Rings 1-3 in (a) Case-1 and (b) Case-2.
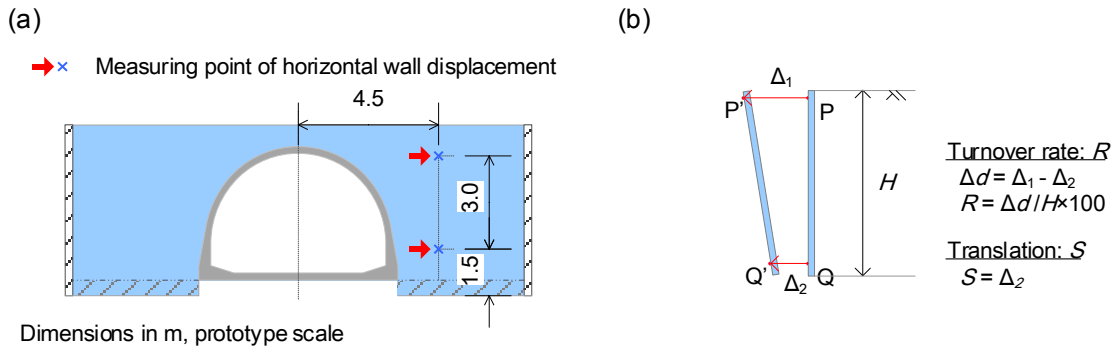
Figure 4.12: Definition of turnover rate (R) and translation (S): (a) measuring location of wall displacement and (b) calculation method of turnover rate and translation.

be dependent on the longitudinal structural connectivity of the culvert models. The difference in the structural connectivity also appeared as a unique embankment deformation. Here, two physical indexes are defined to understand the characteristics of embankment deformation, namely, the turnover rate and the translation, as shown in Figure 4.12. The turnover rate is the value of the difference ($\Delta_d = \Delta_l - \Delta_2$) between the lateral displacements of the upper portion (Δ_l) and the lower portion (Δ_2) divided by the wall height (H). The translation is equal to Δ_2. The transition of the lateral displacement of the mouth wall is based on the relation between the turnover rate and the translation, and is described in Figure 4.13.

From the figure, the order of the deformation amount was Case-0 > Case-2 > Case-1. In Case-2, the embankment deformation due to the culvert longitudinal earthquake becomes more amplified than Case-1. Moreover, the deformation mode of the embankment approaches that of Case-0. This is because, as for the longitudinal shear stiffness of culverts, separated culverts are weaker than connected culverts, which causes the larger deformation of the embankment in Case-2.
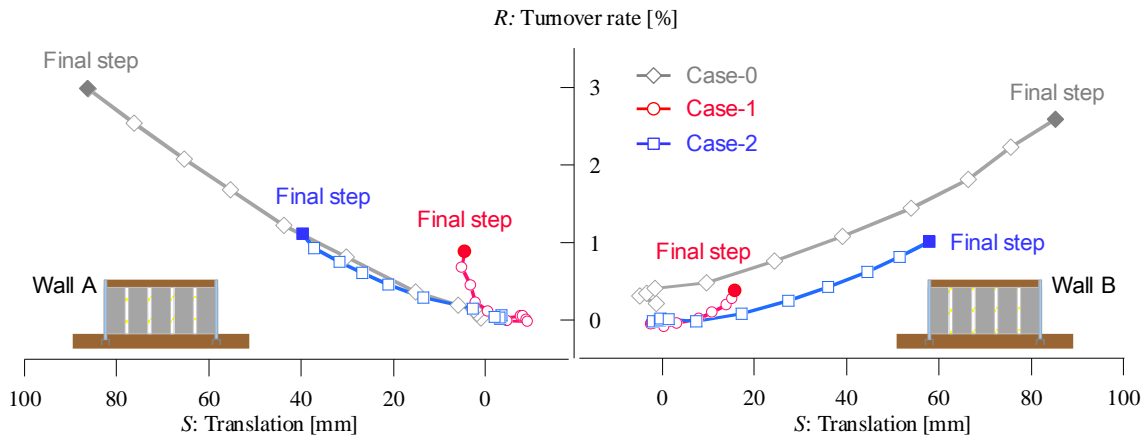
Figure 4.13: Displacement mode of mouth walls in all excitation steps.
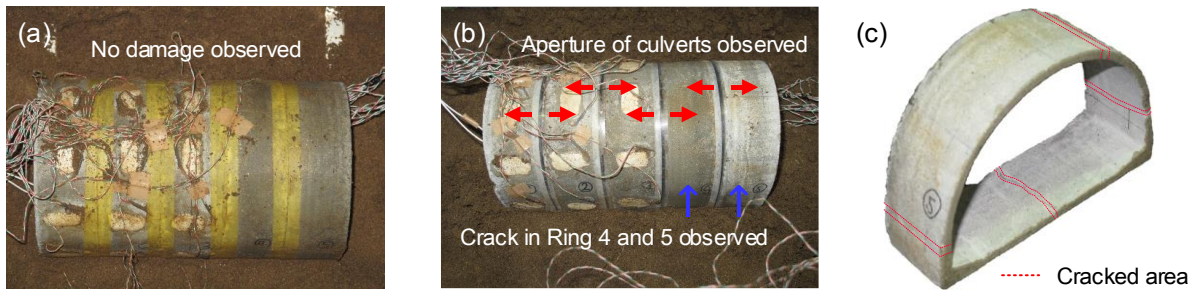
Figure 4.14: Arch culvert models after excitation in (a) Case-1 and (b) Case-2. (c) Ring 5 in Case-2 is chosen to show the cracked area.

When focusing on the culvert model after excitation, shown in Figure 4.14, the difference in the amount of embankment deformation seems to be correlated with the damage to the culvert models. In Case-1, no significant damage to the culverts themselves is observed. In Case-2, on the other hand, the culverts near the mouth inclined toward the outside, and apertures were observed in the culverts. In addition, Ring 4 and Ring 5, without strain gauges, had cracks at the feet and the shoulder, as shown in Figure 4.14 (c). The reason why Rings 1, 2, and 3 in Case-2 had no damage, even after repeated excitations, is that the coating material used to attach the strain gauges may have increased the stiffness of the three rings. Although there is a relation between the damage to the separated culverts and the magnitude of embankment deformation, the reason why the cracks occurred in Rings 4 and 5 in Case-2 will be discussed later based on the internal force of the arch culverts.

4.3.3 Response accelerations of culvert model

In this section, the response accelerations of the culvert model are discussed to figure out the different embankment deformations due to the longitudinal structural connection of the culverts. Figure 4.15 shows the response accelerations of Ring 1 (culvert) named R1, Wall A (mouth wall model) named W2A, and the upper portion inside of the embankment named 3A; details on their arrangement are shown in Figure 4.8. The hysteresis curves are described with the respective response accelerations and the input wave given by the recorded acceleration via 1C of the ground foundation. The curves were
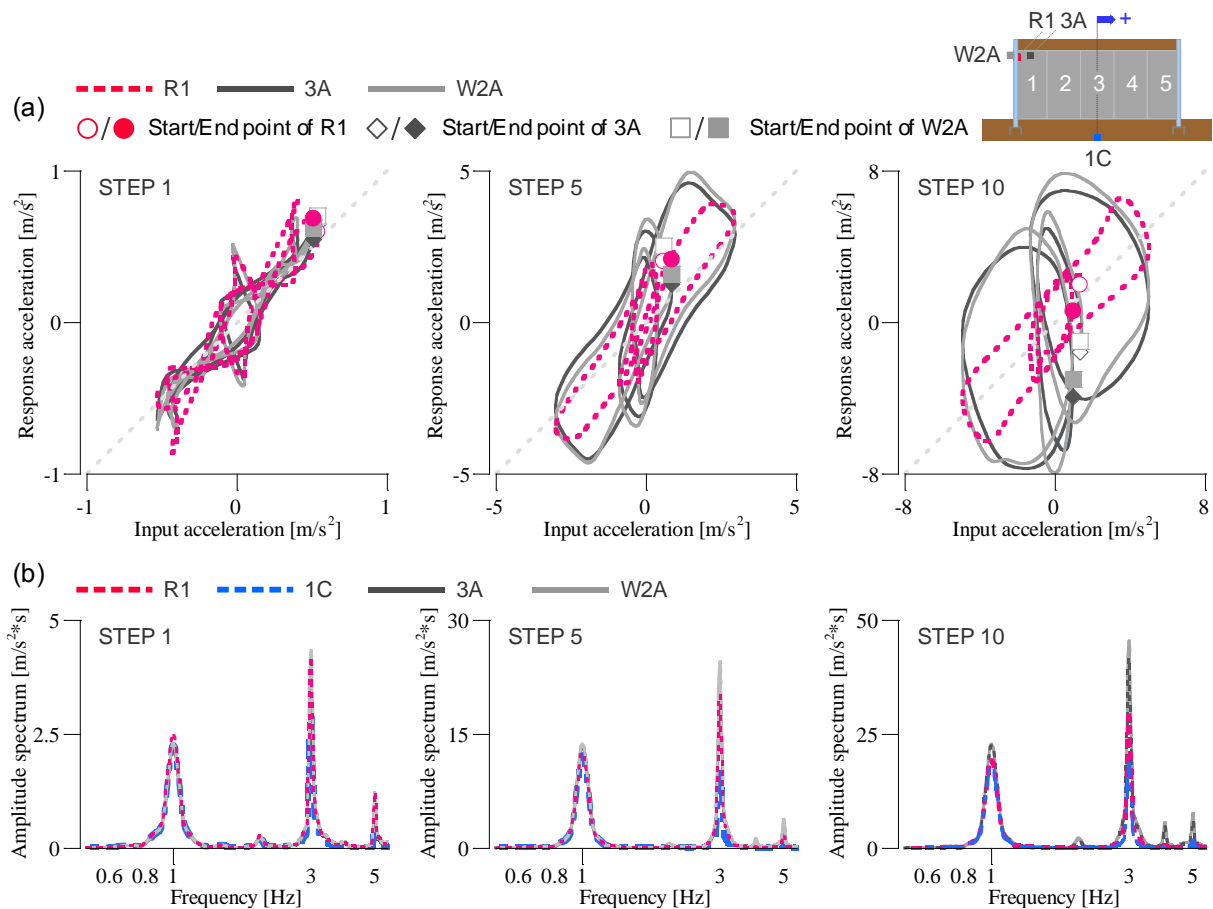
Figure 4.15: Response acceleration of R1, 3A, and W2A in Case-1: (a) hysteresis curves of response acceleration and (b) Fourier Amplitude Spectrums in STEPs 1, 5, and 10.

described from $t = 20.00 \sim 20.98$ s in each excitation step. To calculate the Fourier spectrum, Fast Fourier Transform was used with 8192 data samples and a sampling interval of 0.005 s.

From the figures, focusing on the hysteresis curves, R1 showed a linear response with the input wave of 1C; however, Wall A and A3 showed amplified behavior. From the Fourier spectrums, the frequency domains of R1, 1C, 3A, and W2A showed 1 Hz as a primary vibration mode and 3 Hz as a secondary vibration mode of the vibration in the culvert longitudinal direction. Focusing on the Fourier spectrum of 3 Hz, the magnitude of the Fourier spectrum at 3 Hz is clearly amplified in 3A and W2A compared to R1.

The results of Case-2 are shown in Figure 4.16. It is seen that, in Case-2, the nonlinear amplified behavior of R1, 3A, and W2A with the increase in excitation steps is clearly different from that in Case-1. In addition, R1 showed a larger hysteresis curve than either 3A or W2A. From the Fourier spectrums, as in Case-1, the frequency domains of R1, 1C, 3A, and W2A showed 1 Hz as a primary vibration mode and 3 Hz as a secondary vibration mode of the vibration in the culvert longitudinal direction. On the other hand, the magnitude of the Fourier spectrum at 3 Hz is clearly larger in R1 than in either 3A or W2A.

The amplification factors of 1 Hz and 3 Hz in Case-1 and Case-2 are summarized in Figure 4.17.
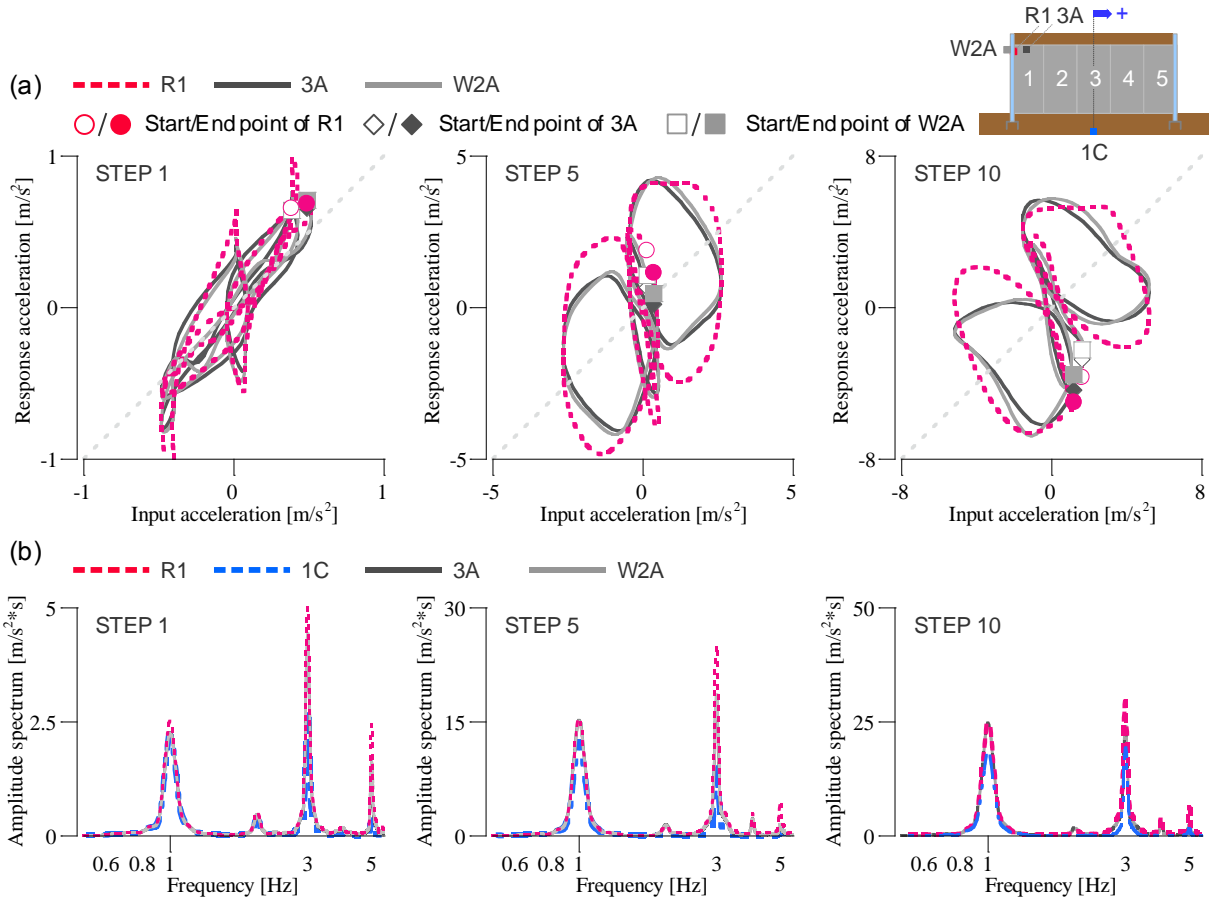
Figure 4.16: Response acceleration of R1, 3A, and W2A in Case-2: (a) hysteresis curves of response acceleration and (b) Fourier Amplitude Spectrums in STEPs 1, 5, and 10.
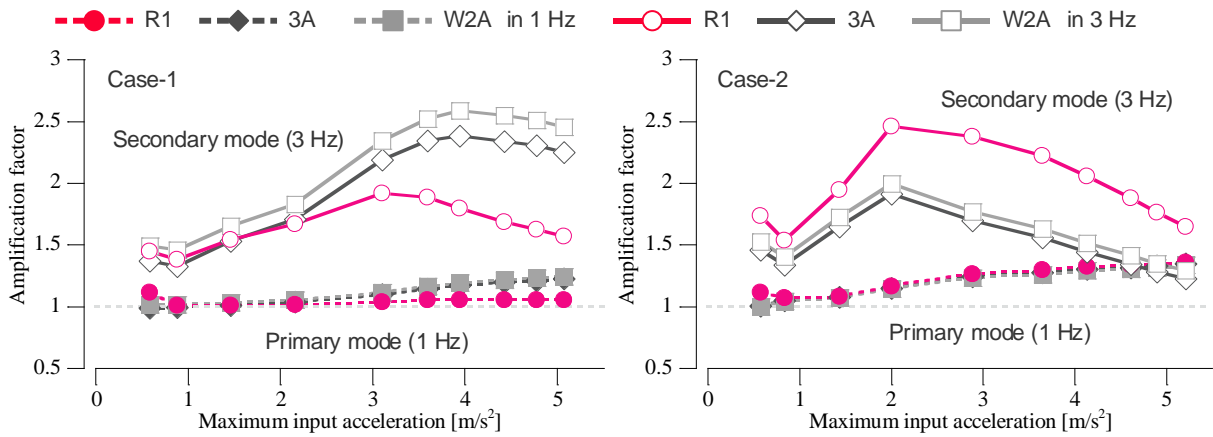
Figure 4.17: Comparison of vibration modes in Case-1 and Case-2. 1 Hz is the primary mode of vibration in the culvert longitudinal direction and 3 Hz is the secondary mode.

The amplification factors are given by dividing a certain Fourier amplitude spectrum by that of 1C. From the figures, the magnitude correlation of R1, 3A, and W2A is as follows: W2A > 3A > R1 in Case-1 after STEP 3 and R1 > W2A > 3A in Case-2 over all the excitation steps. In short, the longitudinal vibration of the culvert in Case-1 was smaller than that of the mouth wall and the embankment, while the opposite tendency appeared in Case-2.

In Case-1, with the increase in excitation steps, the stiffness of the embankment continued to decrease due to its deformation. However, the stiffness of the connected culverts remained constant; there was no damage observed in the culvert model (Refer to Figure 4.14 (a).). Therefore, the reduction in stiffness of the embankment led to the amplified vibration of the embankment and the mouth wall compared to the connected culverts.

In Case-2, on the other hand, the separated culverts seem to easily follow the embankment deformation. The shear stiffness in the culvert longitudinal direction is relatively lower than that in the surrounding ground due to the connecting condition. As a result, the culvert itself shows larger vibration than the embankment. Moreover, the vibration of the separated culverts induced the internal deformation of the embankment, which induced a faster reduction in the stiffness of the embankment compared to Case-1. Therefore, as shown in Figure 4.16 (a), in STEP 10, the shape of the hysteresis curves for R1, 3A, and W2A seem to almost match each other. This is because the relative stiffness of the culvert and the embankment with the mouth continued to decrease with the repeated excitation.

Accordingly, Case-2 showed larger embankment deformation than Case-1 because the vibration of the separated culverts caused the internal deformation of the surrounding ground. The longitudinal structural connection of the culverts is an important countermeasure in that it decreases the harmful influence of the culverts' vibration on the embankment and prevents the longitudinal deformation of the embankment.

4.3.4 Seismic behavior during excitation

To understand the seismic behavior of the culverts due to the structural connection, focus is placed on the time history of the vertical earth pressure from $t = 20.00 \sim 21.25$ s at STEP 5 (maximum input acceleration of 2.5 m/s^2). The time history of the vertical earth pressure and the response acceleration in Case-1 and Case-2 are shown in Figure 4.18. The gray zone in Figure 4.18 means the time domain when the value at the bottom anterior of the vertical earth pressure (close to Wall A) is increasing. In this time domain, Ring 1 is inclining toward Wall A.

Focusing on the gray zone in Case-1, the values for both earth pressure gauges are increasing in this phase. In addition, the amplitude of the earth pressure at Ring 3 is decreasing compared with Ring 1. This indicates that, in Case-1, the connected culverts seem to incline forward and backward in the united body of the five culverts.

On the other hand, from the time history of the vertical pressure in Case-2, the earth pressure working on the bottom slab at Ring 1 and Ring 3 changes to the opposite phase. While Ring 1 is inclining toward Wall A, the earth pressure working on the anterior portion of the bottom slab is increasing and that on the posterior portion is decreasing. Moreover, the amplitude of the earth pressure at Ring 1 and Ring 3 is almost at the same level.

From the above results, the deformation behavior in Case-1 and Case-2 is schematically described in Figure 4.19. Connecting the culverts, like in Case-1, makes all the culverts behave integrally, and the vertical earth pressure from the foundation ground works on the whole bottom slab of the culverts.
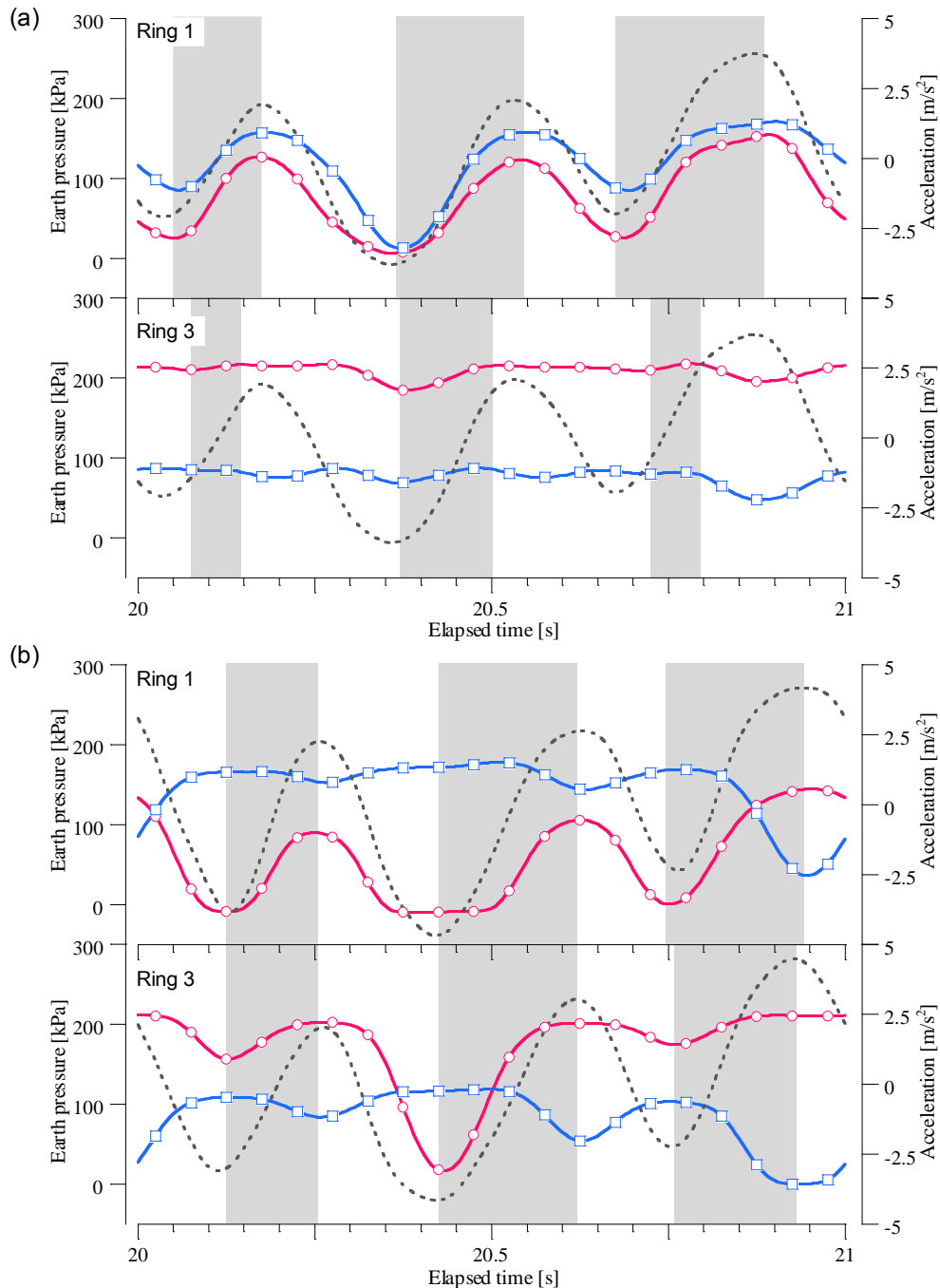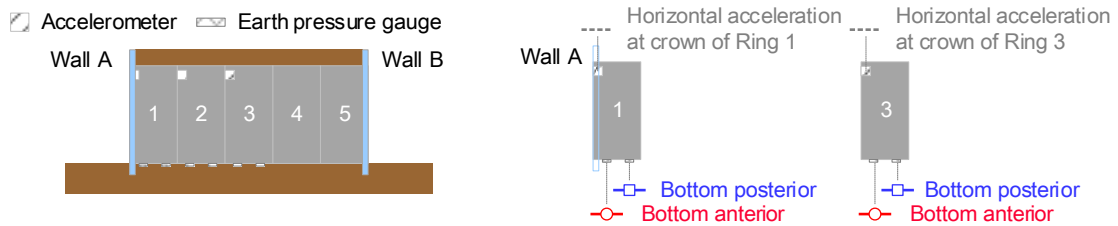
Figure 4.18: Time history of vertical pressure acting on bottom slab and response acceleration at arch crown of culverts in (a) Case-1 and (b) Case-2 at STEP 5 (maximum input acceleration is 2.5 m/s^2).
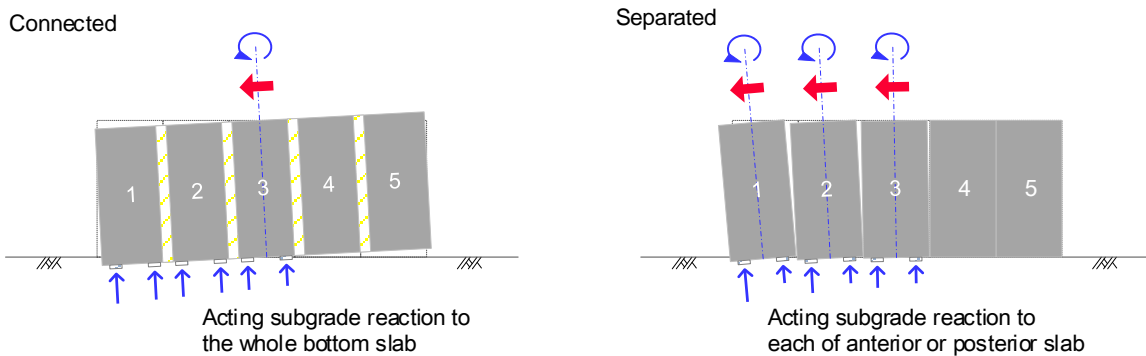
Figure 4.19: Schematic drawings of longitudinal seismic behavior in connected culverts and separated culverts.

Separating the culverts, like in Case-2, makes each culvert behave independently, and the vertical earth pressure from the foundation ground is concentrated on the anterior or the posterior portion of the bottom slab.

4.3.5 Internal forces of arch culvert model

To clarify the mechanism of the damage to the arch culvert model shown in Figure 4.14 (c), the ratio of the maximum bending moment to the bending crack moment, named 'M_{max}/M_{cr}', was calculated in the final excitation step, STEP 10. The results are shown in Figure 4.20. As was shown in Figure 4.14 (b), no cracks were observed in Rings 1 to 3 in Case-2. Accordingly, the final state of the internal forces of the culverts can be the key to clarifying the failure mechanism of Rings 4 and 5.

From the figures, it can be seen that, in Case-1 and Case-2, M_{max}/M_{cr} was commonly larger in the side wall and the invert of the arch culvert model. As one of the clear differences, the dispersion of M_{max}/M_{cr} at the side wall and the invert due to the location of the arch culvert was smaller in Case-2 than in Case-1, which seems to be related to the stress condition of the arch culvert by the structural connectivity, as described in Figure 4.19. This indicates that, in Case-2, bending cracks at the invert or the sidewall are likely to occur despite the position of the arch culvert. Moreover, a crack will firstly occur at the invert and then appear on the inward surface of the invert due to the inward bending moment acting on the invert.

The crack mechanism of the arch culvert models in Case-2 is assumed based on the overall experimental results, as follows. Separating the culverts caused the rigid rotation of each arch culvert due to the embankment deformation, which caused a large reaction force from the foundation ground on the invert of the arch culvert model with the amplified embankment deformation. That is why the inward bending moment on the invert of the arch culvert firstly reached the bending crack moment and then the crack appeared on the surface of the inside of the arch culvert. Accordingly, there is a kind of chain reaction, and cracks supposedly occur one after another on the sidewall and the arch crown continuously in deccending order with the magnitude of M_{max}/M_{cr}.

4.4 Conclusions

In this chapter, two-hinged arch culverts, installed in an embankment, were modeled. The seismic
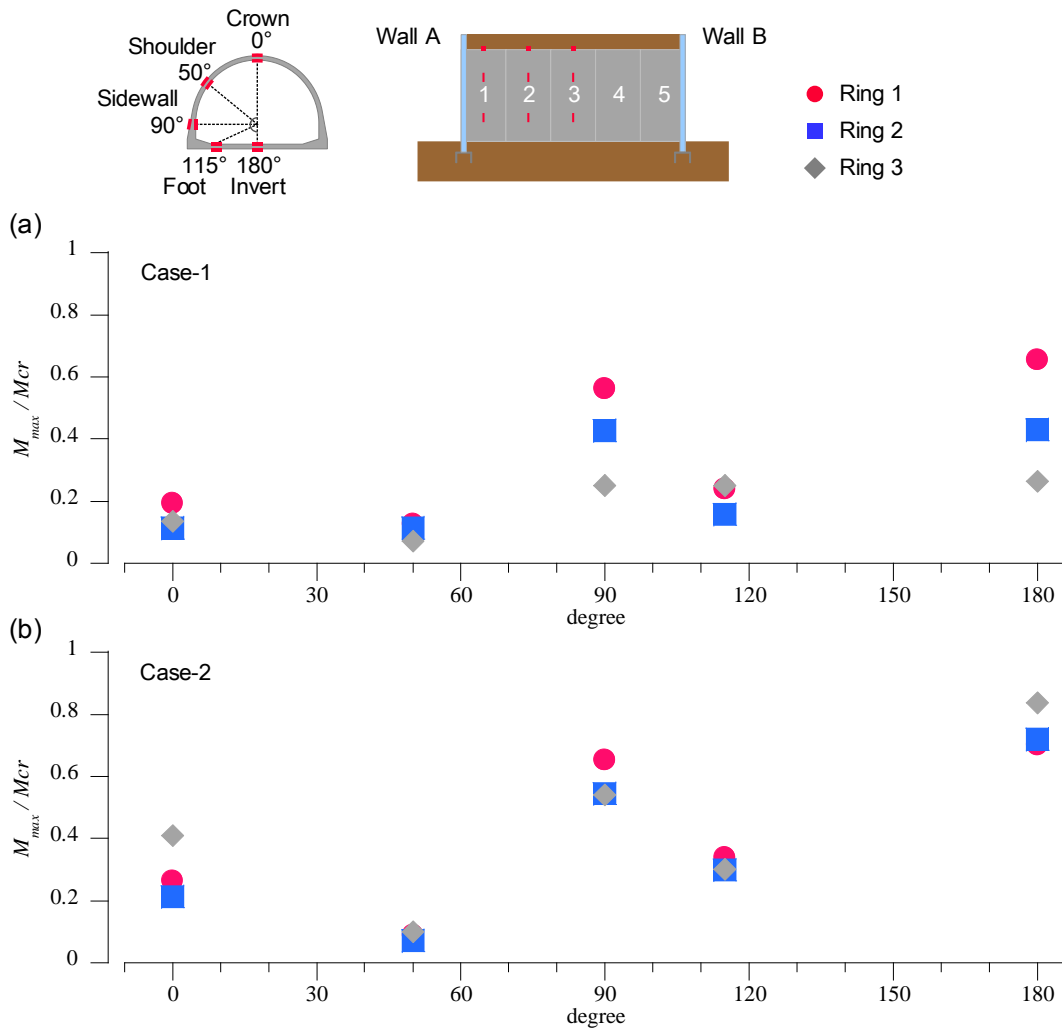
Figure 4.20: Ratio of M_{cr} and M_{max} at each measured portion of Rings 1-3 in (a) Case-1 and (b) Case-2. M_{cr} is defined as the bending crack moment and M_{max} is the maximum bending moment during excitation of STEP 10 (maximum input acceleration is 5.0 m/s^2)

behavior of the culverts was investigated with an earthquake wave of 1 Hz. The following conclusions can be drawn from the results.

1) The initial condition of the bending moment working on the bottom slab of the arch culverts and the supporting mechanism of the upper load were found to depend on the connecting condition. Connected culverts caused an enlargement of the bending moment working on the bottom slab at both ends of the culverts. Separated culverts maintained the homogenous bending moment and the vertical earth pressure working on the bottom slab of each culvert.

2) Separating the culverts allowed each culvert to behave independently in the embankment. In addition, when buried culverts were carefully observed, apertures and cracks were found in them. The large reacting force from the ground foundation may have induced bending cracks on the invert of the arch culvert model, which also caused bending cracks of the sidewall and the arch crown. This unrestrained behavior resulted in apertures at the interconnecting sections of the culverts and a decrease in the longitudinal shear stiffness of the culverts with the

amplified embankment deformation.

3) Connecting the culverts was seen to cause all the culverts to behave integrally during an earthquake. Under this experimental condition, connecting the culverts was advantageous in the seismic resistant design from the viewpoints of preventing apertures from occurring in the culverts during excitations in the culvert longitudinal direction and reducing the embankment deformation and the internal forces of the arch culverts.

References

Association of Modularch Construction Method (2017): *Engineering Manual for Modularch*, *Geo-Research Institute* (in Japanese).

Investigative Committee of Manual for the Design and Construction of Techspan Construction Method (1998): *Manual for the Design and Construction of Techspan Construction Method (Draft)*, *Advanced Construction Technology Center* (in Japanese).

Japan Road Association (2012): *Specifications for Highway Bridges Vol. V: Seismic Design* (in Japanese).

Public Works Research Center (2014): *Manual for the Design and Construction of Reinforced Earth Wall, 4th Revised Edition* (in Japanese).

Technological Examination Committee of Techspan Construction Method (2014): *Comparison Outline of Revised Items in Manual for the Design and Construction of Techspan Construction Method (Draft)*, *Advanced Construction Technology Center* (in Japanese).

Chapter 5 Dynamic centrifuge tests on patterns of embankment shape

5.1 Introduction

In the Great East Japan Earthquake (11 March 2011), particularly in the old-type three-hinged arch culverts, severe damage occurred, such as deformation of the mouth wall, numerous cracks in the arch members, and patterned chipping of the foundation. These damaged culverts had one point in common, namely, they had either shallow soil cover or an asymmetrical embankment load in the culvert longitudinal direction due to the embankment slope and no longitudinal connection of the culverts far from the mouth of the culvert. Therefore, the aim of this chapter is to clarify the influence of embankment shape patterns on the seismic behavior in the culvert longitudinal direction. Dynamic centrifuge tests on three-hinged arch culvert models were carried out for various embankment geometries.

5.2 Experimental setup

Centrifuge shaking table tests were conducted under a gravitational acceleration of 50 G using the geotechnical centrifuge device at Kyoto University's Disaster Prevention Research Institute (DPRI). A soil chamber, 340 mm (H) ×450 mm (W) × 300 mm (D), was employed. Figure 5.1 shows schematic drawings of the three-hinged arch culvert and the model embankment including the arch culvert. Three-hinged arch culverts were modeled with a length of 28.8 m with a reinforced earth wall and constructed on a 5-m-deep layer of soil. In the experiment, the mouth portion of the culverts was modeled with a half-length section, 14.4 m in length, due to the limited dimensions of the soil chamber.

5.2.1 Precast arch culvert model

Figure 5.2 shows schematic drawings of the prototype and the model of the three-hinged arch culvert. The arch culvert model was designed based on the current type (Figure 5.2 (a)), which has an invert foundation. As was shown in the Figure 2.3, the hinge structure has a core rod in the old type and a knuckle shape in the current type. In both types of three-hinged arch culverts, grouting is conducted at the hinge of the arch crown. Additionally, in the current type, a concrete beam, called a "crown beam", is attached to the crown of the arch members to longitudinally connect all the arch members. To focus on the seismic effect of the embankment shape, the current type of three-hinged arch culvert was modeled with a simpler structural connection of the arch members. The arch model member was made of aluminum and its thickness was adjusted to match the bending stiffness of a real RC member. The material properties of the model and the prototype are given in Table 5.1.

Each arch member was arranged in a staggered distribution as in the actual construction method with a combination of half-depth of the arch members and full-depth of the arch members. As for the hinges, the crown hinge was formed in a simply butted condition and the foot hinges were tightly tucked with L-shaped angles and sponges. A rubber sheet was used under the arch feet to prevent slipping. In the actual construction, slight volumetric changes in the rubber sheet are expected to function as hinges of the arch feet. To model the overall, longitudinal connection by the crown beam, masking tape was attached to the crown of the arch model members (Figure 5.2(a)). The joints of each arch culvert were
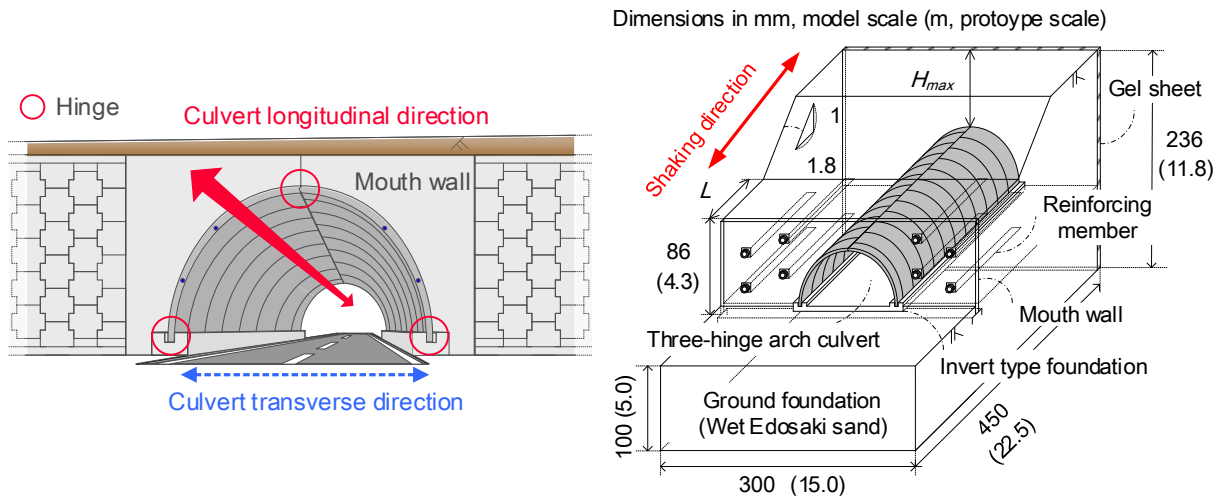
Figure 5.1: Schematic drawings of (a) three-hinged arch culvert installed in embankment and (b) experimental model.
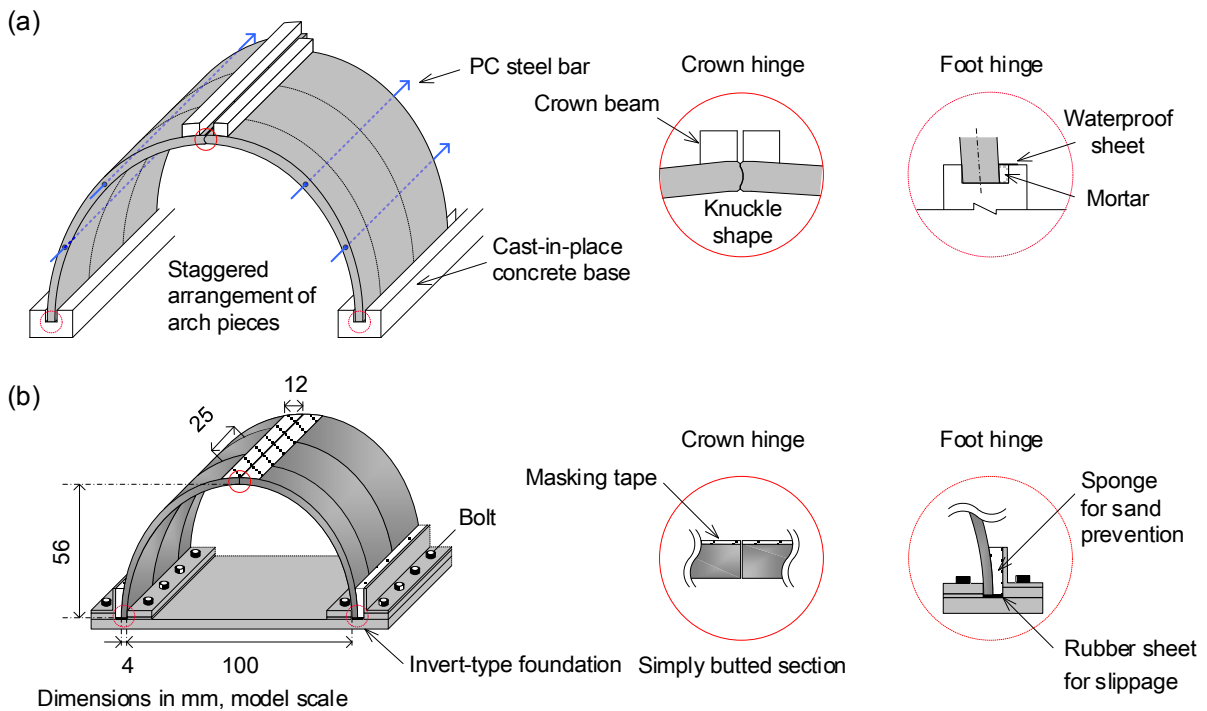
Figure 5.2: Schematic drawings of (a) prototype and (b) model of three-hinged arch culverts.

Table 5.1 : Material properties of real structure and model in prototype scale.

Properties		Unit	Prototype (RC)	Model (Aluminum)
Specific gravity	-	-	2.40	2.70
Young's modulus	E	[kN/m^2]	2.95×10^7	7.06×10^7
Depth	a	[mm]	1250	1250
Thickness	b	[mm]	250	200
Flexural rigidity	EI	[kN・m^2]	4.80×10^4	5.88×10^4
Shaft rigidity	EA	[kN]	9.22×10^6	1.77×10^7

covered with polypropylene sheets to prevent the intrusion of sand.
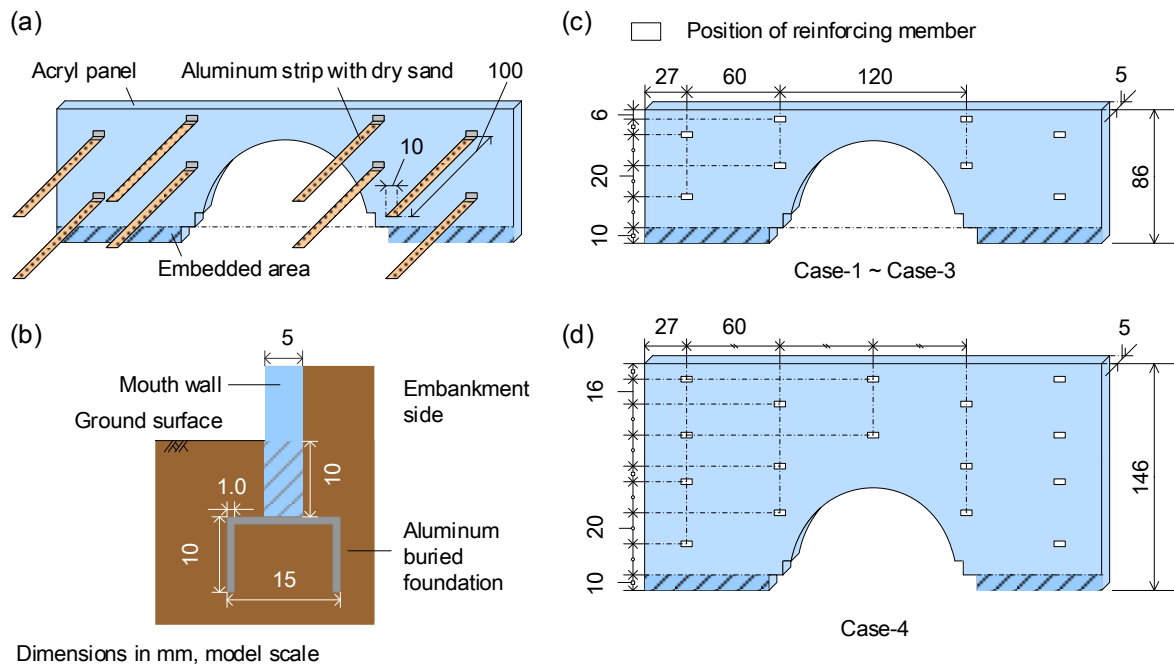
Figure 5.3: Schematic drawings of (a) mouth wall model based on reinforced earth wall, (b) embedment of mouth wall, and (c) arrangements of reinforcing members in Cases 1-3, and (d) in Case-4.

5.2.2 Modeling mouth wall of culvert

Generally, mouth walls of three-hinged arch culverts are constructed as perpendicular reinforced soil walls. The wall structure is different near the mouth versus the rest of the reinforced soil wall, as shown in Figure 5.1 (a). The wall near the culvert mouth is composed of two large concrete panels, which are joined by grouting. The other part of the wall is constructed as a typical reinforced earth wall. The wall in this experiment represents only the integrated wall near the culvert. Figure 5.3 shows the modeling of the mouth wall. A 5-mm-thick acrylic panel was used for the wall model. Aluminum plates, 0.1 mm in thickness and 10 mm in width, were employed for the reinforcing members. The foundation of the wall model was made of an aluminum angular plate with a thickness of 1 mm and a depth of embedment of 0.5 m in the prototype scale. The length of the reinforcing members was designed based on the reinforced earth wall, 4.3 m in height, and does not consider the influence of the culvert structure. Fs, the safety factor of earthquakes, was set to be more than 1.2. Hence, the length of the reinforcing members was unified to be 5.0 m in the all cases.

5.2.3 Experimental cases

To set the shape of the embankment as a parameter in the experiment, the minimum and maximum overburdens and the gradient of the embankment slope need to be determined. In the Manual for the Design and Construction of Techspan Construction Method (1998), the minimum overburden considering the traffic load is regulated to 1.0 m, which is a reference of 1.0 m in the prototype scale in this centrifuge test. As for the maximum overburden, 4.0 m in prototype scale was chosen under the limitation of the dimensions of the soil chamber. The gradient of the embankment slope was chosen based on the Japan Road Association (2010). The standards for slope gradients are shown in Table 5.2.

Table 5.2: Standards of slope gradient in road embankments (Japan Road Association, 2010).

Embankment material	Height [m]	Gradient	Remarks
Well-graded sand (S),	Less than 5.0 m	1:1.5 ~ 1:1.8	The left-hand side condition is applied to the
Gravel or graved with fines (G)	5.0 – 15.0 m	1:1.8 ~ 1:2.0	embankment which satisfies the compaction
Poorly-grades sand (SG)	Less than 10.0 m	1:1.8 ~ 1:2.0	standard shown in Chapter 5 of the Japanese Road
Rock lump	Less than 10.0 m	1:1.5 ~ 1:1.8	Embankment Guideline with the foundation ground
(including debris)	10 – 20 m	1:1.8 ~ 1:2.0	which has enough bearing capacity to support the
Sandy soil (SF), hard lean clay and hard clay	Less than 5.0 m	1:1.5 ~ 1:1.8	embankment without water-logging. () means the
(hard clay and day accumulated in diluvium,			general classification as a representative name. The
Kanto roam and so on)	5.0 – 10.0 m	1:1.8 ~ 1:2.0	embankment without the standard gradient requires
Volcanic cohesive soil (V)	Less than 5.0 m	1:1.8 ~ 1:2.0	a stability analysis.
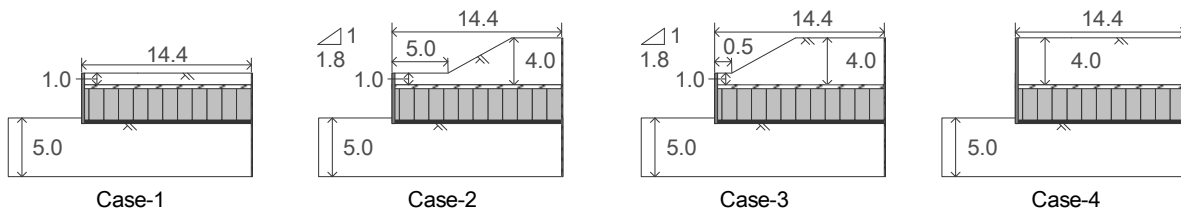
Dimensions in m, prototype scale

Figure 5.4: Experimental cases due to patterns of embankment shapes.

According to the design criteria, a gradient from 1:15 to 1:18 is selected for the embankment height of 0.0 ~ 0.5 m and well-graded sand is used for compaction. In this experiment, the gradient was 1:1.8.

From the above minimum and maximum overburdens and the gradient of the embankment slope, four types of experimental cases were set. Figure 5.4 shows the experimental cases: Case-1 is an embankment with an overburden of 1.0 m in prototype scale; Case-2 is an uneven embankment with overburdens of 1.0 m and 4.0 m with a slope transition distanced 5.0 from the mouth wall of the culvert; Case-3 is an uneven embankment with overburdens of 1.0 and 4.0 with a slope transition distanced 0.5 from the mouth wall of the culvert; and Case-4 is an embankment with an overburden of 4.0 m in prototype scale.

5.2.4 Procedure for making ground model

Hinge types of arch culverts must be built to specific standards and applicable to both embankment and foundation soils (Technological Examination Committee of Techspan Construction Method, 2014). Therefore, the ground model here was made by compacting wet *Edosaki* sand to D_c = 92% and w = 17.6% (= w_{opt} of *Edosaki* sand). Figure 5.5 shows the procedure for making the embankment model, while Figure 5.6 shows the completion of the embankment model in each experimental case. The present experiment models the half-section of the embankment in a rigid chamber, which restrains the displacement at the boundary between the side wall of the chamber and the embankment. Additionally, the reflected wave will largely influence the embankment model of the half-section. That is why different behavior will appear compared to the actual embankment shape. Therefore, based on the experiments for the gel sheet described in Chapter 3, a gel sheet, with a thickness of 2 mm and compressive stiffness of 0.07 N/mm^2, was set onto the side wall of the rigid chamber which is a perpendicular area against the input wave direction.
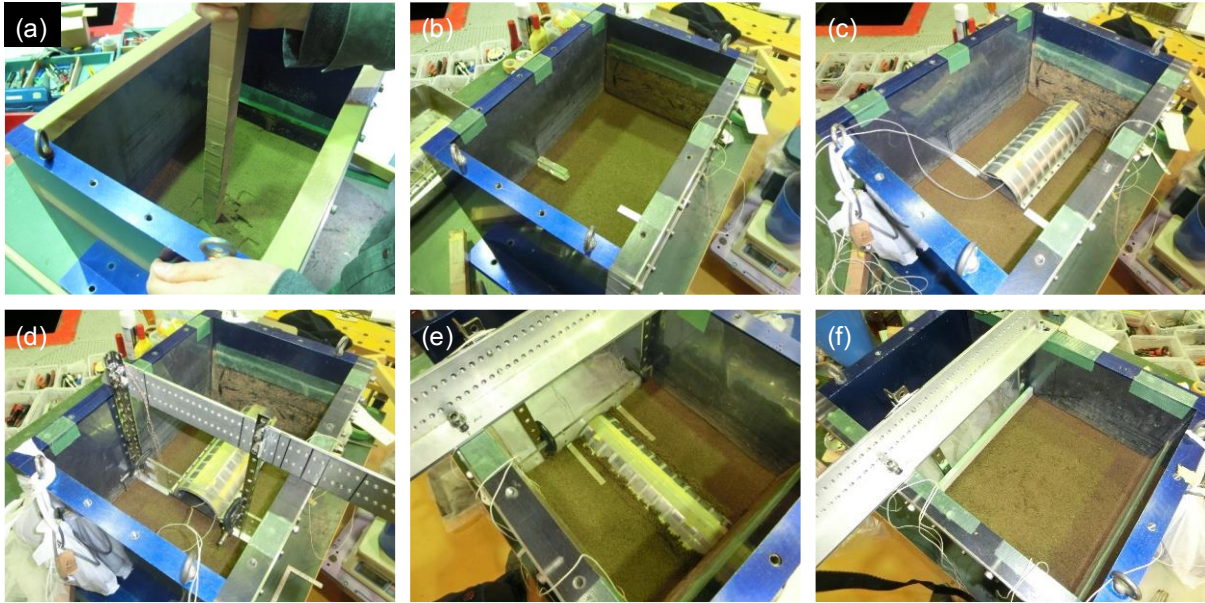
Figure 5.5: Procedure for making embankment model: (a) making foundation with wooded rectangular timber, (b) setting foundation for mouth wall, (c) setting culvert model, (d) setting mouth wall, (e) attaching reinforcing members with mouth wall model, and (f) filling of super-embankment.
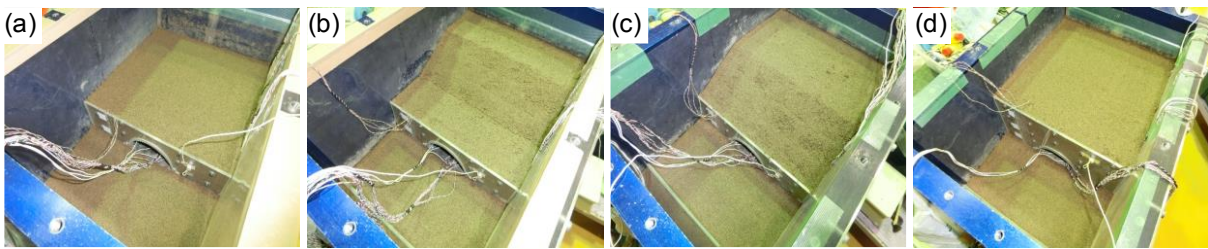
Figure 5.6: Completion of embankment model in (a) Case-1, (b) Case-2, (c) Case-3, and (d) Case-4.

5.2.5 Test instrumentation

Figures 5.7 and 5.8 show the arrangements of the test instrumentations in Cases 1-3 and Case-4, respectively. Definitions for the positive direction in wall displacement and response acceleration are also presented in the figures. The positive direction of the wall displacement and the response acceleration are on the left-hand side of the figures. The measurement items are summarized as follows:

1) Response accelerations of the culvert, mouth wall, and embankment
2) Horizontal displacement of the mouth wall
3) Earth pressure on the mouth wall

5.2.6 Input wave

In this experiment, 10 steps of excitation were applied to observe the gradual deformation of the embankment. The initial step, STEP 0, was defined as the time it took to reach 50 G of centrifugal acceleration. A continuous wave with 20 cycles of sine waves was applied with a taper of the prototype, 1 Hz. It was input 10 times, from STEPS 1 to 10, with a gradual increase of 0.5 m/s^2 to observe the gradual deformation of the embankment. Figure 5.9 shows the input wave of the shaking table at STEP
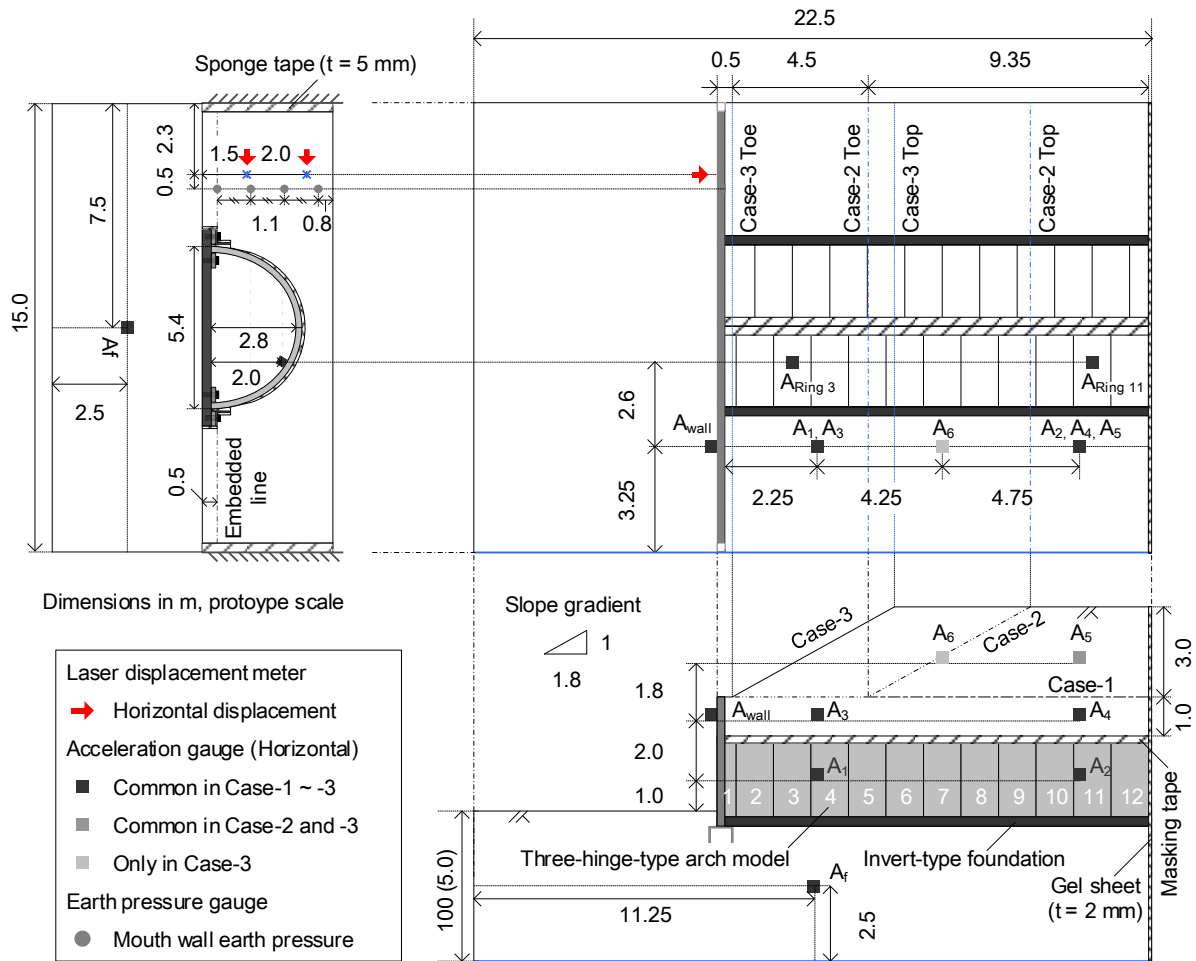
Figure 5.7: Test instrumentations in Cases 1-3.

5 in which the maximum acceleration is 2.5 m/s^2. The wave was input by controlling the displacement of the vibration table. The frequency of the input wave is 1.0 Hz, the same value as that in Chapter 4.

5.3 Results and discussions

The test results are discussed by considering the residual deformation of the embankment by the repeated excitations. This is because an attempt is made to investigate the response behavior throughout all the excitation steps. The values of the results are converted to the prototype scale.

5.3.1 Deflection mode of mouth wall

In Figure 5.10, the transitions of the wall displacements are summarized. The definitions of the physical quantities of the turnover rate, translation, and migration area (Figure 5.10(a)) are as follows: The turnover rate is the value of the difference ($\Delta_d = \Delta_1 - \Delta_2$) between the lateral displacements of the upper portion (Δ_1) and the lower portion (Δ_2) divided by the wall height (H); the translation is equal to Δ_2; and the migration area is the product of the lateral displacement at the center of the wall ($\Delta_m = (\Delta_1 + \Delta_2) / 2$)) and the wall height ($H$). The figure shows the following relations:

Turnover rate: Case-4 > Case-3 > Case-2 > Case-1
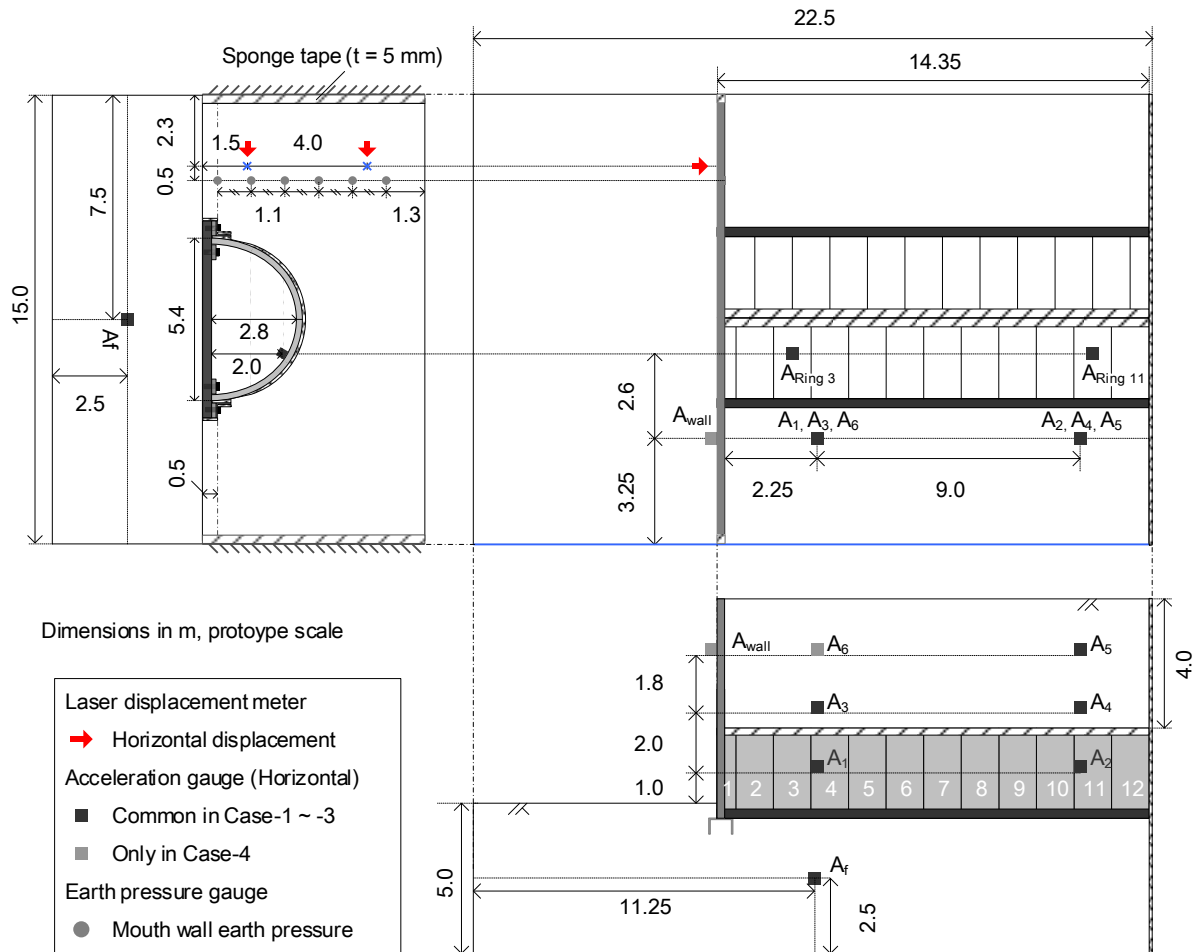
Figure 5.8: Test instrumentation in Case-4.
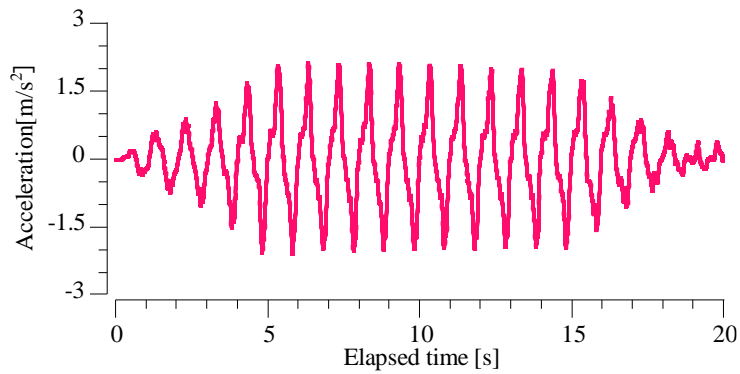
Figure 5.9: Input wave: a continuous wave with 20 cycles of sin waves. The wave is created with a taper of the prototype, 1 Hz and 2.5 m/s² in magnitude.

Translation: Case-3 > Case-4 ≑ Case-2 > Case-1
Migration area: Case-4 > Case-3 > Case-2 > Case-1

The migration area is the path area of the wall model during excitation; it can be considered as an expression of the amount of embankment deformation. The length of the reinforcing members is
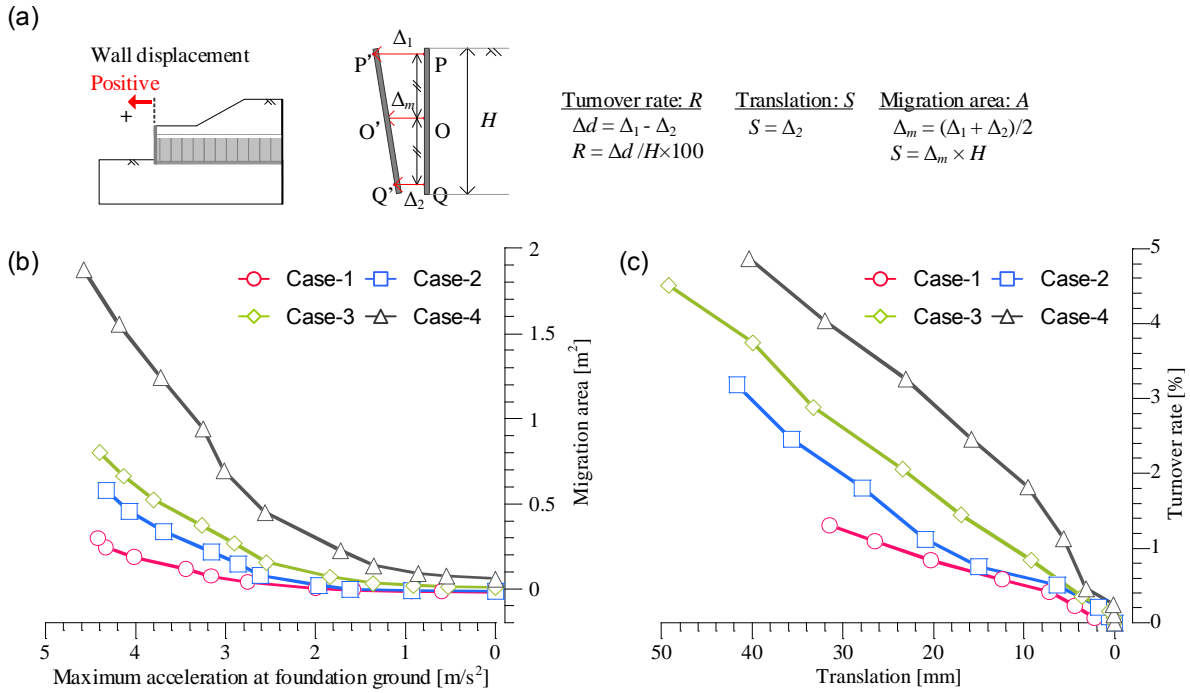
Figure 5.10: Transitions of wall displacements: (a) definitions of turnover rate, translation, and migration area, (b) maximum acceleration at foundation ground at each excitation step vs. migration area, and (c) translation vs. turnover rate.
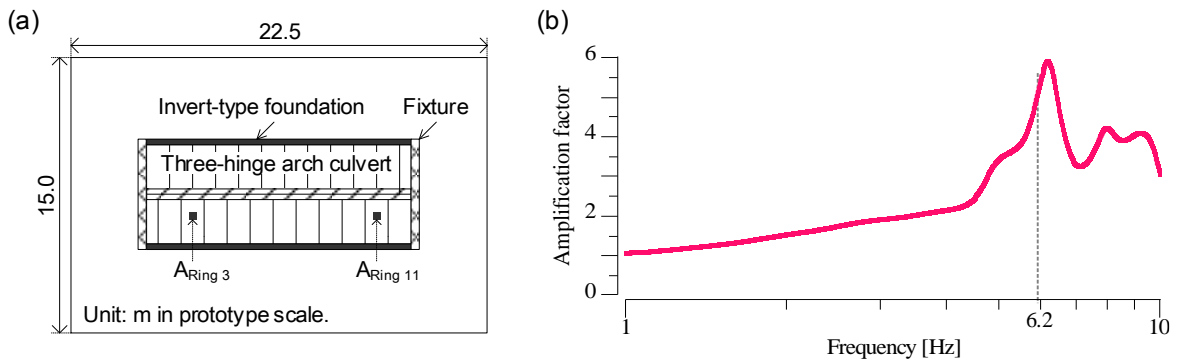
Figure 5.11: Experiment for investigating seismic characteristic of culvert model: (a) a schematic drawing of experimental model from top view and (b) amplification factor of A_{Ring3} in frequency domain.

constant across all the experimental cases, which may be the reason for the decreased deformation seen in Case-4. However, the migration area increased proportionally to the gross weight of the embankment model.

5.3.2 Seismic response of culverts and ground

To evaluate the influence of the culvert on the response acceleration of the embankment, in advance, the seismic characteristic of the culvert model was confirmed. In the experiment, under 50 G of centrifugal acceleration, the white noise was input in the culvert longitudinal direction. Figure 5.11 shows the experimental setup and the amplification ratio of the Fourier spectrum at A_{Ring3}. To calculate the Fourier spectrum, Fast Fourier Transform was used. The sampling data were 65536 and the sampling interval

was 0.005 s. From the figure, the amplification factor of Ring 3 showed the peak value at 6.2 Hz.

Figure 5.12 shows the response accelerations in time history and frequency domain of Ring 3 (A_{Ring3}), Ring 11 (A_{Ring11}), A_3 just above Ring 3, and A_f of the foundation ground, respectively. For the frequency domain, FFT was used as the preliminary experiment: the sampling data were 8192 and the sampling interval was 0.005 s. From the figure, the difference in Cases 1-4 appeared mainly in the frequency domain. The Fourier spectrum of more than 3.0 Hz was increased proportionally in the order of Case-4 to Case-1. This is because the natural frequency of the culvert model was 6.2 Hz, as shown in Figure 5.11. In 3.0 Hz, 5.0 Hz, 7.0 Hz and so on, which were from the secondary mode of the input wave, the Fourier spectrum of the culvert model was amplified; this caused a larger influence on the whole embankment model with the increase in the ratio of the culvert space in the embankment volume.

Figure 5.13 shows the transitions of the maximum response accelerations at A_3, A_{Ring3}, and A_{Ring11} over all the excitation steps. As for the X-axis, the maximum response acceleration of the foundation ground was used in both positive and negative directions. The maximum response acceleration is given by the average of the negative and positive peak values from $t = 10.00$ to 20.00 s. In Figure 5.13, the maximum accelerations in the left and right directions are plotted. According to the figure, the amplification of the response acceleration and the difference between A_{Ring3} and A_{Ring11} decreased more for cases with greater embankment cover. This is because an increase in soil cover strengthens the confining pressure acting on the culverts, which reduces the amplification of the response acceleration. On the other hand, in Case-1, the response acceleration of A_{Ring3} exceeded that of A_{Ring11} as well as that of A_3 at STEPS 8, 9, and 10.

As is shown in Figure 5.13, the relation of the response acceleration among A_3, A_{Ring3}, and A_{Ring11} changed at STEP 8. To explain this relation, the hysteresis curves of the response accelerations are depicted in Figure 5.14 from $t = 13.50$ to 14.48 s. In the figure, the start and end points of the hysteresis curves are plotted.

The mutual relationship among A_3, A_{Ring3}, and A_{Ring11} in each experimental case is visible at peak response acceleration No. 3, at which the leftwards response acceleration is maximum. In Case-1, the response acceleration of A_{Ring3} exceeded that of A_{Ring11}. On the other hand, in Case-2 and Case-3, the response acceleration of A_{Ring3} was less than that of A_{Ring11}, and the difference between A_{Ring3} and A_{Ring11} was small. Compared with the curved shape of Case-1, the curved shapes of A_3, A_{Ring3}, and A_{Ring11} converge in Case-2 and Case-3. Moreover, the curved shapes of A_3, A_{Ring3}, and A_{Ring11} almost coincide with each other in Case-4.

From the above results, the following can be concluded. In Case-1, where the overburden depth is a constant 1.0 m in the culvert longitudinal direction, the seismic response exceeds that of the surrounding ground, and the highest amplification is observed at the mouth. In Case-2 and Case-3, a difference in the acceleration values is seen between Ring 3 and Ring 11, but the difference decreases with increasing soil cover for the culverts. On the other hand, in Case-4, where the overburden depth is a constant 4.0 m in the longitudinal direction, the integrated behavior of the culverts and the surrounding ground is shown due to the large confining stress.

Figure 5.15 shows, in the present experiment with a seismic wave of 1 Hz, the relation between
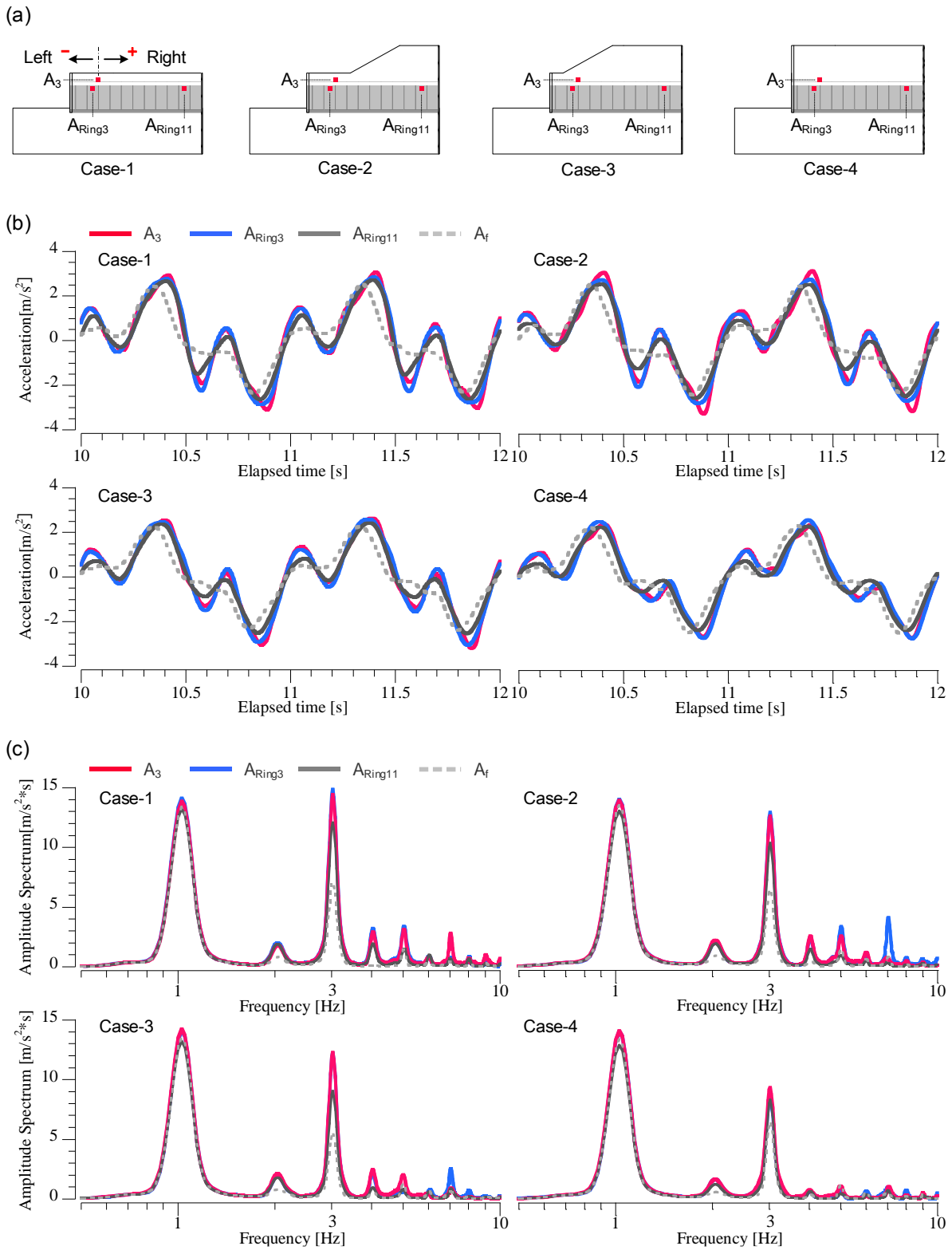
Figure 5.12: Response accelerations in STEP 5 (target maximum acceleration is 2.5 m/s^2): (a) schematic drawings of measuring points and response acceleration, (b) in time history, and (c) in frequency domain of A_{Ring3}, A_{Ring11}, and A_3.
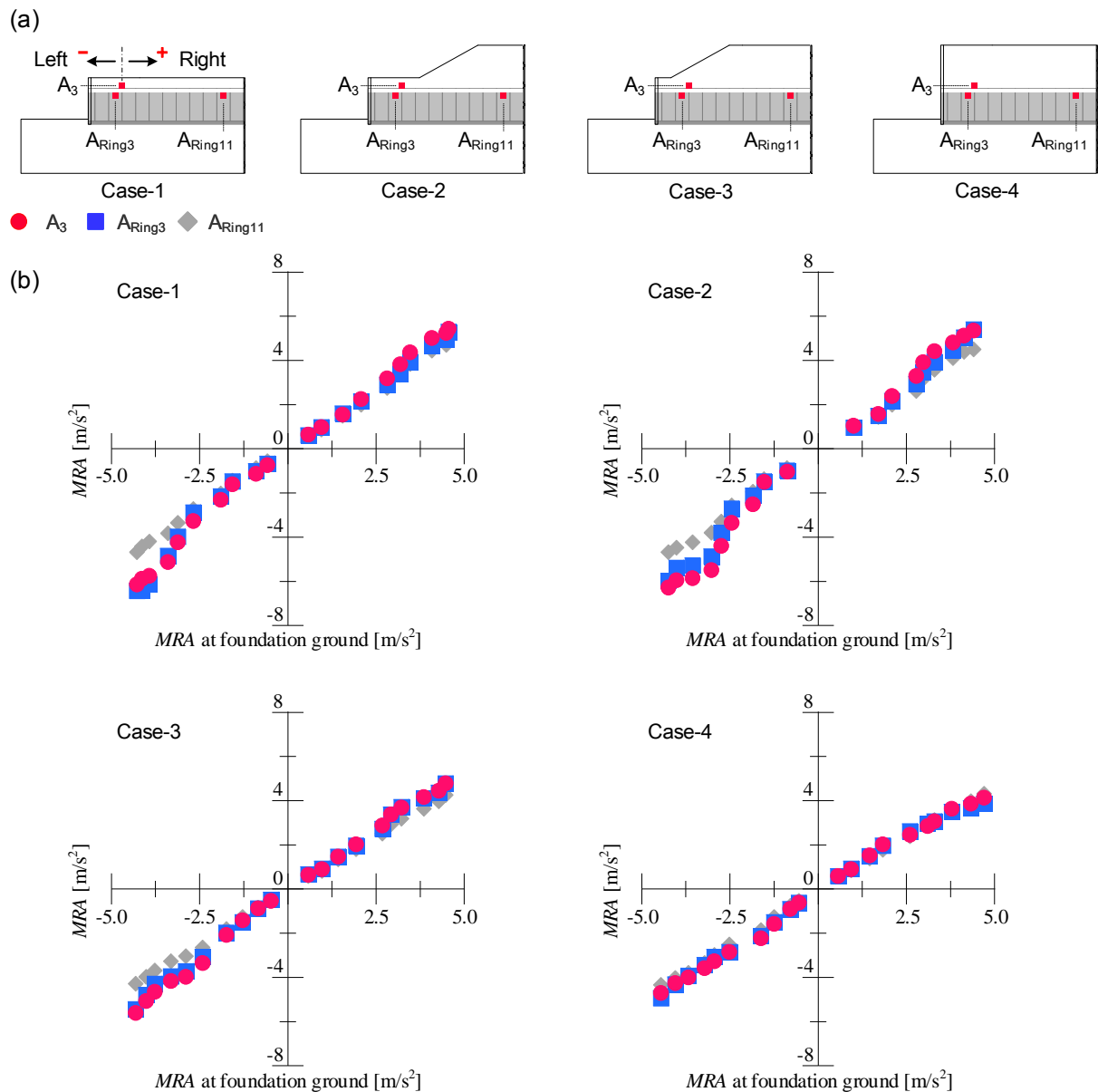
Figure 5.13: Translations of maximum response accelerations of A_3, A_{Ring3}, and A_{Ring11} over all excitation steps: (a) schematic drawings of measuring points and (b) *MRA* (Maximum Response Acceleration) at A_{Ring3}, A_{Ring11}, and A_3 vs. *MRA* at foundation ground.

the seismic mode of the embankment with a culvert and the confining pressure due to the overburden. With the small overburden, the response acceleration of the culvert was largely amplified at the mouth of the culvert where the smallest combined stress from the embankment was acting. That is why the response behavior of the culverts exceeds that of the surrounding ground. With the larger overburden, the confining stress of the embankment is increased, so that the amplification of the response behavior of the culverts at the mouth of the culverts seems to be suppressed. However, as shown in Figure 5.10, the increase in the wall displacement during the longitudinal seismic wave, due to the increase in the gross weight of the embankment, should be given some attention.
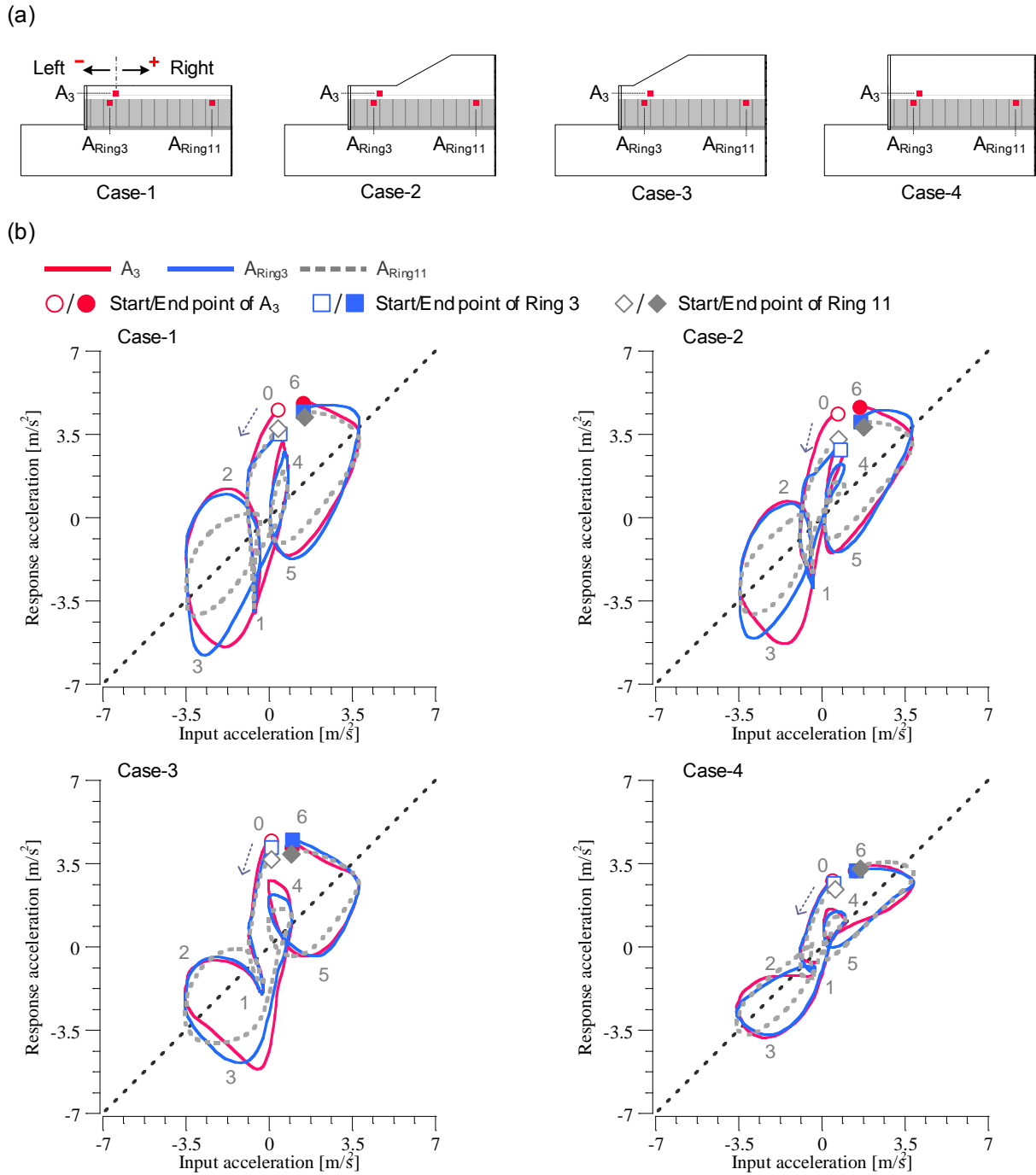
Figure 5.14: Hysteresis curves of response accelerations of A_3, A_{Ring3}, and A_{Ring11}: (a) Case-1, (b) Case-2, (c) Case-3, and (d) Case-4.

5.3.3 Embankment model after excitation

Figure 5.16 shows the embankment model surface after excitation with marked lines on the cracked areas. As seen in the figure, longitudinal cracks were observed in Cases 1-3 near the small soil cover area at the mouth. The cracks run along the arch crown and seem to have been caused by tensile forces in the culvert transverse direction. The compressive deformation on the sides of the culverts is thought
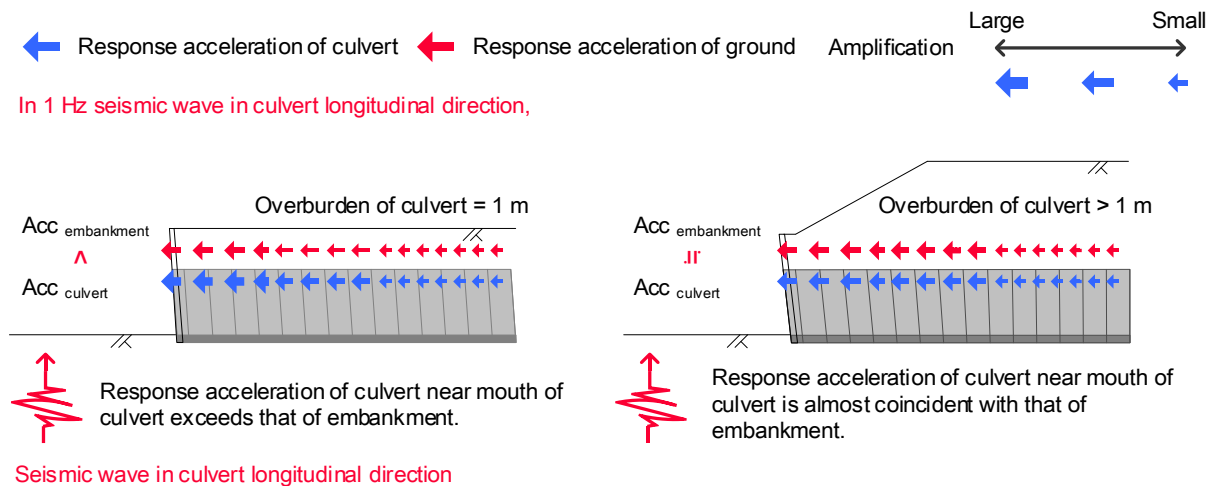
Figure 5.15: Seismic mode in culvert longitudinal direction due to pattern of embankment shape.
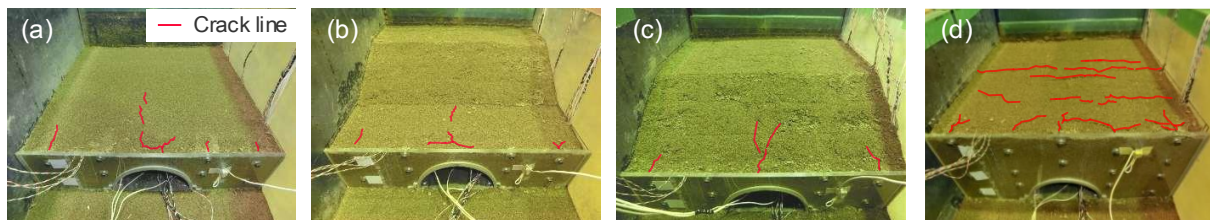
Figure 5.16: Cracked surface of crown of embankment models: (a) Case-1, (b) Case-2, (c) Case-3, and (d) Case-4.

to have created tensile force on the ground surface in the crown area. On the other hand, in Case-4, large cracks occurred in the culvert transverse direction in the central area of the embankment surface. This is because large deformation of the mouth wall caused tension on the surface of the embankment. While the enlargement of the earth cover has the advantage of restraining the seismic behavior of culverts in the longitudinal direction, the larger transverse deformation of the embankment surface should be considered.

Figures 5.17 and 5.18 show the mouth of the culvert before and after excitation, respectively. In this experiment, the hinge was designed as a simply butted section. That is why this hinge model would collapse more easily than an actual knuckle hinge. However, as seen in the figures, even when the embankment has large deformation, no slippage of the crown hinge is observed.

5.4 Conclusions

In this chapter, dynamic centrifuge model tests were conducted focusing on the influence of the embankment shape on the seismic performance of three-hinged arch culverts in the longitudinal direction. The following conclusions can be drawn from the results of this chapter:

1) The deformation of an embankment in the culvert longitudinal direction increases proportionally to the gross weight of the soil.
2) The seismic behavior of culverts in the longitudinal direction is closely related to the degree of overburden.
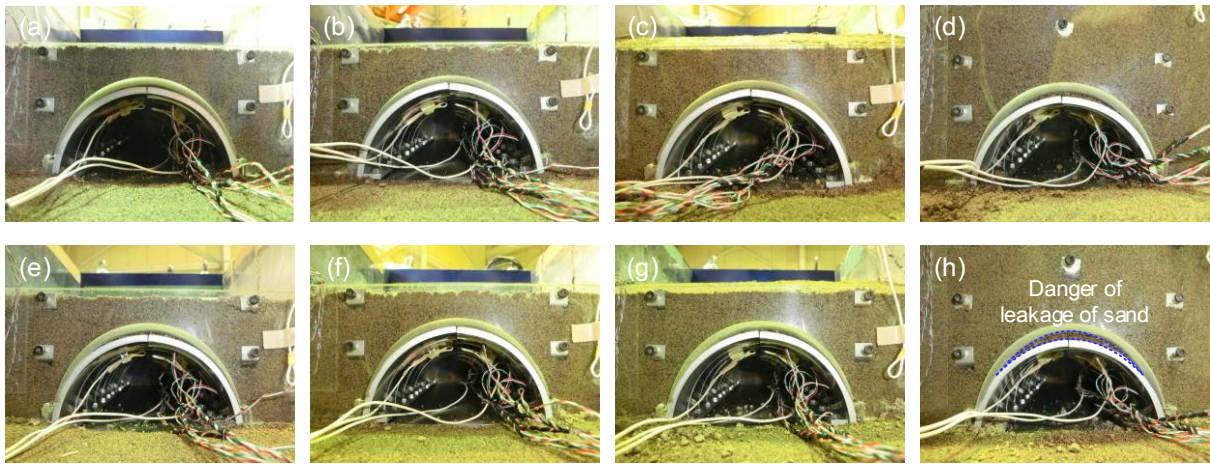
Figure 5.17: Mouth of culvert before and after excitations: (a) and (e) Case-1, (b) and (f) Case-2, (c) and (g) Case-3, and (d) and (h) Case-4.
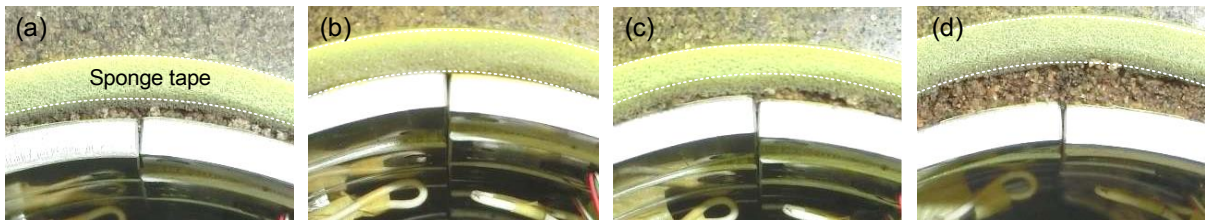
Figure 5.18: Enlarged view of arch crowns: (a) Case-1, (b) Case-2, (c) Case-3, and (d) Case-4.

3) Shallow soil cover, such as 1.0 m, allows the response acceleration of culverts to be amplified and to exceed that of the surrounding soil at the mouth. Conversely, deep soil cover, of more than 4.0 m, causes the culverts to respond as an integrated body with the surrounding soil.

4) In the experiment in which the entire overburden was more than 1.0 m and in which the hinge was a simply butted section, no slippage of the hinge portion was observed during repeated excitation in the longitudinal direction.

References

Association of Modularch Construction Method (2017): *Engineering Manual for Modularch*, *Geo-Research Institute* (in Japanese).

Abe, T. and Nakamura, M. 2014. *The use of and the caution in the application of the culvert constructed by large pre-cast element in the expressway construction*, *The Foundation Engineering & Equipment*, Vol. 42, No. 4, pp. 8-11. (in Japanese)

Investigative Committee of Manual for the Design and Construction of Techspan Construction Method (1998): *Manual for the Design and Construction of Techspan Construction Method (Draft)*, *Advanced Construction Technology Center* (in Japanese).

Japan Road Association (2010): *Road Earthwork Guidelines - Guidelines for Embankment Work* (in Japanese).

Japan Road Association (2012): *Specifications for Highway Bridges Vol. V: Seismic Design* (in Japanese).

Technological Examination Committee of Techspan Construction Method (2014): *Comparison Outline of Revised Items in Manual for the Design and Construction of Techspan Construction Method (Draft)*, *Advanced Construction Technology Center* (in Japanese).

Public Works Research Center (2014): *Manual for the Design and Construction of Reinforced Earth Wall, 4th Revised Edition* (in Japanese).

Chapter 6 Numerical analysis of seismic behavior in culvert longitudinal direction

6.1 Introduction

In this chapter, elasto-plastic FEM analyses of the seismic behavior in the culvert longitudinal direction are discussed. Based on the previous experimental results, 2D and 3D dynamic analyses are conducted considering the seismic effect of the longitudinal structural connectivity and the embankment shape. In the 2D FEM analysis, the applicability of the modeling of the structural connectivity is verified through a dynamic analysis of the simplified culvert model. In the 3D FEM analysis, the seismic behavior in the culvert longitudinal direction of three-hinged arch culverts is verified through the modeling of the structural connectivity of the culverts.

6.2 Outline of 2D elasto-plastic FEM analysis

Through the dynamic centrifuge tests results of Chapters 4 and 5, it was found that the structural connectivity and the embankment shape of culverts largely influence the seismic performance of precast arch culverts. On the other hand, according to the design manual for the hinge type of precast arch culverts (Association of Modularch Construction Method, 2017 and Investigative Committee of Manual for the Design and Construction of Techspan Construction Method, 1998), the longitudinal design does not consider the seismic effect, but does consider the prevention of the slipping of the arch members due to the longitudinal slope of the foundation ground and the ground settlement. This is because there is no evaluation method for the longitudinal seismic performance of culverts.

Therefore, in this chapter, elasto-plastic FEM analyses are conducted to develop a new evaluation method for the longitudinal seismic performance of hinged arch culverts by considering the seismic effects due to the structural connectivity and the embankment shape. The analysis conditions are: the modeling of the structural connectivity, the analysis mesh, the interface of the soil and the culvert, and the input wave.

6.2.1 Modeling of longitudinal structural connectivity

Figure 6.1 shows the deformation mode of culverts with an embankment due to the culvert longitudinal direction for the observed deformation in the dynamic centrifuge tests of Chapter 4 and the FEM modeling. From Figure 6.1(a), the longitudinal seismic behavior of the culverts can be explained by the rigid rotation and the sliding of the culverts with the deformation of the embankment. Therefore, in this FEM analysis (Figure 6.1(b)), the rigid rotation of the culverts was controlled with the bilinear spring elements arranged at the structural connection of the culverts, while the separation and slip were controlled with joint elements arranged at the interface of the culvert and the soil. The embankment deformation was modeled by an elasto-plastic constitutive model, the *cyclic mobility model*, as mentioned in Chapter 3.
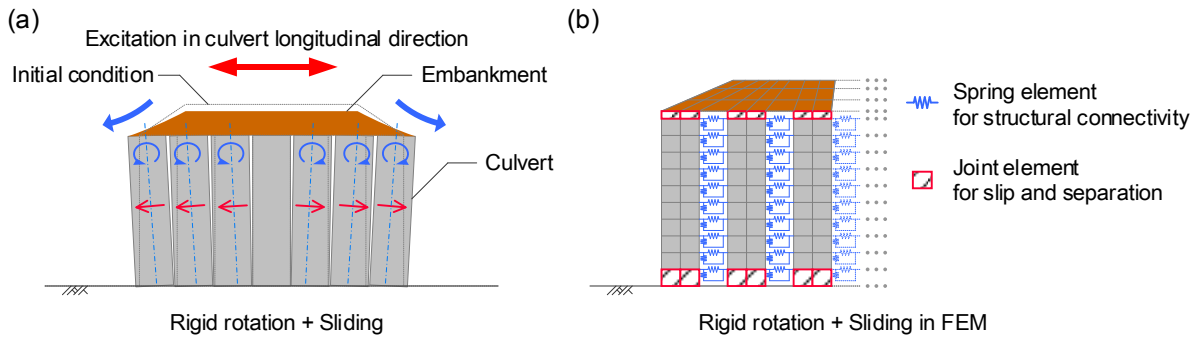
Figure 6.1: Deformation mode of culverts due to seismic wave in culvert longitudinal direction: (a) observed deformation mode in experiment and (b) modeling by FEM.
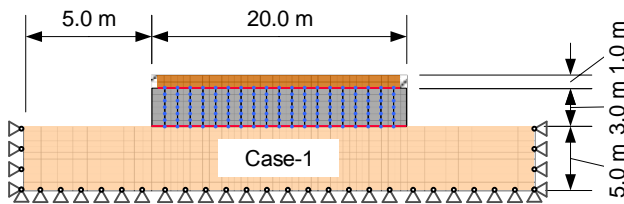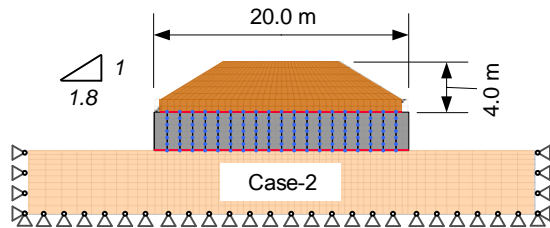
Figure 6.2: Analysis mesh and cases considering shape of embankment and structural connection in both separated and connected conditions.

6.2.2 Analysis mesh and case

Figure 6.2 shows the analysis mesh for two cases. The analyses focused on 20 sets of precast arch culverts, 1.0 m in length, on a 5-m-thick foundation ground. As shown in the figures for Case-1 and Case-2, four analysis cases are given under the separated or connected condition with an overburden having a thickness of 1.0 m or 5.0 m.

6.2.3 Interface of soil and culverts

The solutions for contact-impact problems by a grid scheme and a particle method, such as the finite element method and the moving particle simulation, are based on Lagrange's method of undetermined multipliers (Hughes et al., 1976) or the penalty method (Zienkiewicz, 1977). In particular, the penalty method is equivalent to inserting a spring element into each of the contact points. Therefore, the implementation of the simulation is relatively simple, although there is a problem of vibrations in the structure at higher order modes (Suzuki and Toi, 1987). However, the present study aimed to express the separated and connected culverts with the simple physical meaning. In this numerical analysis, a bilinear spring element is inserted into each contact node of the culvert elements by referring to the

(a)

Bilinear model

F

$k_{compression2}$

$k_{compression1}$

u_n

$k_{tension1}$

u_p

D

$k_{tension2}$

Step: j-1

$u_{i,j-1}$ $u_{i+1,j-1}$

Step: j

$u_{i,j-1}$ $u_{i,j}$ $u_{i+1,j}$ $u_{i+1,j-1}$

D_j: $u_{i,j}$ - $u_{i+1,j}$

ΔD_j: $(u_{i,j-1} - u_{i,j}) - (u_{i+1,j-1} - u_{i+1,j})$

F_j: $F_{j-1} + k\Delta D_j$

u : Node composition of spring element

(b)

F

$k_{compressive} = 1.0 \times 10^{10}$ [kN/m]

D

$k_{tensile} = 1.0 \times 10^{10}$ [kN/m]

(c)

F

$k_{compressive} = 1.0 \times 10^{10}$ [kN/m]

D

$k_{tensile} \fallingdotseq 0$ [kN/m]

(d)

$E_{compression1}$	$1.0 * 10^{10}$ kPa
$E_{compression2}$	$3.10 * 10^{7}$ kPa
u_p	$1.0 * 10^{-9}$ m
$E_{tension1}$	$1.0 * 10^{-9}$ kPa
$E_{tension2}$	$1.0 * 10^{-9}$ kPa
u_n	-1.0 m

Figure 6.3: Spring model for contact-impact of culvert elements: (a) bilinear model of spring element, spring constant in (b) connected condition and (c) separated condition, and (d) parameters of separated condition.

Table 6.1 : Material properties of concrete culvert model

Young's modulus	E_e	[kN/m^2]	3.10×10^7
Unit weight	γ	[kN/m^3]	24.5
Poisson's ratio	v	—	0.20
Damping ratio	h	—	0.02

penalty method (Figure 6.3).

The culverts were modeled as an elastic material whose mechanical properties were based on concrete, as shown in Table 6.1. Figure 6.3 shows a spring model of the bilinear spring elements for the nonlinear behavior of the longitudinal structural connection of the culverts. In the connected condition, the compressive stiffness and tensile stiffness are larger than those of concrete. In the separated condition, although the compressive stiffness equals the connected condition, the tensile stiffness is almost zero. The interface of the culverts and the soil has joint elements whose parameters are determined by direct shear tests between mortar and *Toyoura* sand, as shown in Figure 6.4 (Sawamura et al., 2017). Table 6.2 shows the material properties of the joint elements.

6.2.4 Soil properties

The mechanical behavior of the embankment soil was expressed by the cyclic mobility model mentioned in Chapter 3. The foundation ground was modeled as an elastic model whose Young's modulus was based on the design manual for three-hinged arch culverts (Investigative Committee of Manual for the Design and Construction of Techspan Construction Method, 1998). Normally, three-hinged arch culverts
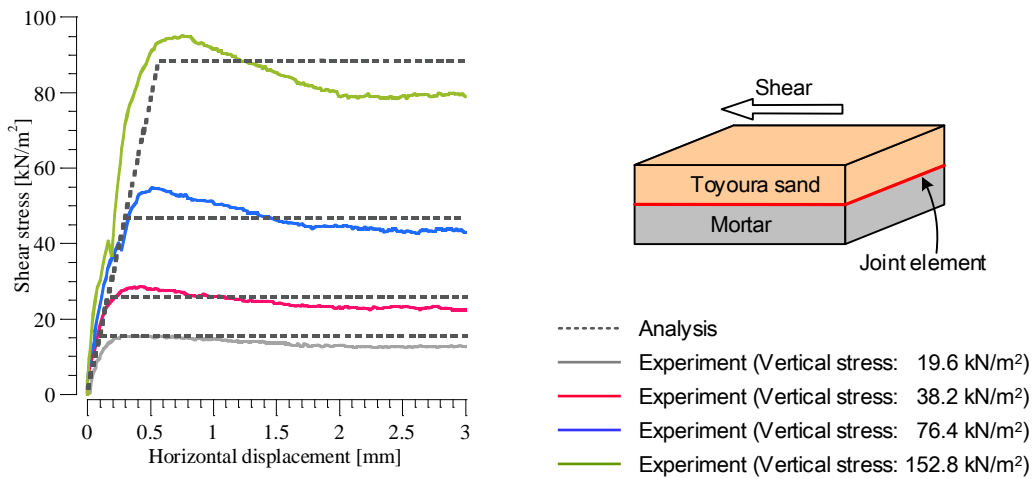
Figure 6.4: Joint profile between soil and culvert by Sawamura et al. (2017).

Table 6.2 : Material properties of joint elements

Shear stiffness	K_s	[kN/m^2]	1.55×10^5
Normal stiffness	K_n	[kN/m^3]	1.55×10^5
Cohesion	c	—	5.00
Internal friction angle	ϕ	—	28.0
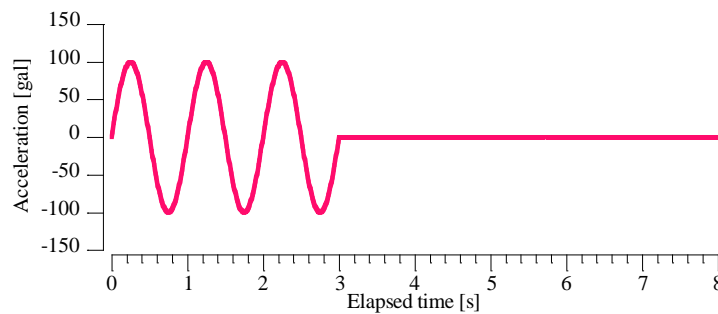
Figure 6.5: Input wave: sin wave with 1 Hz, three cycles, and magnitude of 100 gal.

are constructed for a foundation ground with an SPT value of more than 30 N. Therefore, in this analysis, the Young's modulus of the foundation ground was equivalent to 2800 N = 84,000 kPa (Japan Road Association, 2012); the other mechanical properties were based on *Edosaki* sand.

6.2.5 Initial stress and input wave

The initial stress of the soil and the culverts was determined by a self-weight analysis. Figure 6.5 shows the input wave as a sin wave with 1 Hz, three cycles, and a magnitude of 100 gal. The wave was input at the bottom of the foundation ground. The time interval of the calculation was 0.001 seconds. The time integration was based on the Newmark-β method ($\beta = 1/4$ and $\gamma = 1/2$).

72
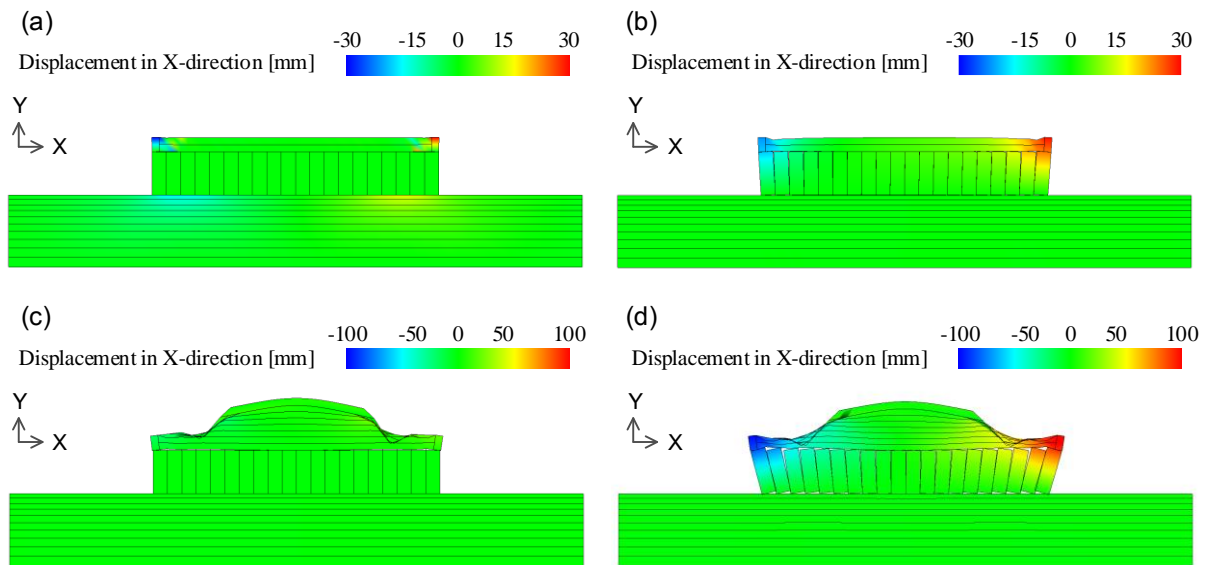
Figure 6.6: Heat map of displacement in X-direction after excitation which is described in 10 times scale as the original one. (a) Case-1$_S$, (b) Case-2$_S$, (c) Case-1$_C$ and (d) Case-2$_C$ after excitation.

6.3 Results of 2D elasto-plastic FEM analysis

6.3.1 Deformed state after excitation

Figure 6.6 shows a heat map of the displacements in the X-direction after excitation. In Case-2$_S$, apertures in the culverts clearly appeared due to the embankment deformation. Moreover, the displacements of the embankment in the separated case exceeded those of the connected case in both Case-1 and Case-2. In short, the deformation of an embankment due to an earthquake is likely to increase with a separated structural connection of the culverts. This deformation tendency due to the structural connectivity matches the deformation tendency seen in the dynamic centrifuge tests of Chapter 4. That is why the current modeling for the structural connectivity of culverts with the spring model can evaluate its seismic effect on the culverts well.

6.3.2 Dynamic behavior at structural connection

Figure 6.7 shows the seismic behavior of the structural connection at the top of the culverts. The focus of the figure is the time history of the displacement or the restoring force of the spring elements located at the top of the culvert element, as shown in Figures 6.7(a) and (b). From Figures 6.7(c) and (d), the displacements are seen to match each other in Case-1$_S$ and Case-2$_S$. The size of the apertures in the culverts increases proportionally as the distance to the mouth of the culverts becomes shorter; SP$_2$ shows the largest aperture of the culverts. From Figure 6.7(e), the amplification of the restoring force in Case-1$_C$ increases toward the tensile force of the spring elements, and finally, the rest of the restoring force remains in the tensile direction. In Case-2$_C$, the tensile force of the spring elements increases as the distance to the mouth of the culverts becomes shorter. The final value of the restoring force is larger than five times that of Case-1$_C$.

Figure 6.8 shows the maximum tensile force of the spring elements arranged at the crown of the
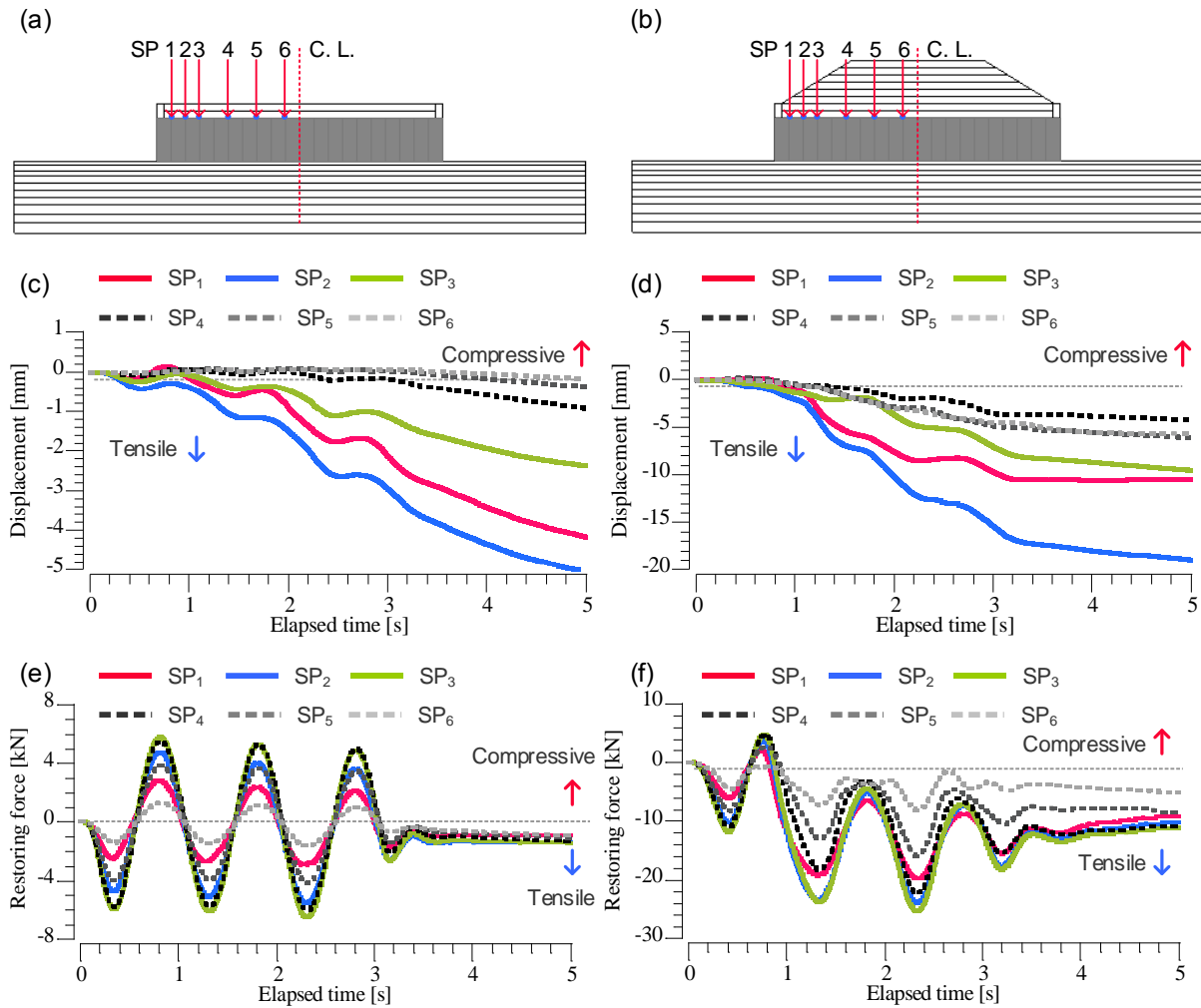
Figure 6.7: Dynamic analysis results for deformation mode of (a) Case-1$_S$ and (b) Case-2$_S$, time history of displacements in X-direction in spring elements of (c) Case-1$_S$ and (d) Case-2$_S$, and time history of restoring force in X-direction in spring elements of (e) Case-1$_C$ and (f) Case-2$_C$.
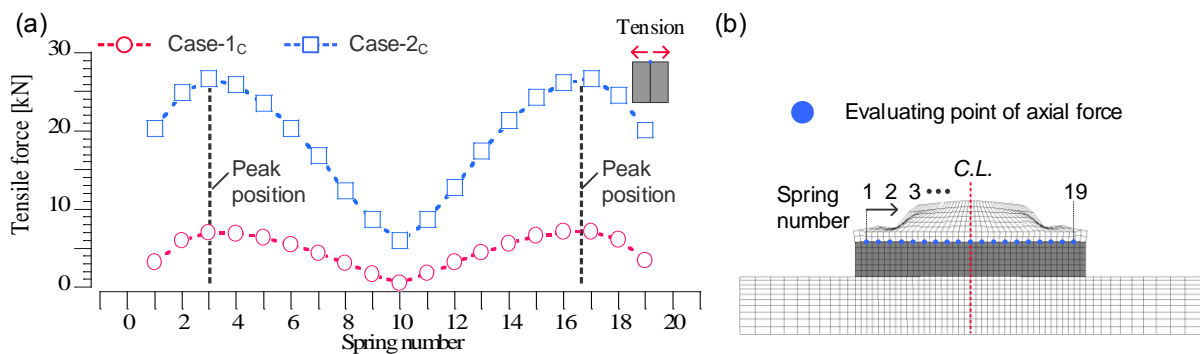
Figure 6.8: Axial force behavior of spring elements in Case-1$_C$ and Case-2$_C$: (a) maximum tensile force at each arch member and (b) evaluating points of axial force in Case-2$_C$ corresponding to those of Case-1$_C$.

arch members in Case-1$_S$ and Case-2$_S$. The peak value appeared at the third arch member from the mouth of each culvert. The magnitude of all the tensile force of the arch members in Case-2$_C$ exceeded that in Case-1$_C$. This is because the tensile force of the arch members is given by the shear force originally due
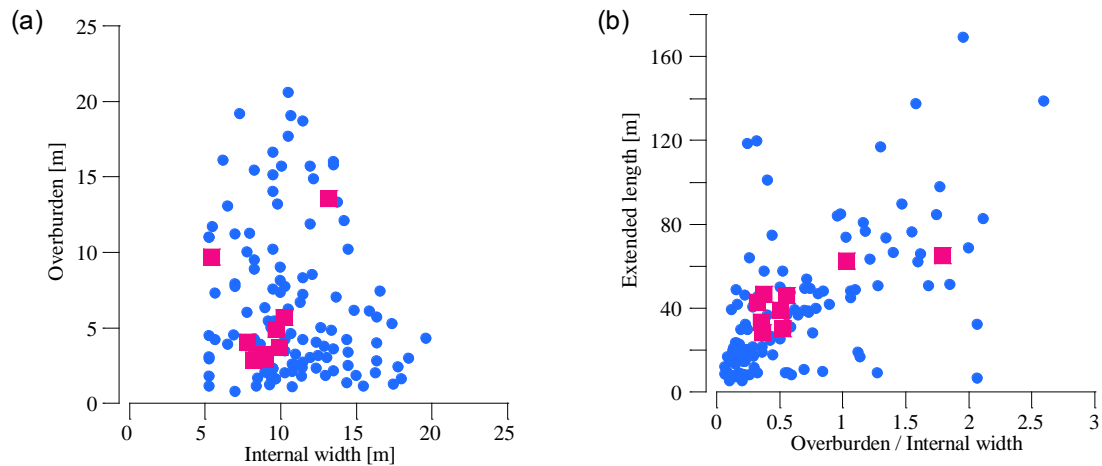
Figure 6.9: Analysis on construction examples of three-hinged arch culverts based on open resource of "*Hokyodo net service* (www.hokyodo.jp)": classifications (a) by internal width and overburden and (b) by overburden ratio (overburden/internal width) and extended length.

to the confining stress of the surrounding ground which is larger in Case-2 than in Case-1.

From the above results, the influence of the longitudinal inertial force on the structural connection was seen to become larger near the mouth of the culverts. Additionally, the influence of the overburden depth on the structural connection was critical to the shear force and caused the apertures in the culverts.

6.4 Outline of 3D elasto-plastic FEM analysis

To verify the modeling of the structural connectivity, its applicability to model the seismic effect of the structural connection and the embankment shape of culverts was confirmed. A 3D elasto-plastic dynamic analysis is conducted, based on the above modeling, to reproduce the seismic behavior in the culvert longitudinal direction of the three-hinged arch culverts. In the present analysis, how the input wave of the culvert longitudinal direction contributes to the unique damage to the arch members is discussed.

6.4.1 Analysis condition

The three-hinged arch culverts in the present analysis were based on the old-type of three-hinged arch culverts (refer to Figure 2.3) considering the examples of disaster taken from the Great East Japan Earthquake (Abe and Nakamura, 2014). Figure 6.9 shows some three-hinged arch culverts damaged in the Great East Japan Earthquake. The damage was seen to be concentrated in areas where the inner width was 10 m and the overburden was 5 m. Here, the extended length is the longitudinal distance of the culverts. The damaged culverts mostly had an extended length of around 20-40 m. This is because precast arch culverts are generally used as underpasses of road embankments, so that the distance of the culverts was chosen in order to satisfy the available distance for the two-lane road on the embankment crown. In this analysis, considering the calculated cost of the prototype scale, an extended length of 20 m was deemed enough to consider the two-lane road on the embankment crown.
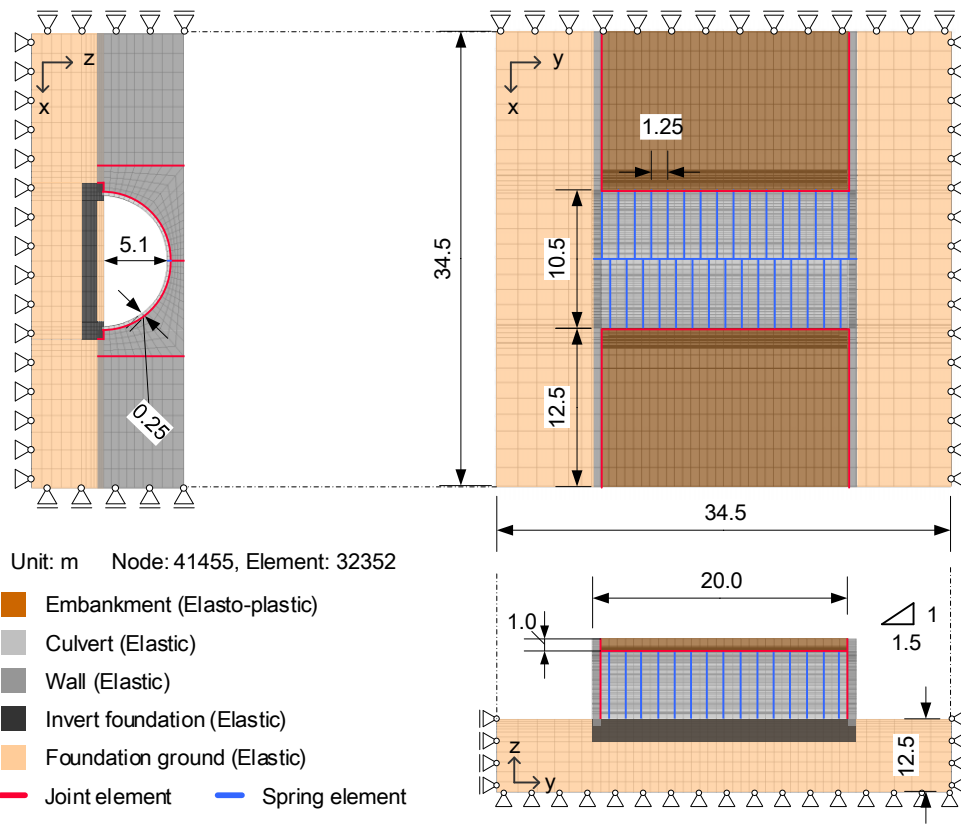
Figure 6.10: Analysis mesh in Case-1.

6.4.2 Analysis mesh and case

Figures 6.10 and 6.11 show the analysis meshes for Case-1 and Case-2, respectively. This study focused on 20-m long three-hinged arch culverts on a foundation ground with a thickness of 5.0 m. The hinge of the arch crown was in a simply butted condition to simplify the hinge modeling of the arch crown. As shown in the two figures, Case-1 had a culvert overburden of 1.0 m and Case-2 had a culvert overburden of 5.0 m. The analysis cases were equivalent to those of the 2D analysis, namely, Case-1$_S$ had separated culverts and an overburden of 1.0 m, while Case-2$_C$ had connected culverts and an overburden of 5.0 m. Through these modelings of the structural connection and the hinge shape, the damage mechanism to the arch members due to the seismic wave in the culvert longitudinal direction was discussed.

6.4.3 Modeling of culvert and interface

Figure 6.12 presents the modeling of the soil-structure interface and the structure-structure interface of the arch elements. The material properties of the culvert were equivalent to those of the 2D modeling. From the figures, it can be seen that the joint elements were arranged on the interface between the arch culvert and the soil for modeling the slip and separation. The bilinear spring elements were arranged in the longitudinal structural connection of the arch members. The hinge of the arch crown was modeled with the bilinear spring elements between the elements of the arch crown, and the hinges of the arch feet were modeled with joint elements between the elements of the arch feet and the foundation.

In this analysis, to express the apertures and the water leakage reported after the Great East Japan
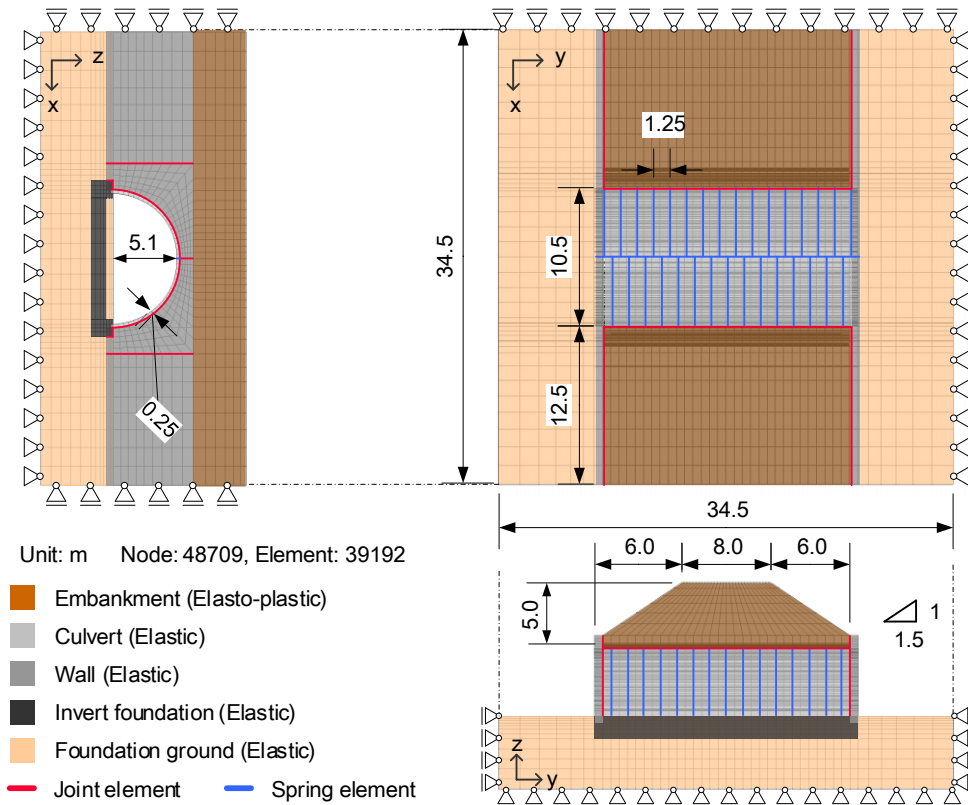
Figure 6.11: Analysis mesh in Case-2.
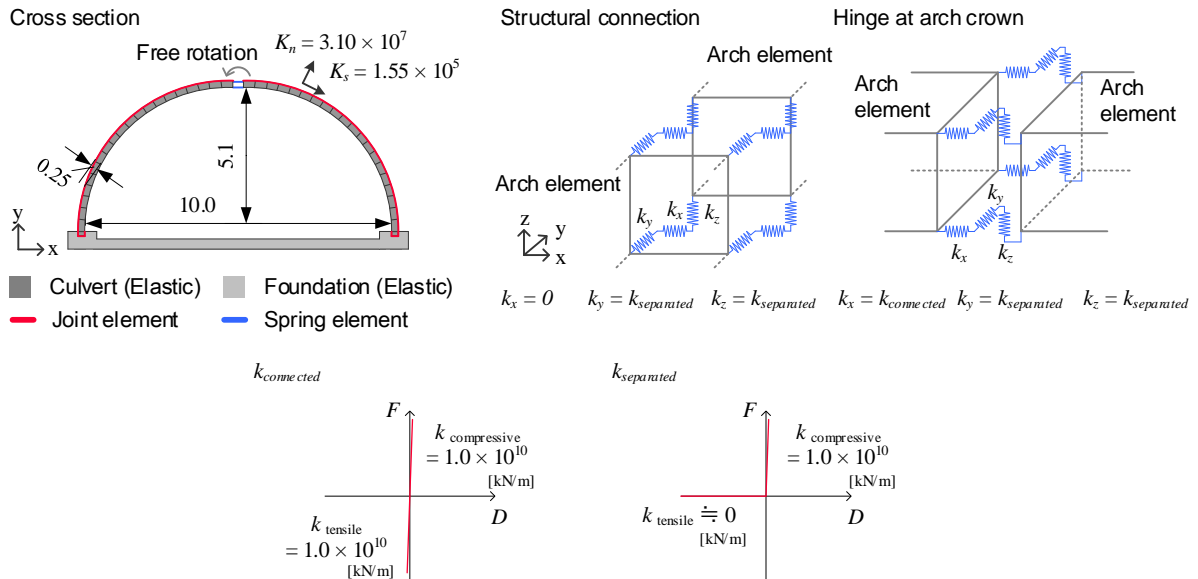
Figure 6.12: Soil-structure interface and structure-structure interface of arch elements.

Earthquake, the arch members were modeled in the separated condition without the structural connection. Therefore, the spring elements were controlled to have tensile stiffness equal to zero under the contactless condition and enough larger stiffness than concrete at the contacts. The hinge at the arch crown was modeled by a rotating stiffness of zero and the hinges at the arch feet were modeled by joint elements, as shown in the figures. The parameters for the joint elements were determined by direct shear
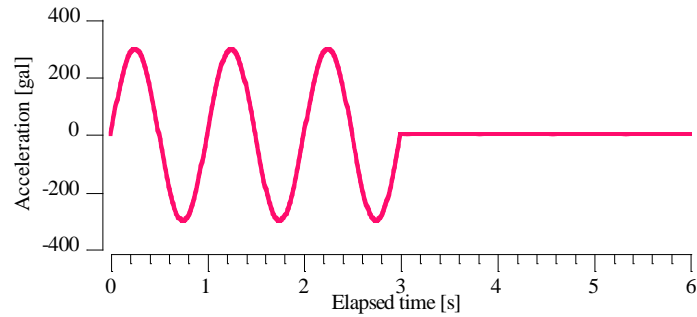
Figure 6.13: Input wave: sin wave with 1 Hz, three cycles, and magnitude of 300 gal.

tests for mortar and *Toyoura* sand, as shown in Table 6.2 (Sawamura et al., 2017).

6.4.4 Model of mouth wall

As was mentioned in Chapter 3, the mouth wall of three-hinged arch culverts is constructed as a perpendicular wall of an embankment generally with a reinforced earth wall. In the dynamic centrifuge tests discussed in Chapters 4 and 5, the unity of the embankment and the mouth wall modeled as a reinforced earth wall was not spoiled during the repeated input of the longitudinal earthquake. Therefore, in this analysis, considering the unity of the embankment and the mouth wall, the mouth wall was modeled as elastic concrete without reinforcing members. The joint elements were arranged at the interface between the soil and the wall, and the shear stiffness was set to have enough larger stiffness so as to express the integral deformation of the embankment with the mouth wall.

6.4.5 Soil properties and initial stress

The soil properties of the embankment and the foundation ground were determined as in 6.2.4. The initial stress of the foundation ground and the culverts was determined through a self-weight analysis of the elastic model. In the elastic model, the Young's modulus of the embankment was four times that of the initial Young's modulus obtained by the triaxial simulation of *Edosaki sand* (Japan Road Association, 2012). The initial stress of the embankment was determined as the K_0 state of the soil, considering the stability of the calculation.

6.4.6 Input wave

For the input wave, a sin wave with 1 Hz, 3 cycles, and 300 gal of magnitude (Figure 6.13) was used to observe the simple seismic behavior. The wave was input at the bottom of the foundation ground in the culvert longitudinal direction. The time interval of the calculation was 0.001 seconds and the time integration was based on the Newmark-β method ($\beta = 1/4$ and $\gamma = 1/2$).

6.5 Results of 3D elasto-plastic FEM analysis

6.5.1 Deformation of embankment and culvert

Figures 6.14(a)-(d) show the transition of the settlement of the embankment for all cases. From the figures, the settlement of the embankment was seen to increase in the separated condition compared to
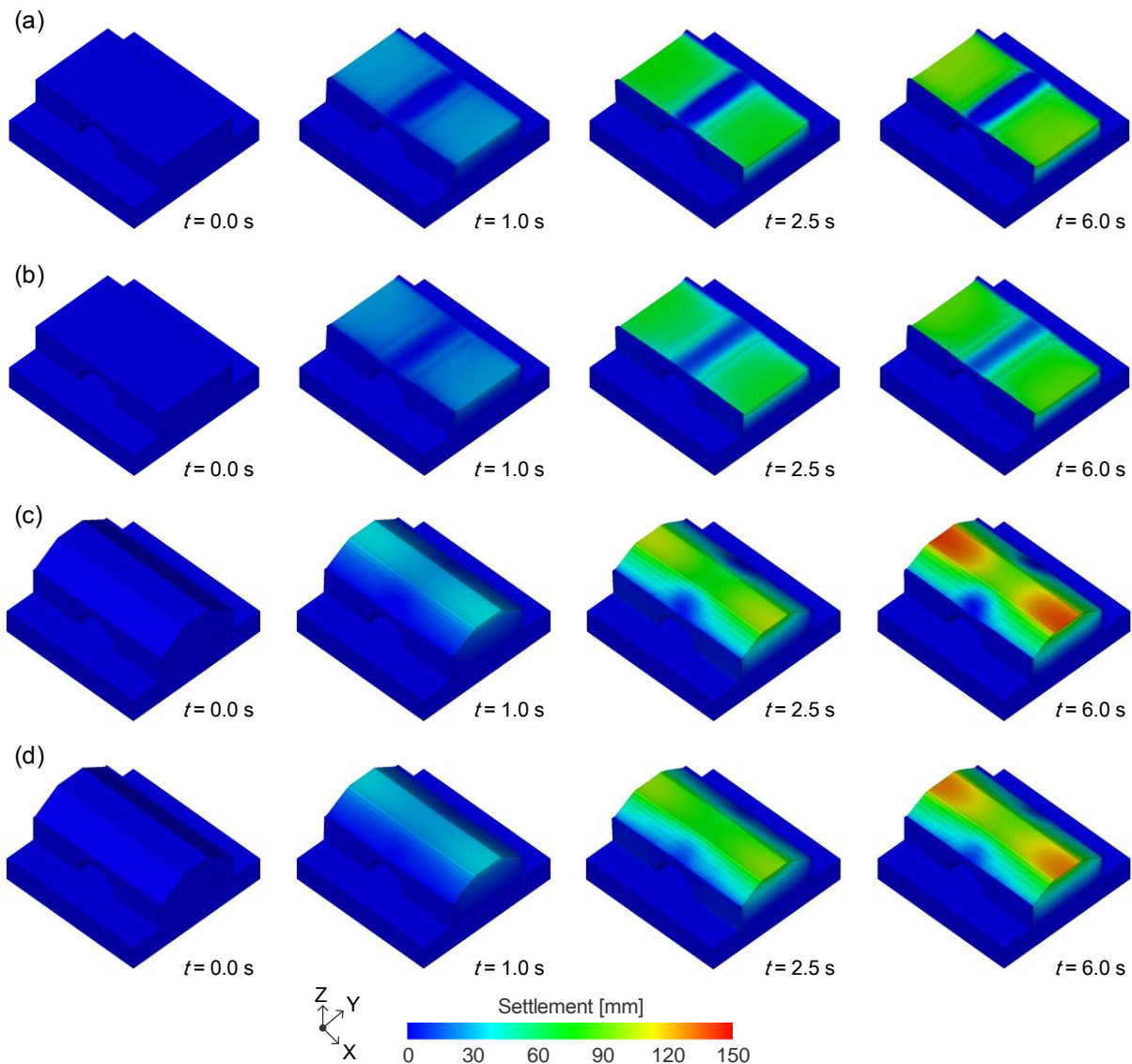
Figure 6.14: Transition of settlement in embankment of (a) Case-1$_S$, (b) Case-1$_C$, (c) Case-2$_S$, and (d) Case-2$_C$.

the connected condition. Figures 6.15(a)-(d) show the wall displacements in the Y-direction. In the separated condition, the wall displacement above the culvert is increased compared to the connected condition. Focusing on the displacements of the culvert, shown in Figures 6.16 and 6.17, the aperture of the culverts is well reproduced in the separated condition although almost no deformation of the culverts was generated after the excitation. The deformation of the culverts caused the larger deformation of the embankment in Case-1$_S$ and Case-2$_S$. This tendency coincides with the results of the experiment discussed in Chapter 4.

Figures 6.18(a)-(d) show the distribution of wall displacement in the Y-direction for all cases after excitation. From the figures, the displacement in the center of the mouth wall increased compared to the other lines of the mouth wall in all cases. Additionally, the amount of displacement in the center of the mouth wall is amplified in the separated condition. Figure 6.19 shows the distribution of wall displacement along the top of the mouth wall. From the figure, the separated condition showed the larger
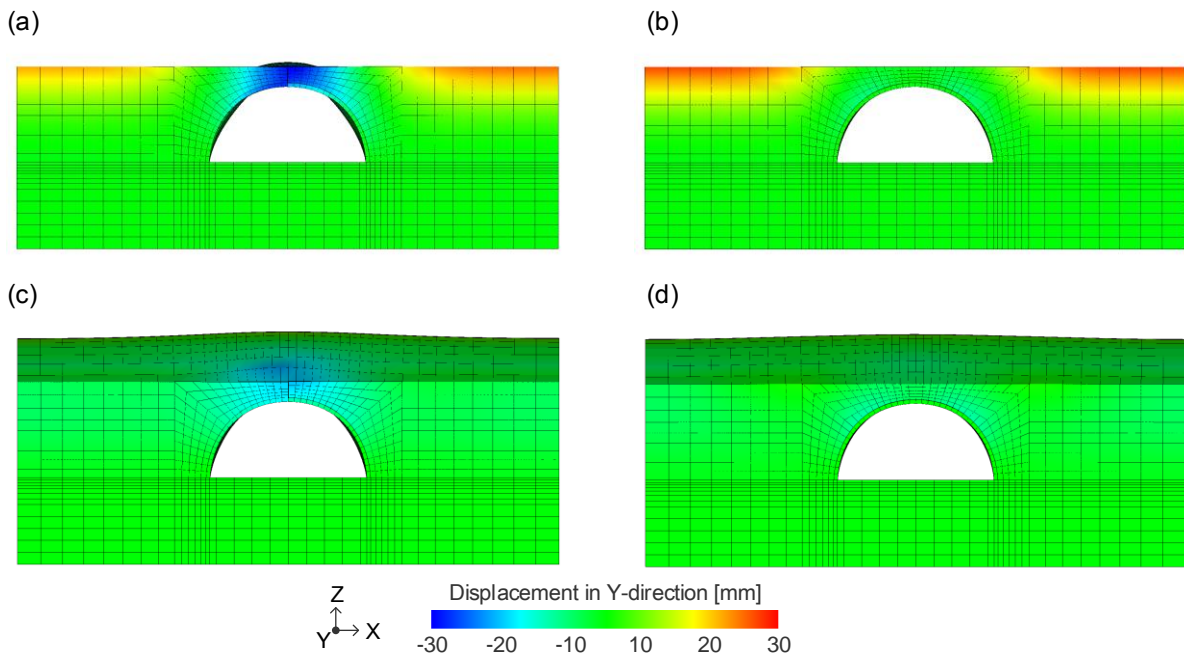
Figure 6.15: Wall displacement in Y-direction of (a) Case-1s, (b) Case-1c, (c) Case-2s, and (d) Case-2c.
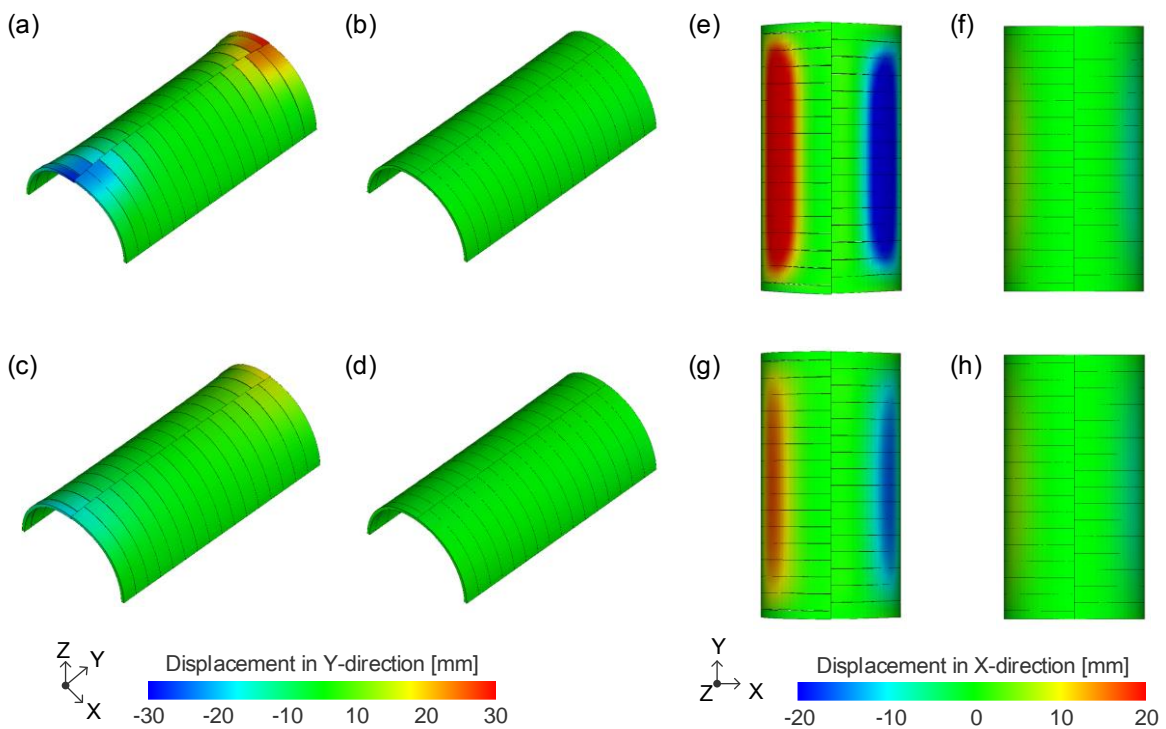
Figure 6.16: Displacement in Y-direction of culverts in (a) Case-1s, (b) Case-1c, (c) Case-2s, and (d) Case-2c and displacement in X-direction of culverts in (e) Case-1s, (f) Case-1c, (g) Case-2s, and (h) Case-2c.

wall displacement at the center of the mouth wall unlike the connected condition.

To discuss the influence on the soil surrounding the culvert, the stress paths are described in Figures 6.20-6.24. From the figures, except for the elements just above the culverts, the shear stress was dominant in the stress paths. Conversely, the change in the stress of the element above the culverts

(a)

t = 0.0 s   *t* = 1.0 s   *t* = 2.5 s   *t* = 6.0 s

(b)

t = 0.0 s   *t* = 1.0 s   *t* = 2.5 s   *t* = 6.0 s

Displacement in Y-direction [mm]

-30 -20 -10 10 20 30
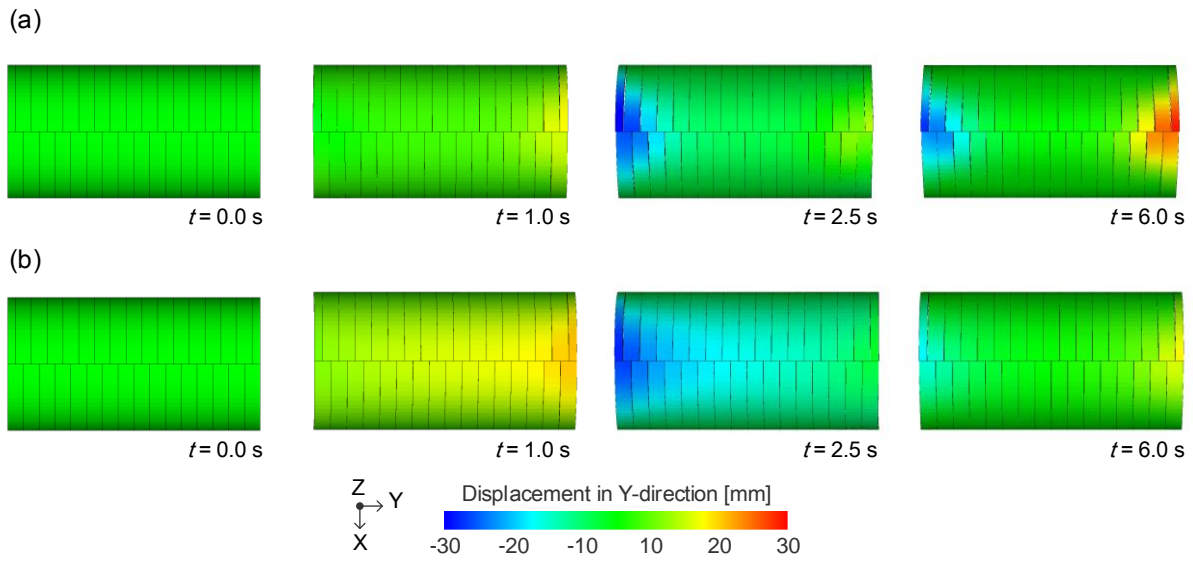
Figure 6.17: Transition of displacement in Y-direction of culverts in (a) Case-1$_S$ and (b) Case-2$_S$.
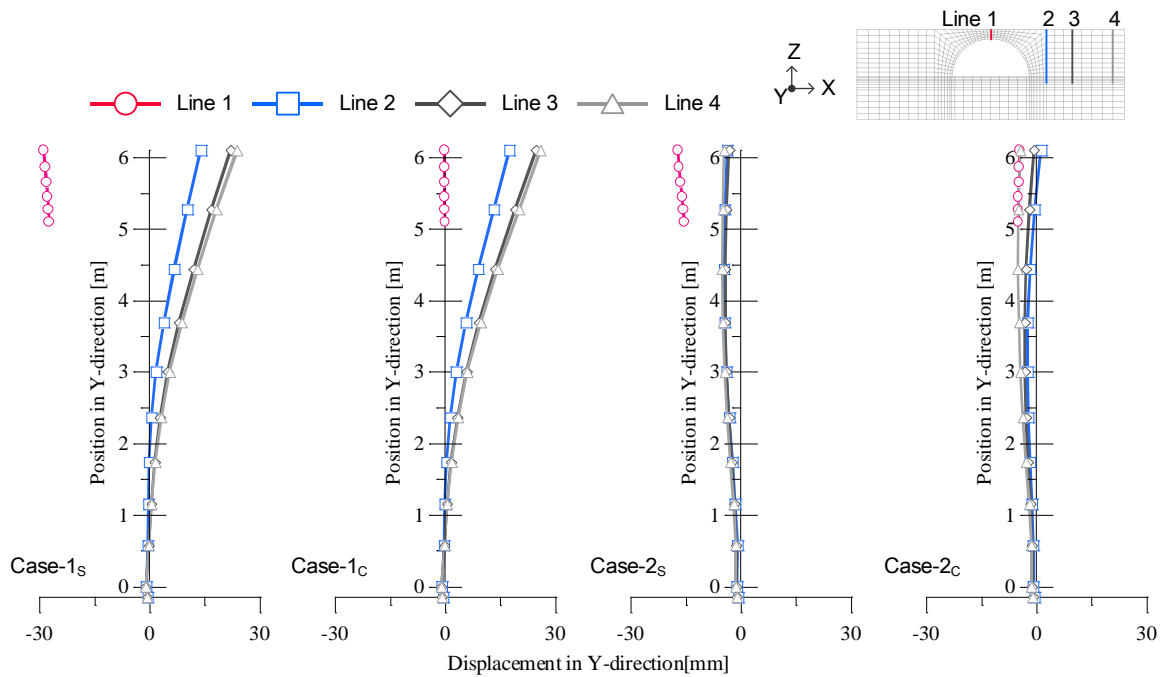
Figure 6.18: Distribution of wall displacement in Y-direction after excitation in (a) Case-1$_C$, (b) Case-1$_C$, (c) Case-2$_S$, and (d) Case-2$_C$.

was smaller in the separated condition than in the connected condition. In short, the increased wall displacement in the separated condition was mainly caused by the deformation of the culvert, but also slightly caused by the reduction in the confining stress of the soil.

From the above results, the separated condition of the culverts was seen to cause the larger deformation of the embankment, particularly near the culverts, compared with the connected condition due to the deformation of the culverts.
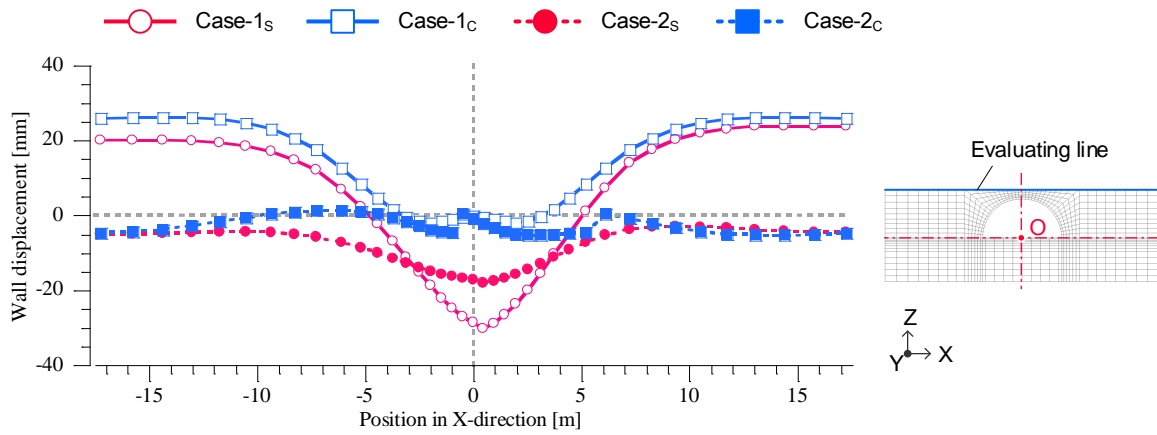
Figure 6.19: Distribution of wall displacement in Y-direction along top of mouth wall of culvert after excitation.
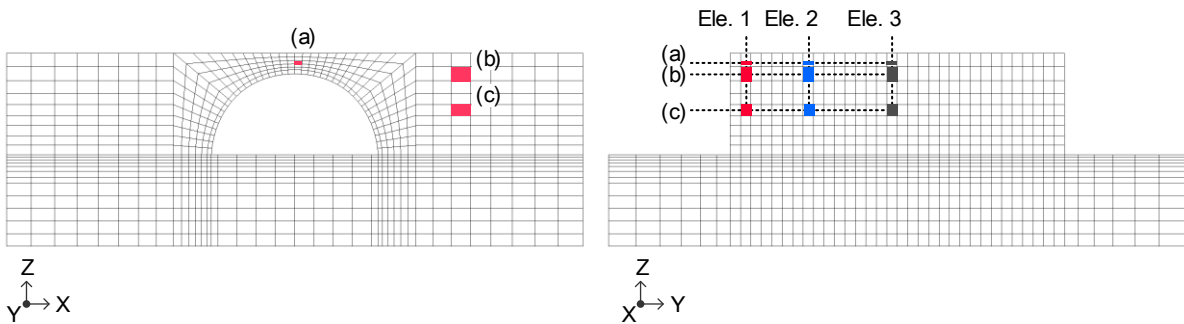
Figure 6.20: Location of the evaluating elements in Figures 6.21-24.
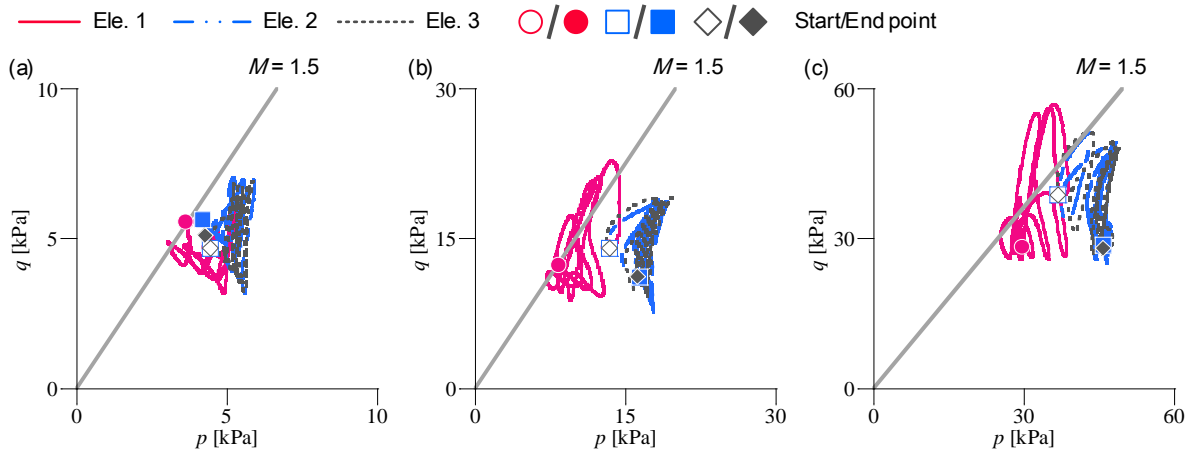
Figure 6.21: Stress path in Case-1$_S$: (a) elements near mouth wall of culvert, (b) elements at center of mouth wall and center of embankment, and (c) elements at center of embankment.

6.5.2 Seismic behavior of culverts

Figures 6.25(a)-(d) show the time histories of the response displacement in the Y-direction at the arch crown. From the figures, both Case-1$_S$ and Case-2$_S$ show amplified magnitude in the negative direction at Ring 1 located at the mouth of the culvert. Significantly, in Case-1$_S$, which has a smaller overburden, the difference in magnitude due to the position was clear, especially near the mouth of the culvert.
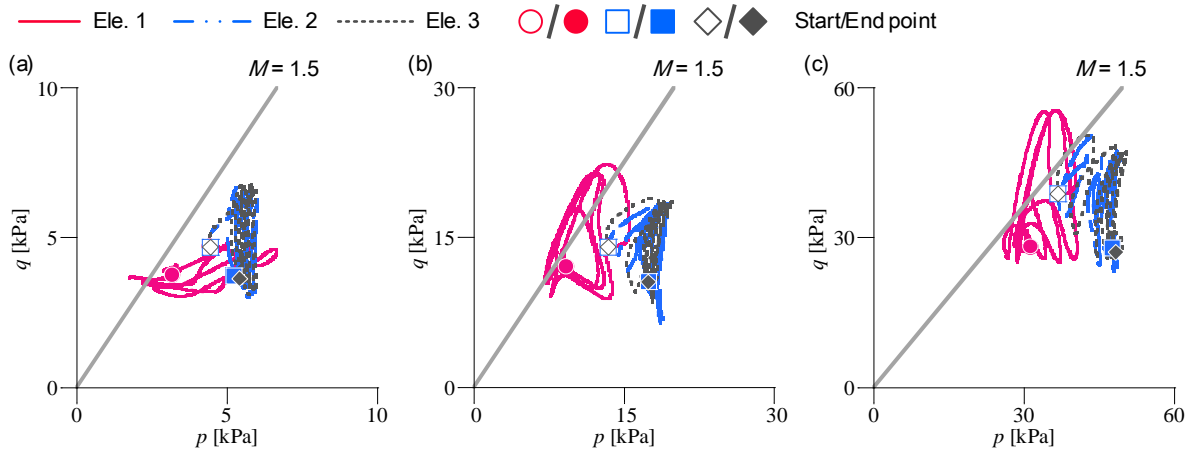
Figure 6.22: Stress path in Case-1$_C$: (a) elements near mouth wall of culvert, (b) elements at center of mouth wall and center of embankment, and (c) elements at center of embankment.
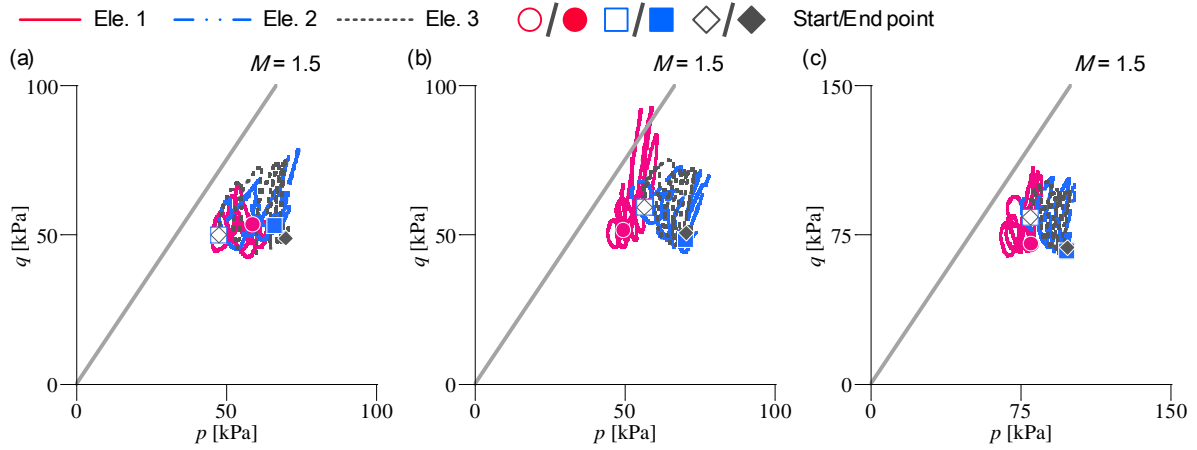
Figure 6.23: Stress path in Case-2$_S$: (a) elements near mouth wall of culvert, (b) elements at center of mouth wall and center of embankment, and (c) elements at center of embankment.
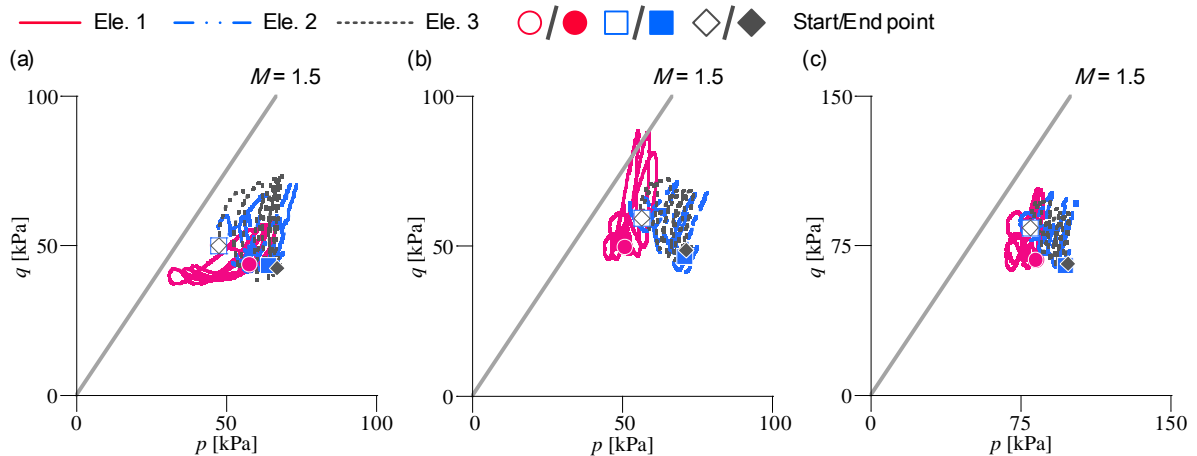
Figure 6.24: Stress path in Case-2$_C$: (a) elements near mouth wall of culvert, (b) elements at center of mouth wall and center of embankment, and (c) elements at center of embankment.
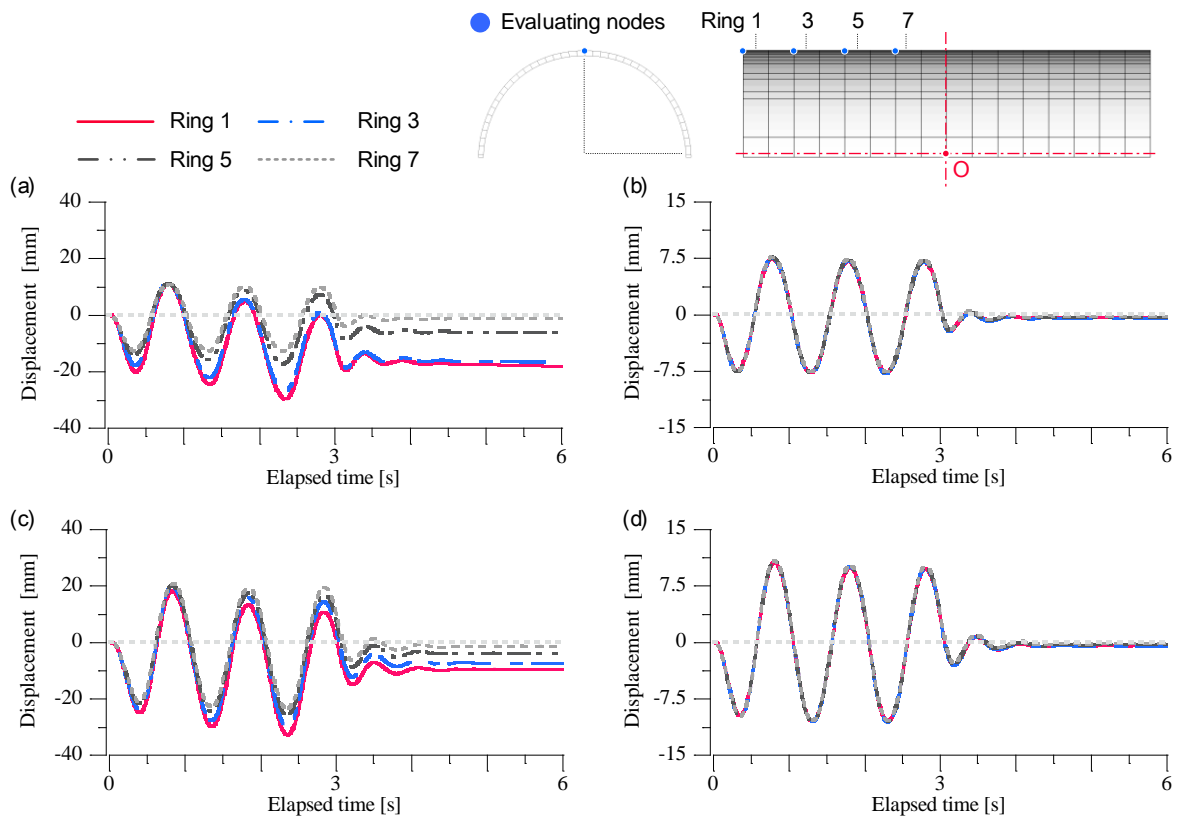
Figure 6.25: Time histories of response displacement in Y-direction at arch crown in (a) Case-1_S, (b) Case-1_C, (c) Case-2_S, and (d) Case-2_C.
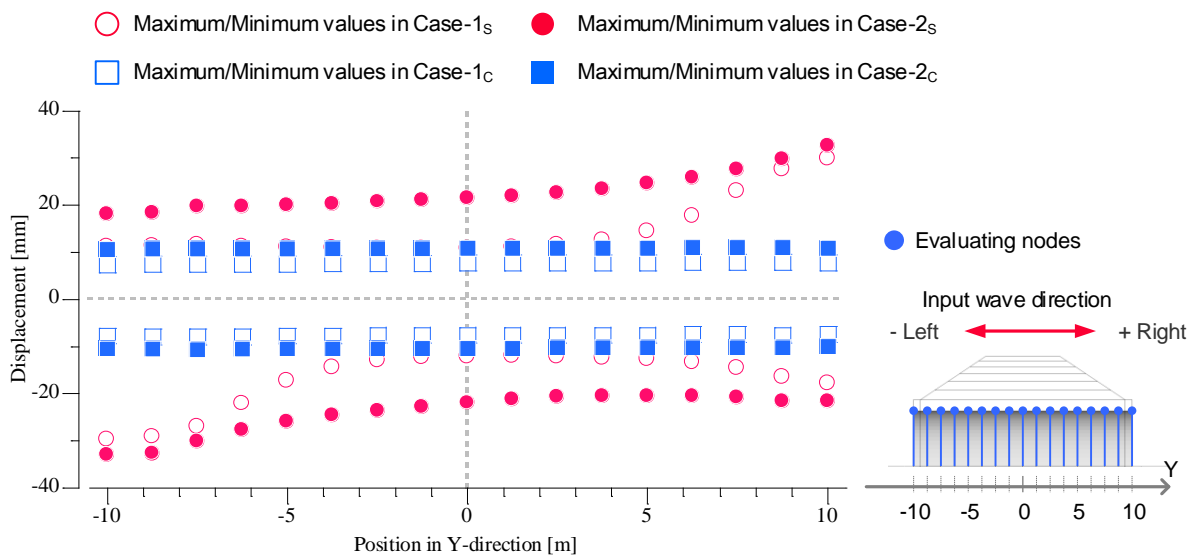
Figure 6.26: Maximum response displacement in Y-direction at arch crown of each arch member.

Additionally, the residual value of the spring's displacement increased in Case-1_S. Conversely, Case-1_C and Case-2_C show united behavior at each position. Hence, the maximum response displacements at half of all the arch members were plotted in Figure 6.26. From the figure, the maximum response displacement of both Case-1_S and Case-2_S exceeded that of both Case-1_C and Case-2_C in the direction
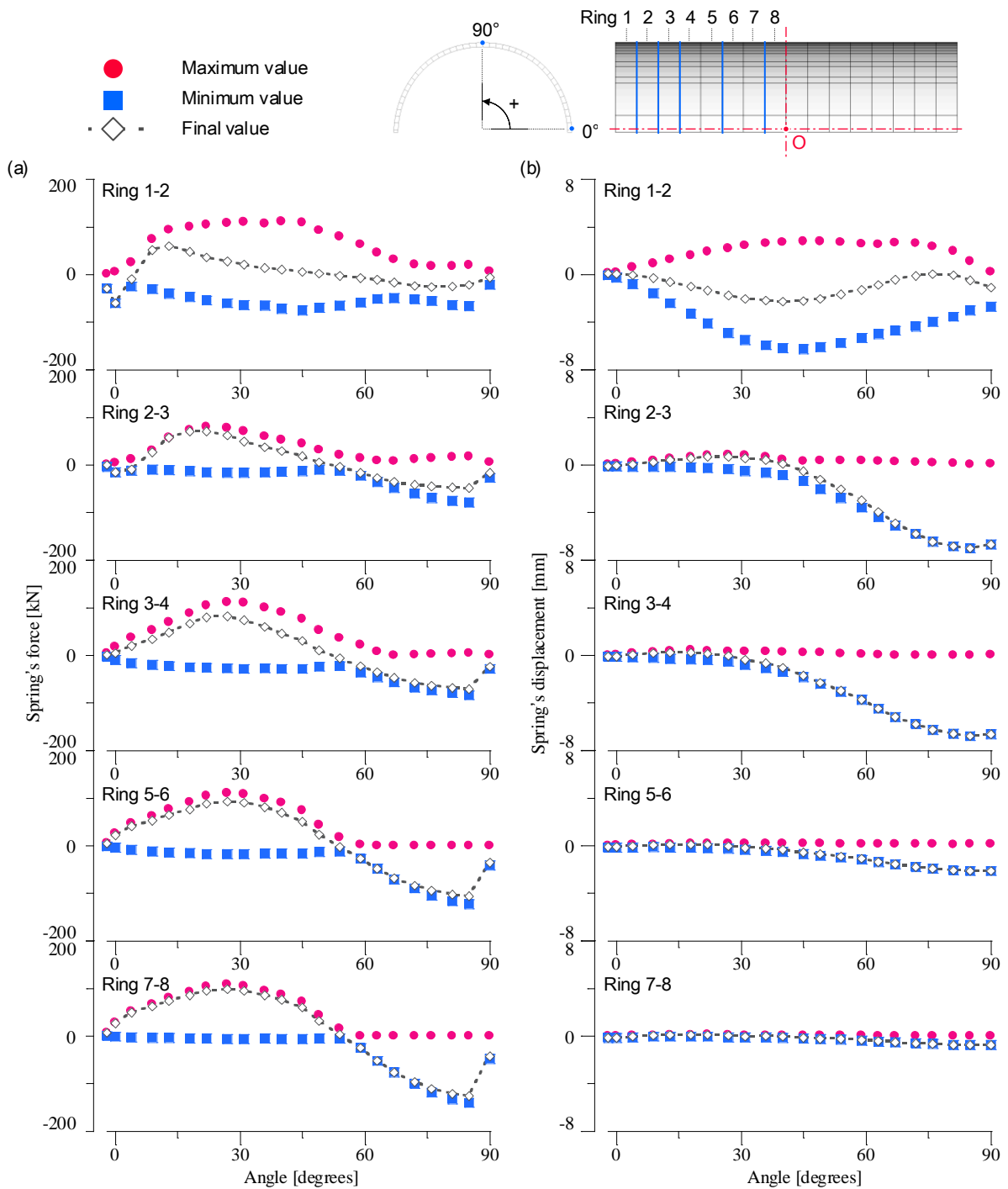
Figure 6.27: Distribution of (a) spring's force in Case-1$_C$ and (b) spring's displacement in Case-1$_S$.

which is from the mouth wall to the outside, and increased at positions closer to the mouth of the culvert. Additionally, in Case-1$_S$, the gradient of the magnitude of the displacement at the arch members near the mouth of the culvert grew larger compared with Case-2$_S$. This is because the smaller overburden of the culvert at the mouth of the culvert caused the smaller confining stress acting on the culvert from the surrounding ground. As a result, the response displacement of the arch members at the mouth of the culvert seems to be amplified and the residual values of the response displacement remain larger. This
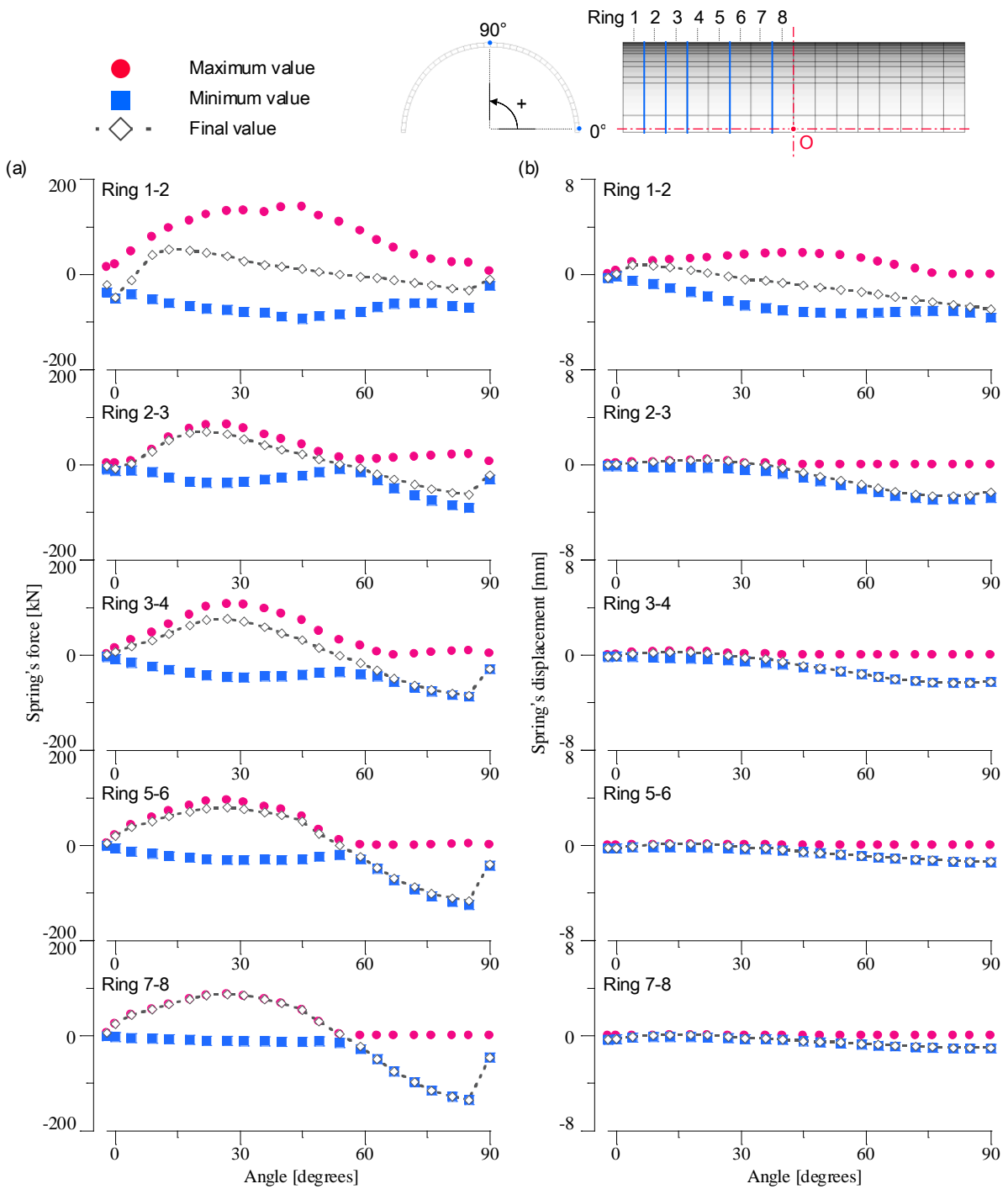
Figure 6.28: Distribution of (a) spring's force in Case-2$_C$ and (b) spring's displacement in Case-2$_S$.

tendency in the response behavior was observed in the dynamic centrifuge tests considering the patterns of overburden addressed in Chapter 5.

To discuss the seismic behavior of the longitudinal structural connection of the culverts, the spring's forces and displacements are plotted in Figure 6.27 and Figure 6.28. The figures show the maximum value, minimum value, and final value due to the seismic wave of the spring's forces and displacements. From the figures, except for the results between Ring 1 and Ring 2, the tensile force and
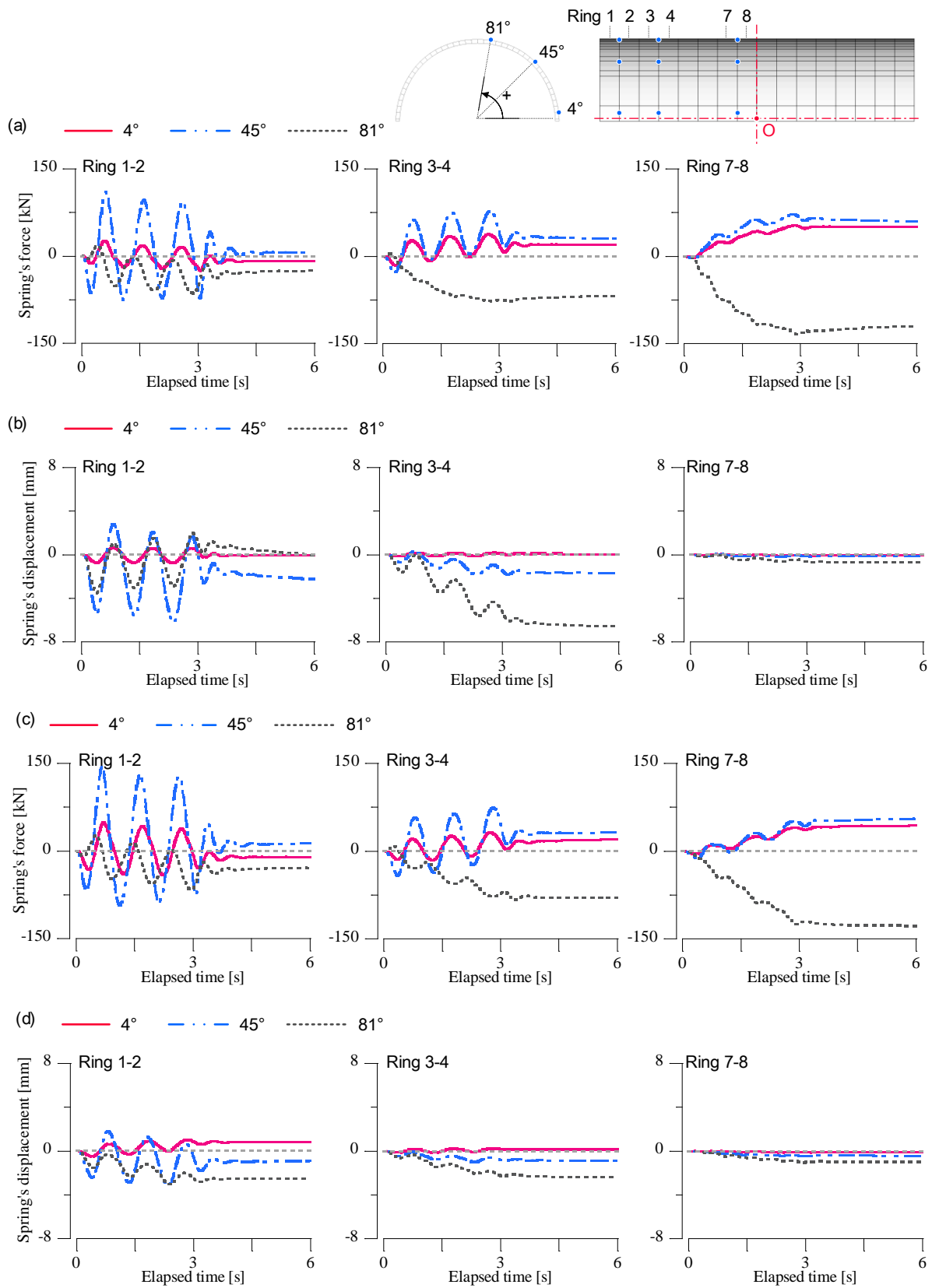
Figure 6.29: Time histories of spring's force and spring's displacement in (a) Case-1c, (b) Case-1s, (c) Case-2c, and (d) Case-2s.
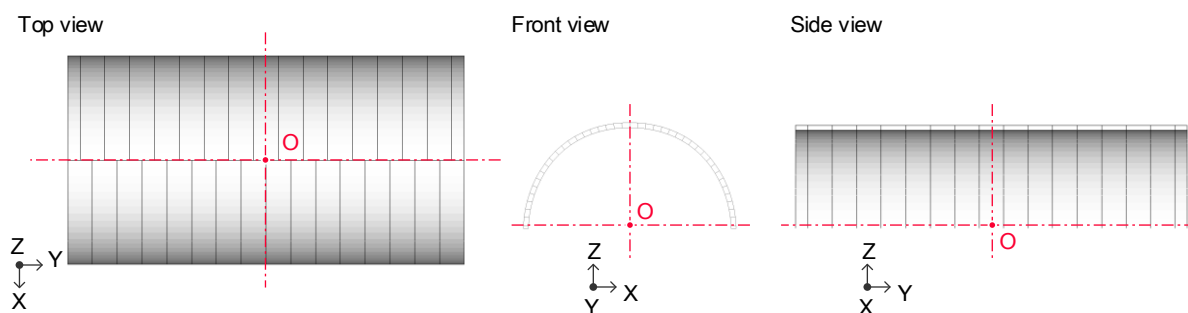
Figure 6.30: Origin of coordinates in present analysis.

the aperture of the culverts mainly occurred in higher positions than the half height of the arch culvert. Additionally, the intersections of the rings, except for Ring 1-2 in Case-1$_S$, showed larger final values compared with Case-2$_S$. From the time histories of the spring's forces and displacements, as shown in Figure 6.29, the tensile force and the aperture of the culvert clearly occurred near the arch crown. These tendencies correspond to the deformation of the culvert shown in Figure 6.29. The increase in overburden caused the higher tensile force in the intersection of the culverts in the connected condition. However, the aperture of the culverts in the separated condition showed a larger value in Case-1$_S$ compared to Case-2$_S$. This tendency matches the response displacement of the arch crown.

From the above results, it is understood that the displacements of arch members are likely to occur in locations under a small overburden where the confining stress from the embankment is weak. Thereby, apertures will appear in culverts whose arch members have a small overburden.

6.5.3 Stress condition of arch culverts

In the Great East Japan Earthquake, characteristic damage, such as continuous chipping of the arch crowns and bending cracks, occurred to the culverts (refer to Figure 2.6). Therefore, for Case-1 and Case-2, the stress conditions during excitation are summarized. Figure 6.30 shows the origin of the coordinates in the present analysis mesh for understanding the direction of the shear stress. Figures 6.31 - 6.33 show the shear stresses occurring in the arch culverts during excitation.

Here, τ_{xy} is the stress that causes the shear deformation in the culvert longitudinal direction in the X-plane. From Figure 6.31, when focusing on the arch crown, τ_{xy} seems to be correlated with the displacements in the Y-direction in both cases. In Case-1$_S$ and Case-2$_S$, stress concentration occurred at the corner of the arch crown near the mouth of the culvert. In Case-1$_C$, Case-2$_C$, and Case-2$_S$, the higher stress distribution of τ_{xy} appeared in the arch members near the mouth. As for Case-1$_C$, the connected condition caused the higher stress concentration. As for Case-2$_S$ and Case-2$_C$, the increase in overburden simply seems to be proportional to the magnitude of the stress.

Here, τ_{zx} is the stress causing the shear deformation in the culvert transverse direction. From Figure 6.32, although τ_{xy} was concentrated on the arch shoulders or the arch crowns in both cases, the areas of stress concentration were different. Both Case-1$_S$ and Case-2$_S$ showed stress concentration occurring on each of the arch members. Conversely, Case-1$_C$ and Case-2$_C$ resist the shear force of all the arch members compared to Case-1$_S$ and Case-2$_S$. In this way, the stress condition of the arch members is different in terms of how the shear force is resisted due to the longitudinal structural
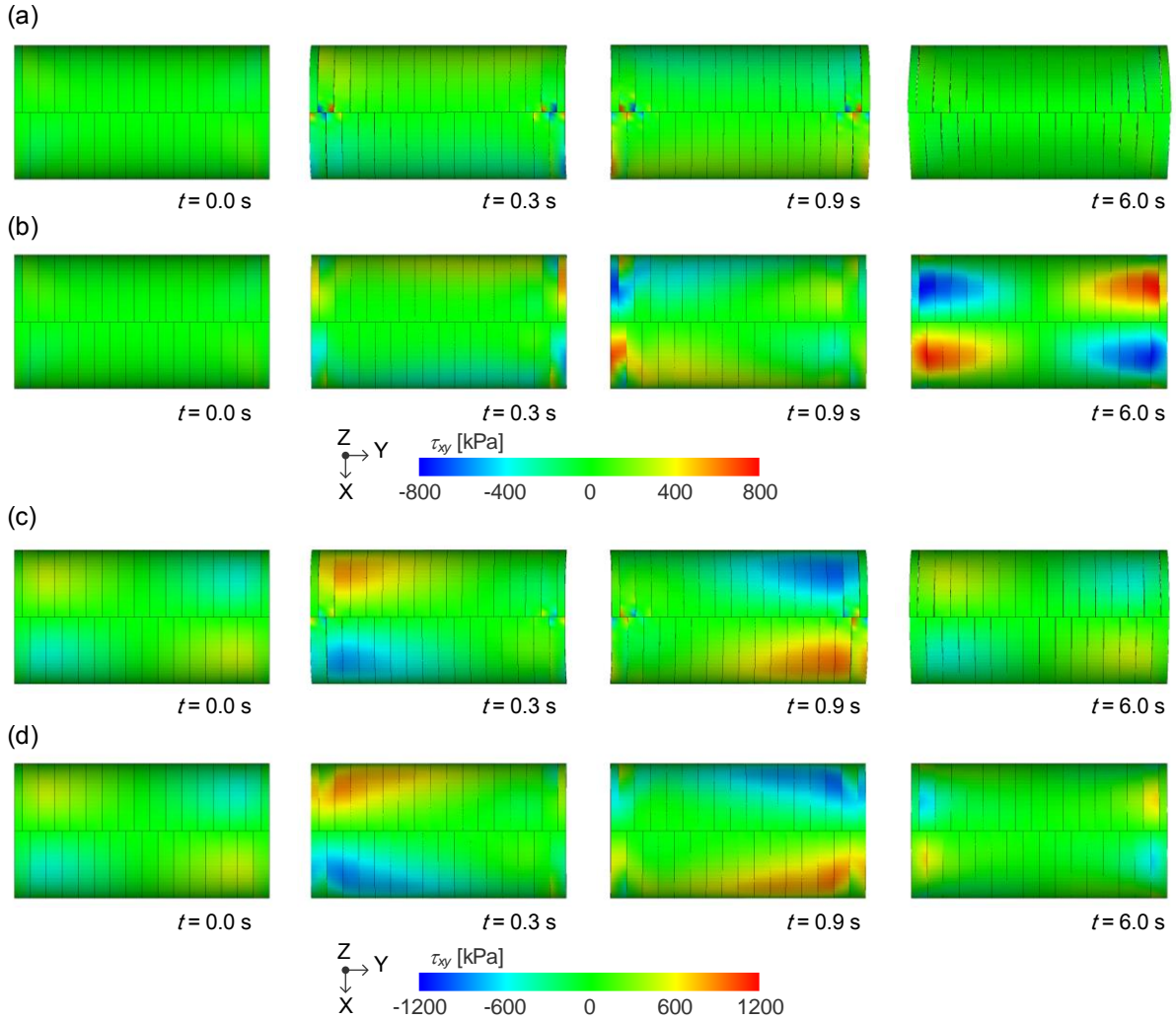
Figure 6.31: Heat map of τ_{xy} on arch crown cross section in (a) Case-1$_S$, (b) Case-1$_C$, (c) Case-2$_S$, and (d) Case-2$_C$.

connectivity.

Here, τ_{yz} is the stress causing the shear deformation in the culvert longitudinal direction in the Z-plane. From Figure 6.33, it is seen that the stress concentration occurred at the feet of the arch members in all cases during excitation. This is because the embankment deformation due to the culvert longitudinal earthquake, observed in Figure 6.14, caused the shear stress of the culvert cross section. Especially in Case-2$_S$ and Case-2$_C$, larger shear stress occurred along the direction of excitation on each of the arch members. The difference between the areas of shear stress concentration appeared as the confining stress of the culverts from the embankment due to the difference in overburden between Case-1 and Case-2.

From the above results, connecting the culverts seems to cause the amplification of the cross-section force along the culvert longitudinal direction because all the arch members resist the shear force. In the connected condition, the local concentration of shear stress on all the arch members will occur, but in the separated condition, the arch members will independently resist the shear force, which will induce the stress concentration of each arch member.
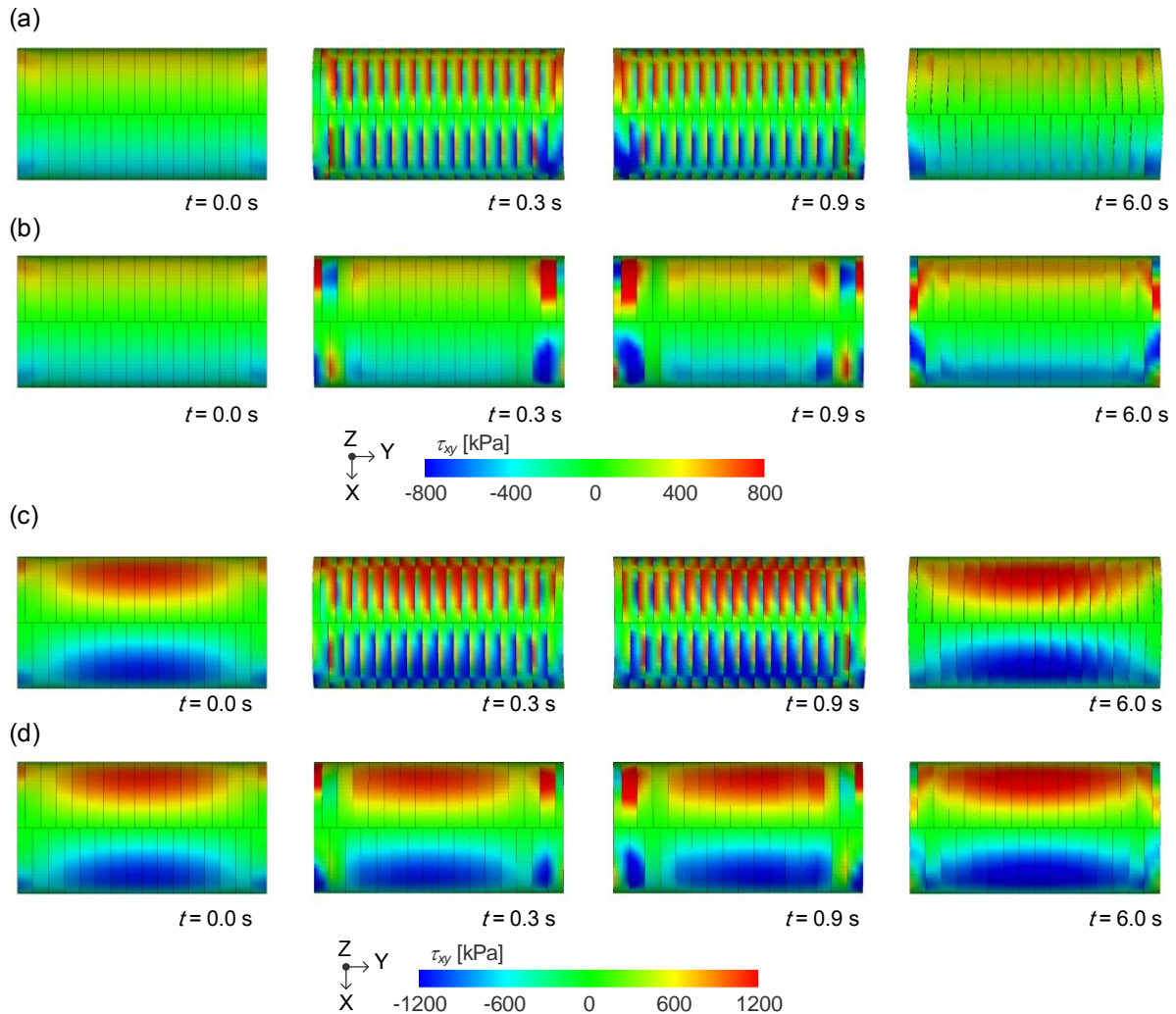
Figure 6.32: Heat map of τ_{zx} on arch crown cross section in (a) Case-1$_S$, (b) Case-1$_C$, (c) Case-2$_S$, and (d) Case-2$_C$.

6.6 Conclusions

In this chapter, 2D and 3D dynamic FEM analyses were conducted to develop a new evaluation method for the seismic performance of precast arch culverts in the culvert longitudinal direction. The obtained results are shown below.

2D dynamic analysis results

1) Bilinear spring elements were applied for structural connectivity in the FEM dynamic analysis. Then, the apertures of the culverts due to the deformation of the embankment could be expressed.

2) In the separated case, the embankment deformation became larger than that of the connected case, which matches the trend appearing in the observed deformation through dynamic centrifuge tests considering the structural connectivity of culverts.

3) The influence of the longitudinal inertial force on the structural connection became larger near the mouth of the culverts. Additionally, the influence of the embankment deformation on the structural connection was found to be critical at the culverts under the slope of the embankment.

(a)

$t = 0.0$ s $t = 0.3$ s $t = 0.9$ s $t = 6.0$ s

(b)

$t = 0.0$ s $t = 0.3$ s $t = 0.9$ s $t = 6.0$ s

Z
X → Y τ_{yz} [kPa]
-800   -400   0   400   800

(c)

$t = 0.0$ s $t = 0.3$ s $t = 0.9$ s $t = 6.0$ s

(d)

$t = 0.0$ s $t = 0.3$ s $t = 0.9$ s $t = 6.0$ s

Z
X → Y τ_{yz} [kPa]
-1200   -600   0   600   1200

Figure 6.33: Heat map of τ_{yz} on inner side of arch members cross section in (a) Case-1s, (b) Case-1c, (c) Case-2s, and (d) Case-2c.

3D dynamic analysis results

1) The difference in overburden appears as a difference in the confining stress acting on the culverts. Three-hinged arch culverts with a small overburden are likely to suffer damage related to the displacement of the arch members such as apertures in the arch members. On the other hand, culverts with a large overburden are likely to suffer damage to the arch members themselves due to the increase in shear stress which is dependent on the overburden depth.

2) The separated condition of the culverts causes the larger deformation of the embankment, particularly near the culverts, compared with the connected condition, due to the deformation of the culverts. This mainly results from the deformation of the culverts due to the decrease in the longitudinal shear stiffness.

3) In the connected condition, the connected culverts resist the shear force with all the arch members; this induces the local concentration of the shear stress on all the arch members. In the separated condition, however, the arch members independently resist the shear force; this induces the stress concentration of each arch member.

References

Abe, T. and Nakamura, M. (2014) *The use of and the caution in the application of the culvert constructed by large pre-cast element in the expressway construction*, The Foundation Engineering & Equipment, Monthly, Vol. 42, No. 4, pp. 8-11. (in Japanese)

Association of Modularch Construction Method (2017): *Engineering Manual for Modularch*, *Geo-Research Institute* (in Japanese).

Hokyodo net service: Construction examples of Techspan construction method (access on 2014/10/10): https://www.hokyodo.jp/2_pa/frame.html (in Japanese)

T. J. R. Hughes, R. L. Taylor, J. L. Sackman, A. Curnier and W. Kanoknukulchai. (1976): A Finite Element for a Class of Contact-Impact Problems, Computer Methods in Applied Mechanics and Engineering, Vol. 8, pp. 249-276.

Investigative Committee of Manual for the Design and Construction of Techspan Construction Method (1998): *Manual for the Design and Construction of Techspan Construction Method (Draft)*, *Advanced Construction Technology Center* (in Japanese).

Japan Road Association (2012): *Specifications for Highway Bridges Vol. V: Seismic Design* (in Japanese).

Sawamura, Y., Matsushita, R., Kishida, K., and Kimura, M. (2017): Evaluation of mechanical behavior of two-hinge precast arch culvert in construction process and its seismic damage morphology through strong earthquake response experiments, *Japanese Geotechnical Journal*, Vol. 15, No. 4, pp. 385-396 (in Japanese). doi.org/10.3208/jgs.12.385

Suzuki, N. and Toi, Y. (1987): Finite Element Analysis of Dynamic Frictional Contact Problems by Using the Penalty Function Method -Consideration on the Penalty Numbers and its Application to the Friction-Excited Vibration Problem-, *Journal of the Society of Naval Architects of Japan*, No. 162, pp. 364-373. doi.org/10.2534/jjasnaoe1968.1987.162_364 (in Japanese)

Technological Examination Committee of Techspan Construction Method (2014): *Comparison Outline of Revised Items in Manual for the Design and Construction of Techspan Construction Method (Draft)*, *Advanced Construction Technology Center* (in Japanese).

Zhang F., Ye, B., Noda, T., Nakano, M. And Nakai, K. (2007): Explanation of cyclic mobility of soils, Approach by stress-induced anisotropy, *Soil and Foundations*, Vol. 47, No. 4, pp. 635-648. dx. doi.org/10.3208/sandf.47.635

Zienkiewicz, O. C., (1977): The Finite Element Method, McGraw-Hill.

Chapter 7 Discussion of damage mechanism of three-hinged arch culverts during the Great East Japan Earthquake

7.1 Introduction

From the previous chapters, the longitudinal seismic behavior of the hinge type of precast arch culvert was discussed through the dynamic centrifuge test and the dynamic FEM analysis. The applicability of the 3D elasto-platic FEM analysis in the longitudinal seismic behavior was confirmed in Chapter 6. Therefore, with the methodology of the experiments and numerical analysis, in this chapter, the mechanism of seismic damage to the three-hinged arch culverts during the Great East Japan earthquake is discussed.

7.2 Seismic damages due to torsional deformation

7.2.1 Characteristics of damage patterns of old-type three-hinged arch culvert

After the Great East Japan earthquake, the damage mechanism of the three-hinged arch culverts was studied based on the field study and the analytical study. Fujiwara et al. (2017) focused on the effect of overburden on the damage of the three-hinged arch culverts based on the damage investigation for 8 three-hinged arch culverts. Figure 7.1 summarized the results of their investigation. As shown in the figures, Fujiwara et al. assumed culvert damages were induced by the continuous inclination in the longitudinal direction of the arch members. Due to the inclination of the arch members, the stress concentration along the vertical direction occurred in the corner of the arch members. However, they could not find the clear contribution of the maximum overburden to the edge defect of the arch members.

Based on the investigation of Fujiwara et al. (2017), Nakamura et al. (2018) conducted the 3D elasto-plastic FEM analysis for the three-hinged arch culverts. They modeled the three-hinged arch culverts in 3D FEM and conducted the static analysis. The applied load was calculated by the dynamic analysis of the 2D model of the culvert longitudinal direction considering the embankment shape. Figure 7.2 summarized the assumed damage to the three-hinged arch culverts and the analysis result. From Figure 7.2, they reproduced the stress concentration on the corner of the arch members correlated with the edge defect of the arch crown by applying the longitudinal displacement to the three-hinged arch culverts. Additionally, the circumferential stress state of the arch members showed the uneven stress distribution, which seems to induce the bending crack of the arch members. They concluded that the effective countermeasure to decrease the degree of the seismic damage in the culvert longitudinal direction was to restrict the longitudinal displacement of the arch members. However, the damage to the foot of the arch member shown in Figure 7.2 was not clearly explained.

7.2.2 Analytical approach to torsional deformation of three-hinged arch culvert

As mentioned above, the damage to the arch members were well discussed including the damage mechanism and the reproduction of the damage stated through the FEM analysis. However, the mechanism of the damage to the mouth wall and the concrete foundation are still unclear. As Abe and Nakamura (2014) mentioned, the distinctive damages to the arch members seems to be caused by the
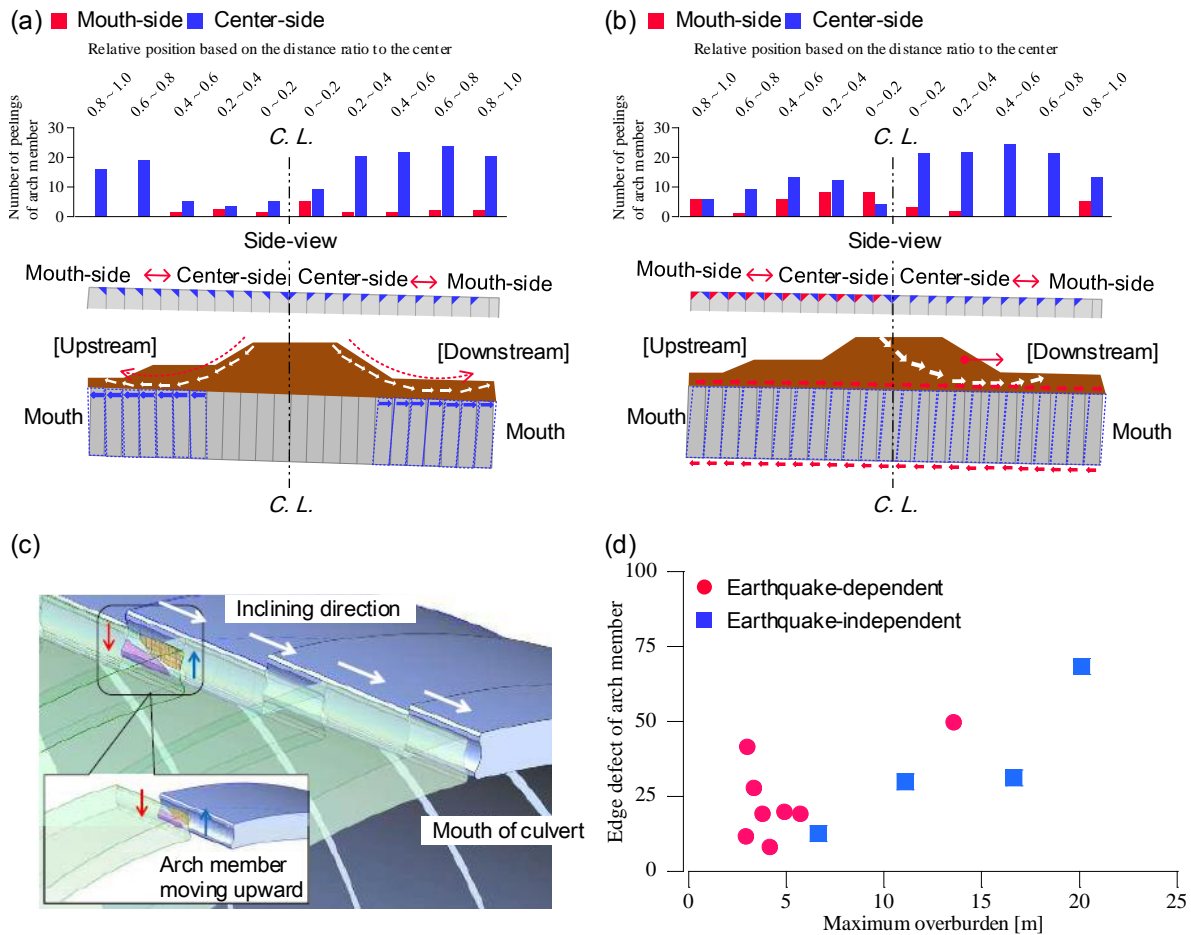
Figure 7.1: Study of seismic damage to three-hinged arch culverts during the Great East Japan earthquake by Fujiwara et al. (2017): (a) Schematic figures of trend of edge defect of arch members in normal condition and (b) after earthquake, (c) a schematic figure of generating edge defect and (d) relation between number of edge defect and maximum overburden.
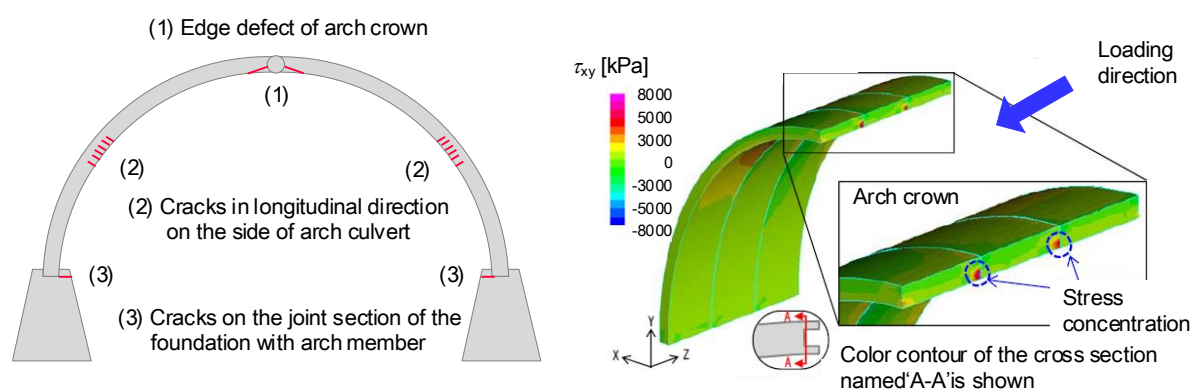
Figure 7.2: Study of damage to three-hinged arch culverts due to the longitudinal seismic behavior by Nakamura et al. (2018): (a) Schematic figures of damage classification due to the Great East Japan earthquake (b) degree of shear stress by static FEM analysis in culvert longitudinal direction.

torsional deflections of each of arch members. Additionally, the seismic effect due to the oblique angle of the culvert may induce the uneven deformation of the mouth wall. This is because the uneven inertial
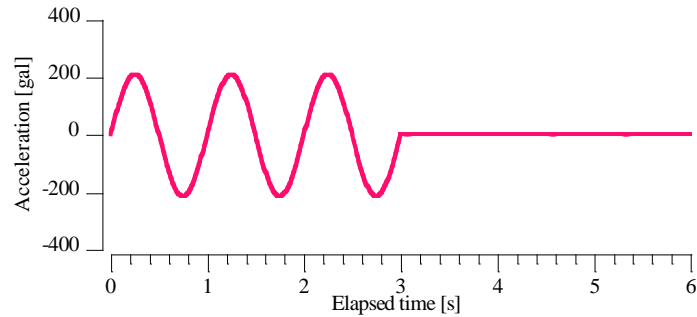
Figure 7.3: Input wave: sin wave with 1 Hz and three cycles.

force of the culvert longitudinal direction is likely to be a trigger of the asymmetrical deformation of the mouth wall.

Therefore, to clarify the mechanism of the seismic damage to the three-hinged arch culverts during the Great East Japan earthquake, this chapter focused on the torsional deformation of the arch members and the seismic effect of oblique angle of the culvert respectively.

The present analysis focused on the seismic behavior in the 45º direction which is assumed to induce the largest torsional deflections of the arch members. In the seismic analyses with the input wave of the 45º direction, the analysis conditions such as analysis mesh (Figure 6.9 and Figure 6.10), mechanical properties of the model, soil-culvert interface and analytical cases were equivalent to the model used in 6.4 except for the input wave direction. The magnitude of input wave direction was 300 gal by adjusting the magnitude of the input wave. Figure 7.3 shows the input wave. In the analysis, the seismic wave was respectively input in X-direction and Y-direction simultaneously on the bottom of the ground foundation, which reproduced the seismic wave in the 45º direction.

7.2.3 Deformation and stress state of culvert

Figures 7.4(a)-(d) show the transition of the settlement of the embankment for all cases. From the figures, the settlement of the embankment was seen to increase in the separated condition compared to the connected condition; this tendency coincident with the results due to the seismic wave in the culvert longitudinal direction. Figures 7.5(a)-(d) show the heat map of the displacements in the Y-direction after the excitation. From the figures, in the separated condition, the wall displacement above the culvert is increased compared to the connected condition. To discuss in detail of the wall displacements, the distribution of wall displacement in the Y-direction for all cases after excitation is shown in Figures 7.6. From the figure, the uneven displacements of the mouth wall are clear in the separated condition. Case-1_S, particularly, showed more uneven deformation of the mouth wall than that of Case-2_S. Figures 7.7 shows the transition of displacements in Y-direction of the culverts in the separated condition. From the figures, the deformation of the culverts of Case-1_S is larger than that of Case-2_S. In short, the magnitude of the uneven deformation of the mouth wall can be increased by the deformation of the culverts.

Figures 7.8(a)-(d) show the time histories of the response displacement in the Y-direction at the arch crown. From the figures, both Case-1_S and Case-2_S show amplified magnitude in the negative direction in the order of Rings 1, 3, 5 and 7. Significantly, in Case-1_S, which has a smaller overburden,
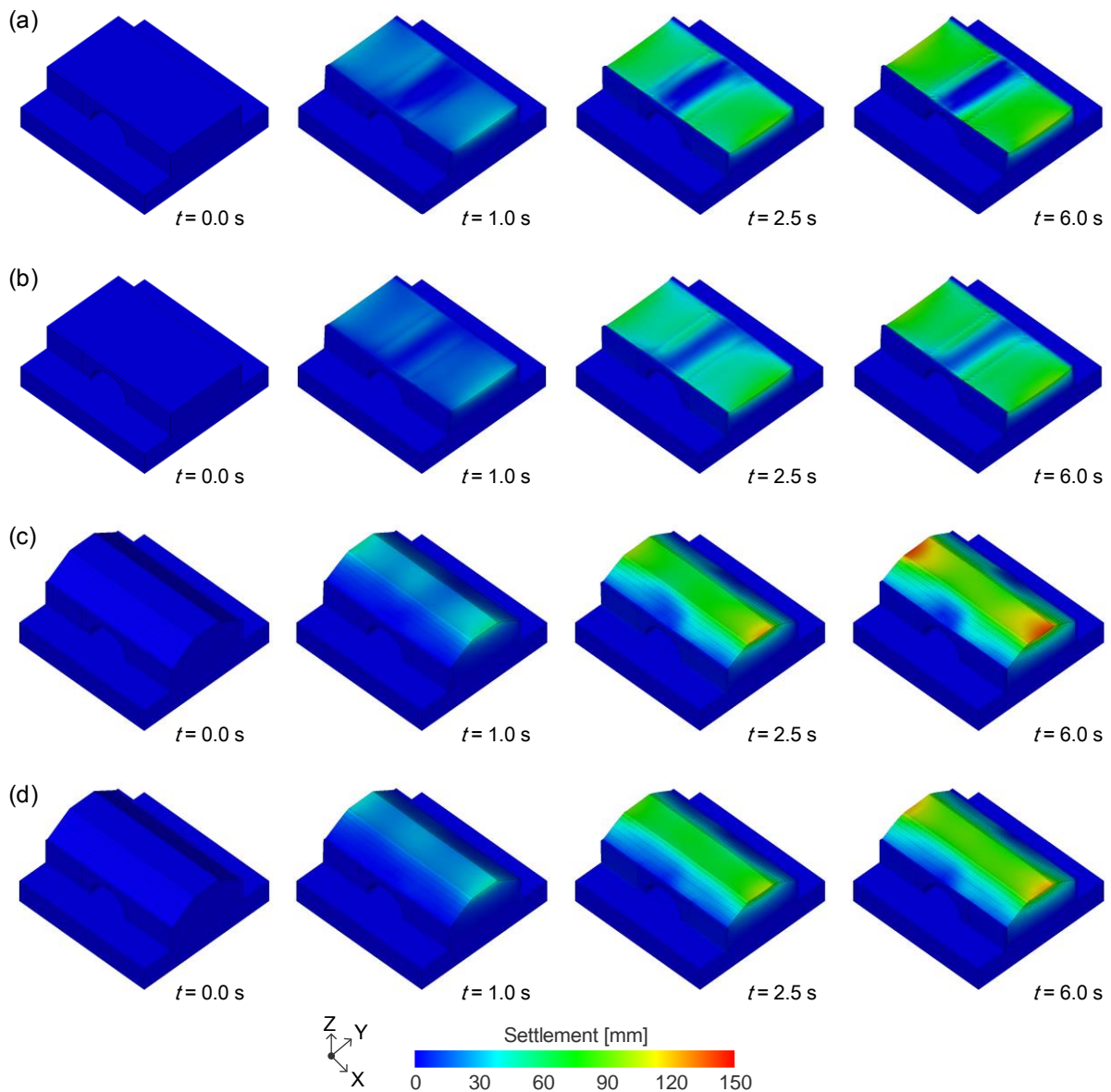
Figure 7.4: Transition of settlement in embankment of (a) Case-1$_S$, (b) Case-1$_C$, (c) Case-2$_S$, and (d) Case-2$_C$.

the difference in magnitude due to the position was clear. The tendency coincident with the results of the seismic behavior in the culvert longitudinal direction. Additionally, the value of the residual displacement was larger in Case-1$_S$ than in Case-2$_S$. Hence, the maximum response displacements at half of all the arch members were plotted in Figure 7.9. From the figure, the maximum response displacement of both Case-1$_S$ and Case-2$_S$ clearly showed the state of the torsional deformation, but it was not seen in Case-1$_C$ and Case-2$_C$; this different patterns of the displacements of the arch culvert induced the different deformation of the mouth wall.

To discuss the damage mechanism of the three-hinged arch culverts due to the torsional deformation, the shear stress state of the culverts is summarized in Figures 7.10 - 7.12. Here, τ_{xy} is the stress that causes the shear deformation in the culvert longitudinal direction in the X-plane. From Figure 7.10, when focusing on the arch crown, in Case-1$_S$ and Case-2$_S$, stress concentration occurred at the
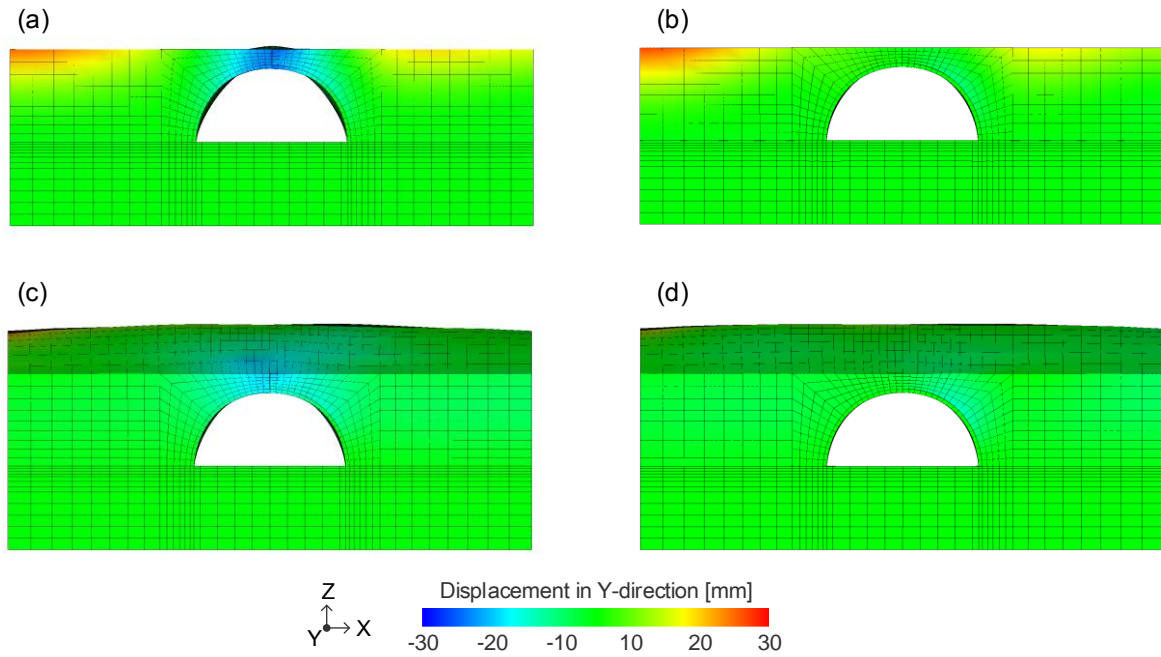
Figure 7.5: Wall displacement in Y-direction of (a) Case-1$_S$, (b) Case-1$_C$, (c) Case-2$_S$, and (d) Case-2$_C$.
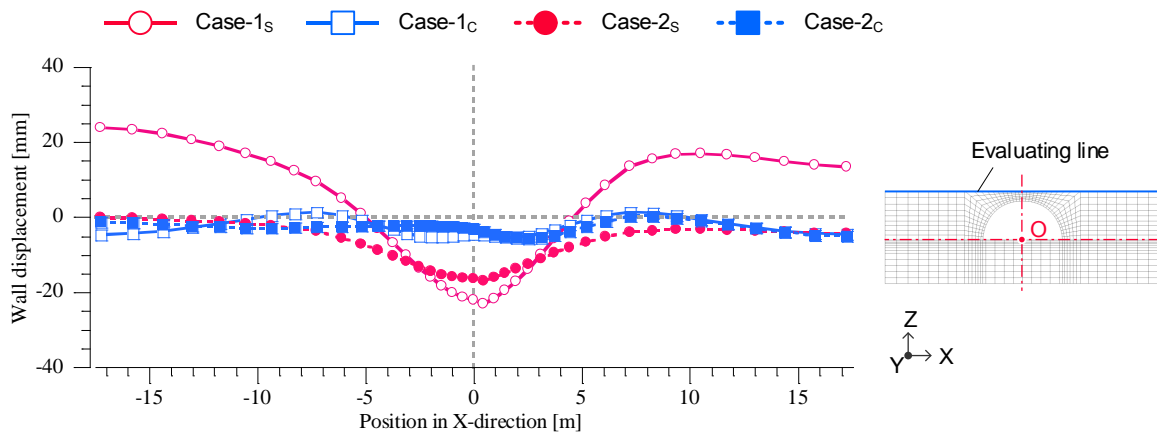
Figure 7.6: Distribution of wall displacement in Y-direction along top of mouth wall of culvert after excitation.

multiple number of the corners of the arch crowns near the mouth of the culvert. In Case-1$_C$ and Case-2$_C$, the higher stress distribution of τ_{xy} appeared in the arch members near the mouth compared to the separated condition; it is due to the longitudinal structural connection. Here, τ_{zx} is the stress causing the shear deformation in the culvert transverse direction. From Figure 7.11, In the connected condition, the difference of the stress level is lower than that in the separated condition during excitation. Moreover, the separated culverts resist this uneven stress by each arch member. This uneven stress level of the arch culverts at both arch shoulders likely to induce the torsional deformation of the culverts.

To discuss the stress concentration which corresponds to the edge defect of the concrete members, the stress state in the detail of the excitation in Case-1$_S$ and Case-2$_S$ is shown in Figure 7.12. Focusing on the result at $t = 0.9$ s and 2.9 s in Figure 7.12(b), the stress concentration on the arch crown and arch foot was simultaneously occurring. This tendency also can be slightly seen in Case-1$_S$.

t = 0.0 s t = 1.0 s t = 2.5 s t = 6.0 s

(b)

t = 0.0 s t = 1.0 s t = 2.5 s t = 6.0 s

Displacement in Y-direction [mm]

-30   -20   -10   10   20   30
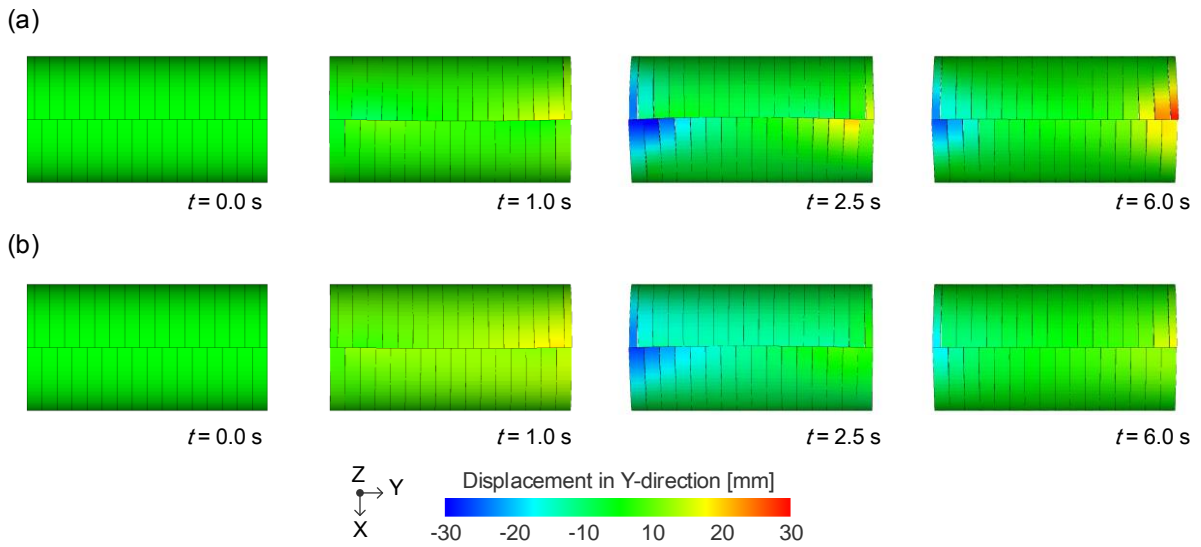
Figure 7.7: Transition of displacement in Y-direction of culverts in (a) Case-1$_S$ and (b) Case-2$_S$.
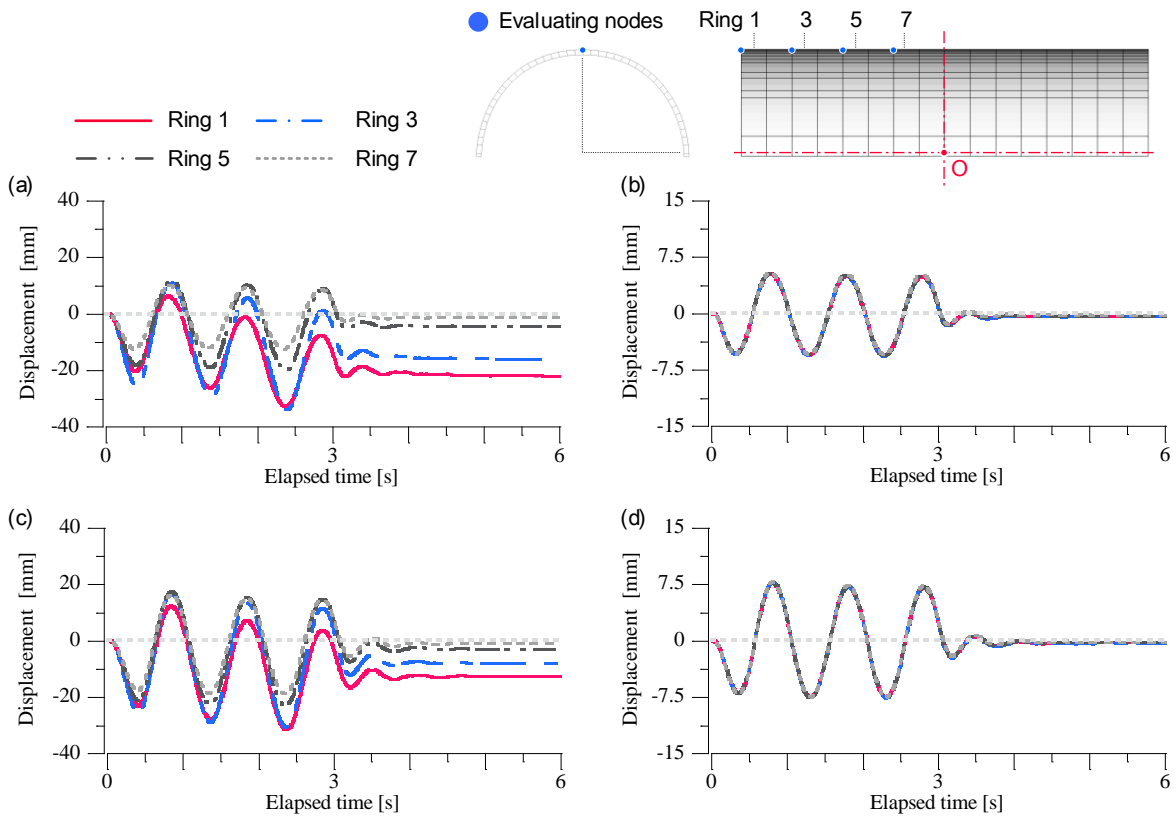
Figure 7.8: Time histories of response displacement in Y-direction at arch crown in (a) Case-1$_C$, (b) Case-1$_C$, (c) Case-2$_S$, and (d) Case-2$_C$.

Figure 7.13 shows the comparison of the obtained stress state in Case-2$_S$ and the assumed damage mechanism by Abe and Nakamura (2014). Focusing on the positional relation between the stress concentration on the arch crown and the arch foot, each of stress concentration location occurred on diagonal lines of the arch members, which proved the clear torsional deformation of the arch members.
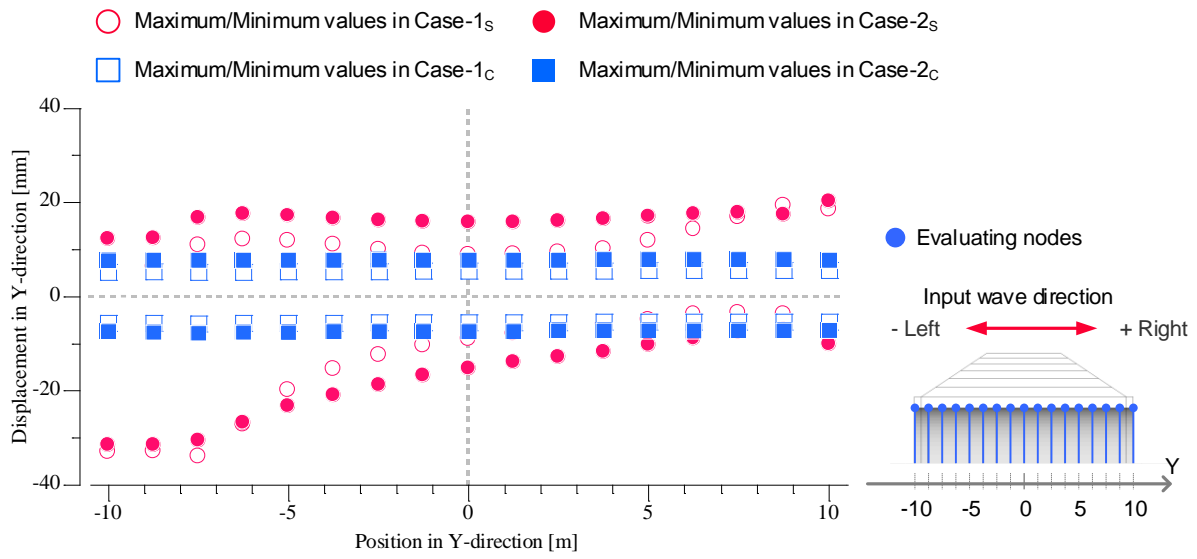
Figure 7.9: Maximum response displacement in Y-direction at arch crown of each arch member.
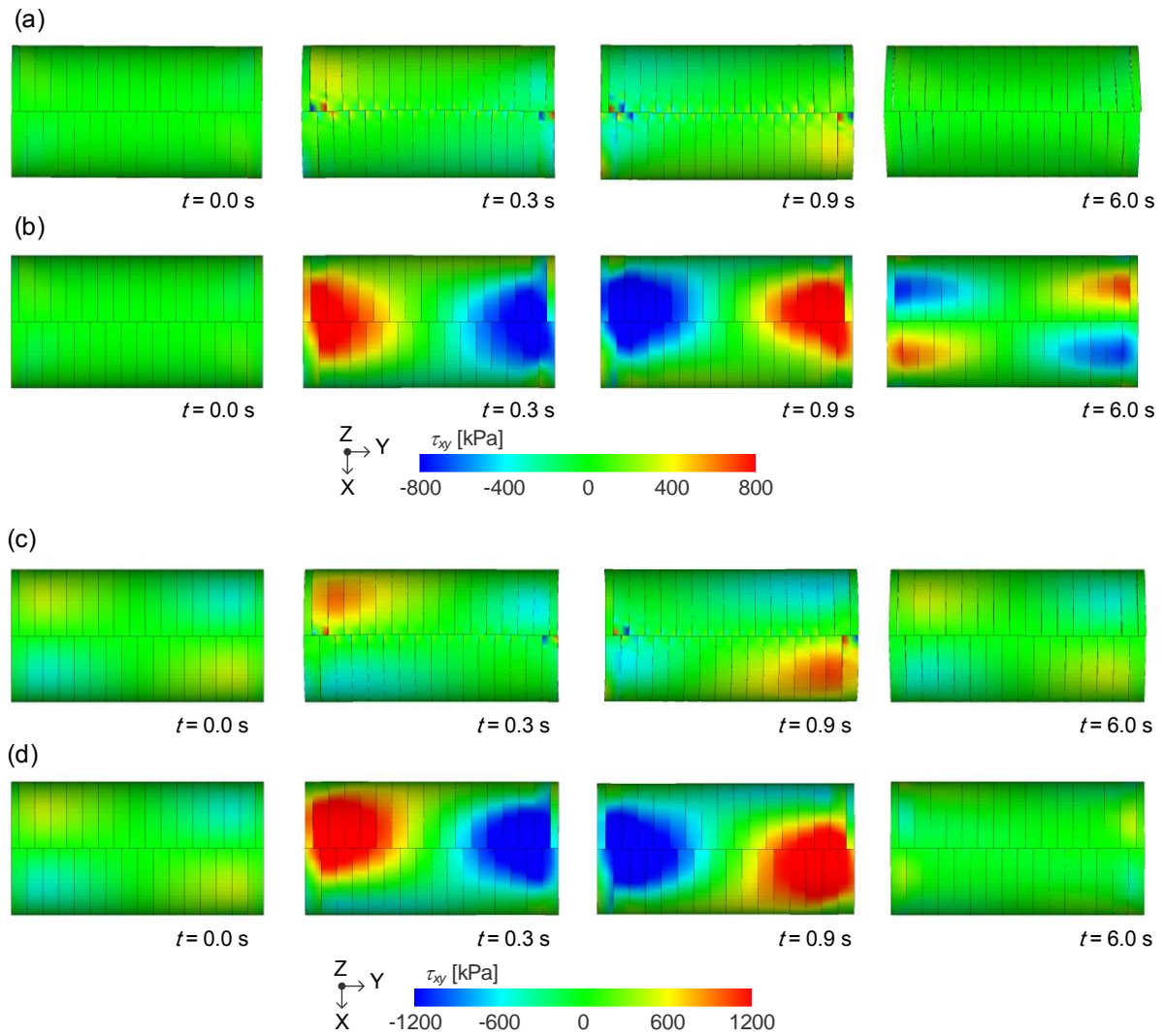
Figure 7.10: Heat map of τ_{xy} on arch crown cross section in (a) Case-1$_S$, (b) Case-1$_C$, (c) Case-2$_S$, and (d) Case-2$_C$.
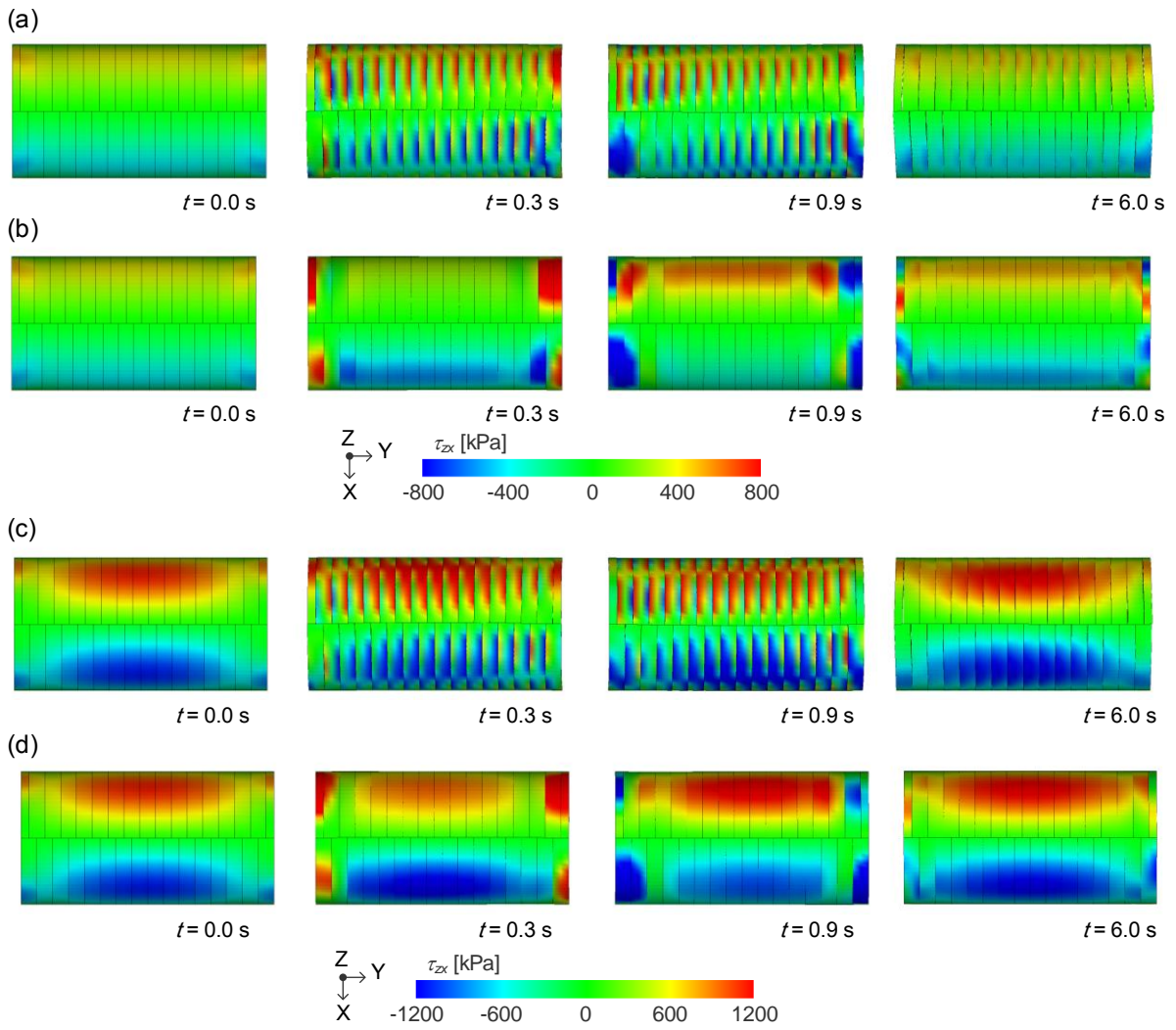
Figure 7.11: Heat map of τ_{zx} on arch crown cross section in (a) Case-1$_S$, (b) Case-1$_C$, (c) Case-2$_S$, and (d) Case-2$_C$.
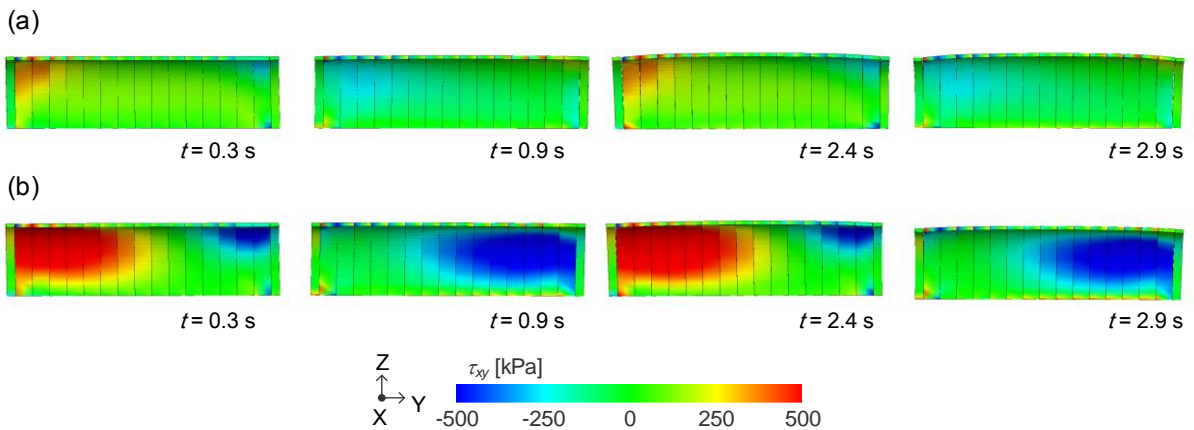
Figure 7.12: Heat map of τ_{xy} on inner side of arch members cross section in (a) Case-1$_S$, (b) Case-1$_C$, (c) Case-2$_S$, and (d) Case-2$_C$.
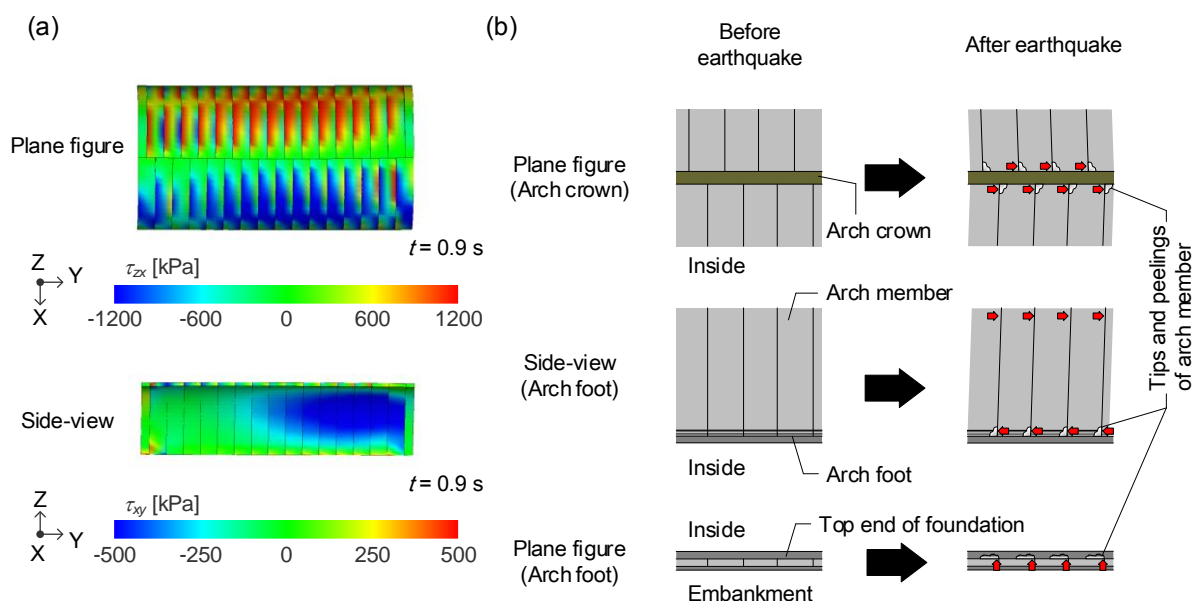
Figure 7.13: Comparison of (a) stress state due to torsional deformation in Case-2s and (b) damage mechanism during the Great East Japan earthquake assumed by Abe and Nakamura (2014).

These stress state in Case-1s and Case-2s match with the damage mechanism suggested by Abe and Nakamura (2014).

The damaged three-hinged arch culvert was old-type and did not have the concrete beam at the arch crown; the combination of this weaker structural connectivity and the torsional deformation of the arch members is likely to induce the specific damages to the arch members such as the edge defect of the arch crown and the concrete foundation.

7.3 Seismic effect of an oblique angle of culverts

7.3.1 Experimental outline

Figure 7.14 shows schematic drawings of the experimental setup and the model of the three-hinged culvert constructed on a wet sand foundation under centrifugal acceleration of 50 G using the rigid soil chamber. The purpose of this experiment is to reproduce the deformation of mouth wall reported by Abe and Nakamura (2014) (Figure 7.14 (a)). The experimental setup is equivalent to the conditions of Chapter 5. Figures 7.14(a), (b), and (c) show the damaged culvert which is the basis for the models and the completed model culverts for Case-Even of a symmetrical overburden and for Case-Uneven of an asymmetrical overburden, respectively. The angle between the model embankment and the culvert in Case-Uneven is 70°, based on the observation of damaged culverts with 60° to 90° angles (Refer to Table 2.2). In the numerical analysis, the accurate modeling of the mouth wall was difficult. Therefore, the dynamic centrifuge test was chosen to reproduce the asymmetrical deformation of the mouth wall.

The mouth wall of three-hinge arch culverts uses a separated wall structure. To consider the structural characteristics of both the mouth wall and the oblique angle condition, the model wall for this experiment was made of two acrylic plates and the reinforcement was modeled with aluminum strips. A continuous tapered 1 Hz wave with 20 cycles of sine waves was applied 10 times, from STEP 1 to STEP
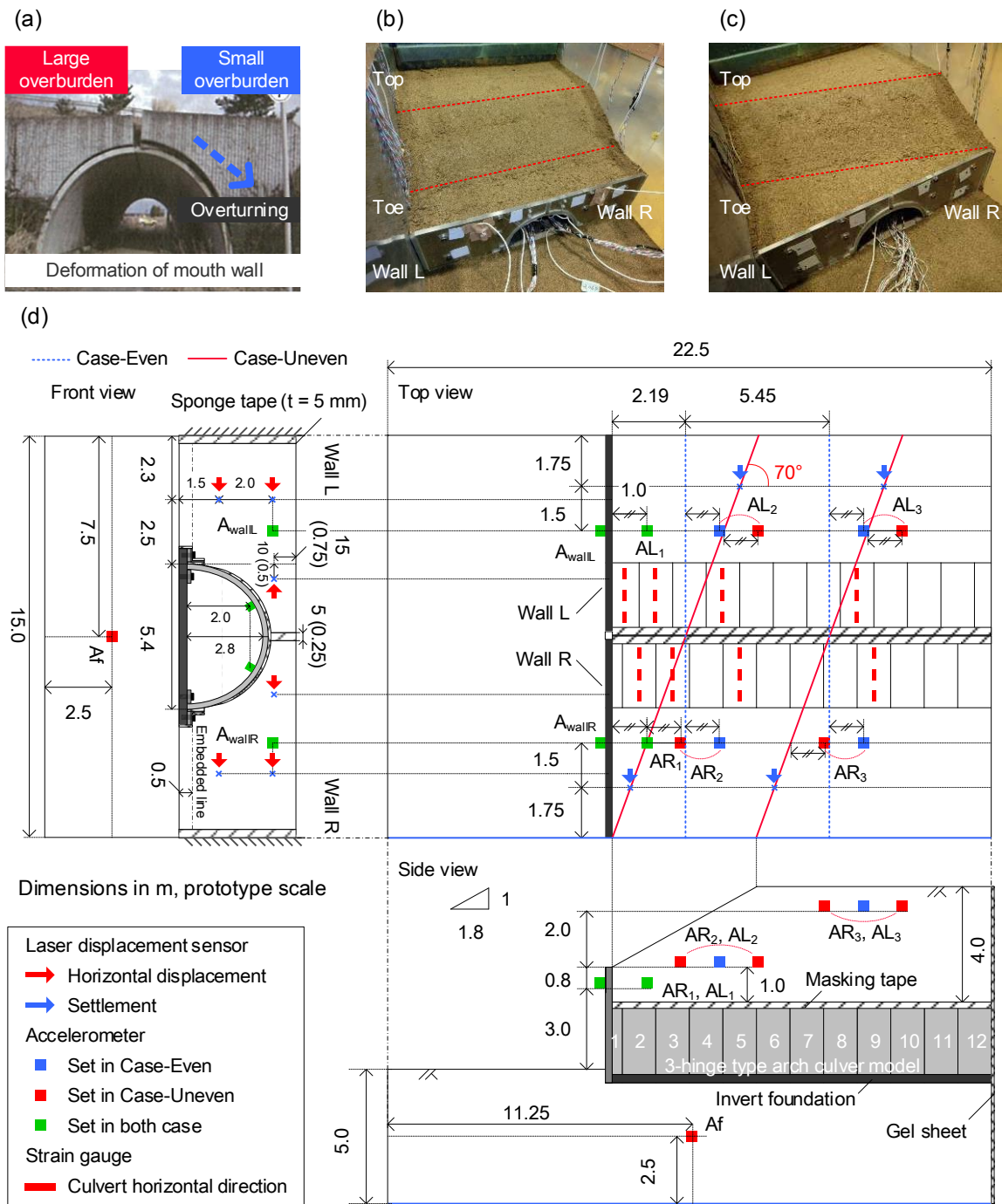
Figure 7.14: Schematic drawing of experimental set-up. (a) Referenced disaster example about the slippage of moth wall during Great East Japan earthquake (March, 11, 2011), (b) Case-Even, (c) Case-Uneven, (d) Experimental set-up of Case-Even and Case-Uneven.

10, with a gradual increase of 0.5 m/s^2 per step.

7.3.2 Experimental results

Figure 7.15 presents the horizontal displacement of the mouth wall after excitation. Both Case-Even and Case-Uneven show larger deformation of Wall R after repeated excitations; it is especially
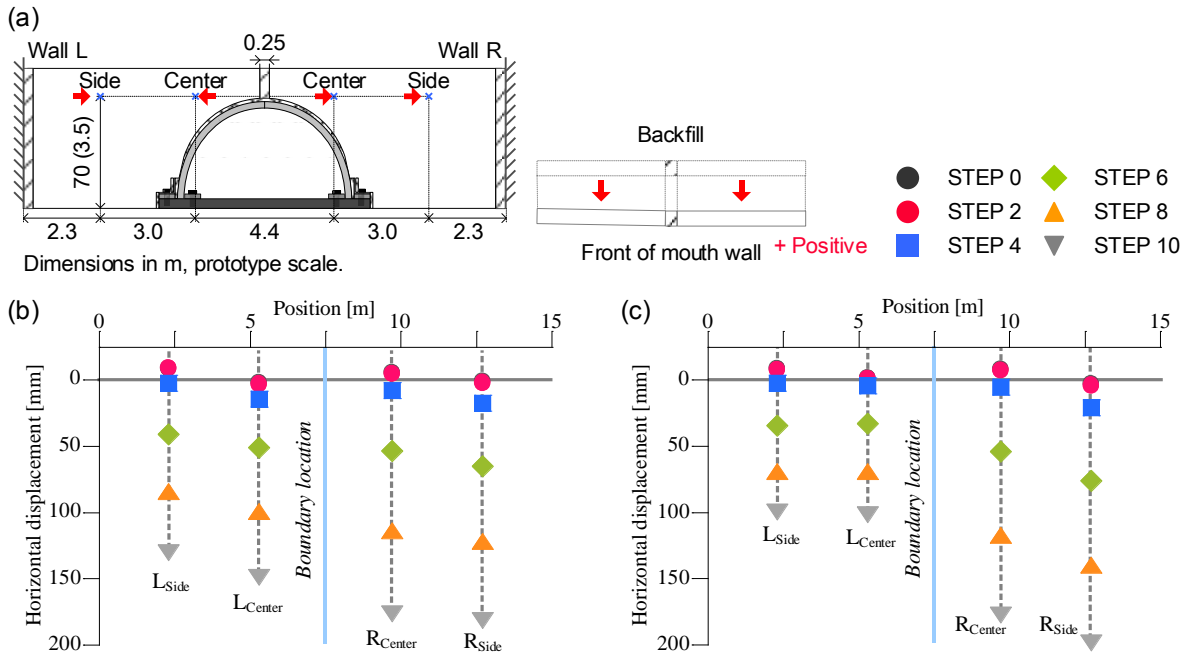
Figure 7.15: Transition of horizontal wall displacement: (a) measuring positions and results of (b) Case-Even and (c) Case-Uneven.
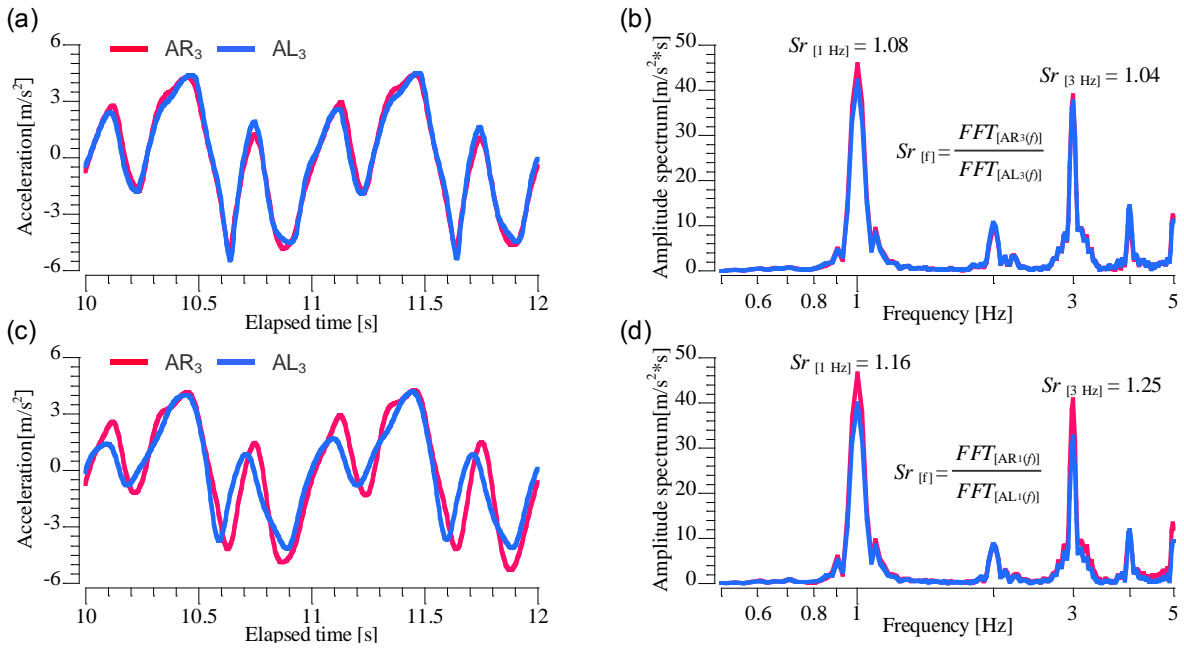
Figure 7.16: Response acceleration of embankment at STEP 6 (Maximum acceleration is 3.0 m/s^2): (a) time history and (b) frequency domain in Case-Even and (c) time history and (d) frequency domain in Case-Uneven.

significant in Case-Uneven. Figure 7.16 shows the response acceleration at the top of the model embankment (AR$_3$, AL$_3$) for STEP 6, whose maximum acceleration is 3.0 m/s^2. Only the results from t = 10.0 s to 12.0 s are shown to clarify the differences in the two cases. In the figure, Sr is defined as the ratio of the Fourier Amplification Spectrum (FAS) given by FAS to AR$_3$ divided by FAS to AL$_3$. In Case-

Even, seen in Figs. 7.16(a) and (b), the response accelerations of AR_3 and AL_3 are almost coincident, while Sr_1 Hz of AR_3 shows amplification of about 10% over AL_3, which is likely to be the cause of the larger deformation of Wall R. In Case-Uneven, AR_3 shows a slightly different waveform from AL_3, and Sr_1 Hz and Sr_3 Hz of AR_3 are amplified by about 16% and 25%, respectively. Case-Uneven seems to experience uneven deformation at the mouth wall due to the uneven amplification and response acceleration at AR_3 and AL_3.

From the above results, the uneven deformation of the mouth wall seems to be caused by the uneven overburden of the culvert. And the magnitude of the deformation of the mouth wall in the longitudinal seismic behavior is proportionally increased with the thickness of overburden. However, in the reported deformation of the mouth wall at the Great East Japan earthquake (Figure 7.14 (a)), the mouth wall with smaller overburden showed the overturning deformation. That is why there are still some factors existing to consider (e.g. type of foundation of culvert, boundary limitation of experiment or combination of uneven overburden and critical direction of input wave). These assumed factors are required to investigate their seismic effect through the various cases of the further numerical analyses.

7.4 Conclusions

In this chapter, through the dynamic centrifuge tests and the 3D dynamic FEM analysis, the seismic damages to the three-hinged arch culverts at the Great East Japan earthquake were discussed. The obtained results are shown below.

1) The observed damages to the arch members such as the edge defect of the arch crown and the arch foot can be explained the combination of the weak structural connectivity of the culverts and the torsional deformation of the arch members. Considering the old type of three-hinged arch culverts suffering the seismic damage, the weak structural connectivity due to the absence of concrete beam at the arch crown induced the critical damages to the arch members.

2) By connecting the culverts, although the cross-sectional force of the arch members will be increased, the independent displacements of the arch members can be suppressed, which can prevent the specific damages to the arch members such as the edge defect of the arch members and the aperture of the culverts.

3) The uneven overburden simply causes the uneven deformation of the mouth wall whose magnitude in the longitudinal seismic behavior is proportionally increased with the magnitude of the inertial force due to the thickness of overburden. However, the reported deformation of the mouth wall at the Great East Japan earthquake showed the opposite trend.

4) In the viewpoints of the clarification of the seismic damage, there still are some factors existing to consider (e.g. type of foundation of culvert, boundary limitation of experiment or combination of uneven overburden and critical direction of input wave). These assumed factors are required to investigate their seismic effect through the various cases of the further numerical analyses.

References

Abe, T. and Nakamura, M. (2014) *The use of and the caution in the application of the culvert constructed*

by large pre-cast element in the expressway construction, *The Foundation Engineering & Equipment*, Monthly, Vol. 42, No. 4, pp. 8-11. (in Japanese)

Fujiwara, Y., Fujioka, I. and Saeki, M. (2017): *Study of overburden effect on three-hinged arch culvert*, *the Proceedings of the JSCE Annual Meeting*, Vol.71, III-460, pp.919-920 (in Japanese).

Investigative Committee of Manual for the Design and Construction of Techspan Construction Method (1998): *Manual for the Design and Construction of Techspan Construction Method (Draft)*, *Advanced Construction Technology Center* (in Japanese).

Nakamura, H., Fujiwara, Y., Fujioka, I., Saeki, M., and Makino, M. (2018): *Study of seismic damage in the culvert direction to three-hinged arch culvert*, *the Proceedings of the JSCE Annual Meeting*, Vol.72, III-132, pp.263-264 (in Japanese).

Technological Examination Committee of Techspan Construction Method (2014): *Comparison Outline of Revised Items in Manual for the Design and Construction of Techspan Construction Method (Draft)*, *Advanced Construction Technology Center* (in Japanese).

Chapter 8 Conclusions and future studies

In the current study, the critical effect of the structural connectivity and the embankment shape on the seismic behavior in the culvert longitudinal direction was confirmed through dynamic centrifuge tests and a 2D and 3D elasto-plastic FEM analyses on the hinge-type of precast arch culverts. Additionally, the damage mechanism of the three-hinged arch culverts brought about by the Great East Japan Earthquake was discussed through a numerical method that can simulate the dynamic soil-culvert interaction due to the longitudinal structural connectivity and the shape of the embankment. The conclusions obtained in each chapter are described below.

In Chapter 2, outlines of culvert structures and a past disaster were given along with an investigation of the seismic performance of the hinge-type of precast arch culverts. As an important issue in the seismic performance of the hinge-type of precast arch culverts, an examination of the damage to the overall culverts and the embankment, occurring in the Great Japan Earthquake, revealed that the design method only for the arch's cross section is insufficient for evaluating the whole culvert structure and the mechanism of such a disaster. On the other hand, past research works on the culvert longitudinal direction focused on the design method of the culvert longitudinal direction, but they did not attain a clear interpretation of the actual damage mechanism corresponding to the inertial force in the culvert longitudinal direction. Additionally, the Great East Japan Earthquake motivated civil engineers to incorporate earthquake resistance into the established precast arch culverts, of which there are currently more than 200 in Japan. However, due to the lack of an accurate evaluation method for the seismic performance of these precast arch culverts, a radical countermeasure against earthquakes cannot be developed.

In Chapter 3, an outline was given of the centrifuge tests discussed in Chapter 4 and Chapter 5 and the numerical analysis performed in Chapter 6. To model the actual construction of the hinge-type of precast arch culverts, *Edosaki* sand with well-distributed particles was used for the ground model prepared by compaction. Additionally, the modeling of the mouth wall, based on a reinforced earth wall, was explained. In the numerical analysis, the outline and the mechanical properties of the elasto-plastic constitutive sand model were described.

In Chapter 4, dynamic centrifuge tests were conducted on precast arch culverts installed in an embankment. The seismic behavior of the culverts was investigated with an earthquake wave of 1 Hz. The following conclusions can be drawn from the results of this chapter.

1) The initial condition of the bending moment working on the bottom slab of the arch culverts and the supporting mechanism of the upper load were found to depend on the connecting condition. Connected culverts caused an enlargement of the bending moment working on the bottom slab at both ends of the culverts. Separated culverts maintained the homogenous bending moment and the vertical earth pressure working on the bottom slab of each culvert.

2) Separating the culverts allowed each culvert to behave independently in the embankment. In addition, when buried culverts were carefully observed, apertures and cracks were found in them. The large reacting force from the ground foundation may have induced bending cracks on the invert of the arch culvert model, which also caused bending cracks on the sidewall and

the arch crown. This unrestrained behavior resulted in apertures at the interconnecting sections of the culverts and a decrease in the longitudinal shear stiffness of the culverts with the amplified embankment deformation.

3) Connecting the culverts was seen to cause all the culverts to behave integrally during an earthquake. Under this experimental condition, connecting the culverts was advantageous in the seismic resistant design from the viewpoints of preventing apertures from occurring in the culverts during excitations in the culvert longitudinal direction and reducing the embankment deformation and the internal forces of the arch culverts.

In **Chapter 5**, dynamic centrifuge model tests were conducted focusing on the influence of the embankment shape on the seismic performance of three-hinged arch culverts in the longitudinal direction. The following conclusions can be drawn from the results of this chapter:

1) The deformation of an embankment in the culvert longitudinal direction increases proportionally to the gross weight of the soil.

2) The seismic behavior of culverts in the longitudinal direction is closely related to the degree of overburden.

3) Shallow soil cover, such as 1.0 m, allows the response acceleration of culverts to be amplified and to exceed that of the surrounding soil at the mouth. Conversely, deep soil cover, of more than 4.0 m, causes the culverts to respond as an integrated body with the surrounding soil.

4) In the experiment in which the entire overburden was more than 1.0 m and the hinge was a simply butted section, no slippage of the hinge portion was observed during repeated excitation in the longitudinal direction.

In **Chapter 6**, 2D and 3D dynamic FEM analyses were conducted to develop a new evaluation method for the seismic performance of precast arch culverts in the culvert longitudinal direction. The obtained results are shown below.

2D dynamic analysis results

1) Bilinear spring elements were applied for structural connectivity in the FEM dynamic analysis. Then, the apertures of the culverts due to the deformation of the embankment could be expressed.

2) In the separated case, the embankment deformation became larger than that of the connected case, which matches the trend appearing in the observed deformation through dynamic centrifuge tests considering the structural connectivity of culverts.

3) The influence of the longitudinal inertial force on the structural connection became larger near the mouth of the culverts. Additionally, the influence of the embankment deformation on the structural connection was found to be critical at the culverts under the slope of the embankment.

3D dynamic analysis results

4) The difference in overburden appears as a difference in the confining stress acting on the culverts. Three-hinged arch culverts with a small overburden are likely to suffer damage related to the displacement of the arch members such as apertures in the arch members. On the other hand,

culverts with a large overburden are likely to suffer damage to the arch members themselves due to the increase in shear stress which is dependent on the overburden depth.

5) The separated condition of the culverts causes the larger deformation of the embankment, particularly near the culverts, compared with the connected condition, due to the deformation of the culverts. This mainly results from the deformation of the culverts due to the decrease in the longitudinal shear stiffness.

6) In the connected condition, the connected culverts resist the shear force with all the arch members; this induces the local concentration of the shear stress on all the arch members. In the separated condition, however, the arch members independently resist the shear force; this induces the stress concentration of each arch member.

In **Chapter 7**, through the dynamic centrifuge tests and the 3D dynamic FEM analysis, the seismic damage to the three-hinged arch culverts at the Great East Japan Earthquake was discussed. The obtained results are shown below.

1) The observed damage to the arch members, such as edge defects at the arch crown and the arch feet, can be explained by the combination of the weak structural connectivity of the culverts and the torsional deformation of the arch members. Considering the old type of three-hinged arch culverts and the seismic damage they suffered, the weak structural connectivity due to no concrete beams at the arch crown induced the critical damage to the arch members.

2) By connecting the culverts, although the cross-sectional force of the arch members will be increased, the independent displacement of the arch members can be suppressed, which can prevent specific damage to the arch members, such as edge defects to the arch members and apertures in the culverts.

3) The uneven overburden simply causes the uneven deformation of the mouth wall whose magnitude in the longitudinal seismic behavior is proportionally increased with the magnitude of the inertial force due to the thickness of the overburden. However, the reported deformation of the mouth wall at the Great East Japan Earthquake showed an irreconcilable trend.

Finally, recommendations for future studies are summarized below.

1) From the viewpoint of the clarification of seismic damage, there are still some factors which need to be considered (e.g., the type of culvert foundation, the boundary limitations of the experiment or the combination of an uneven overburden and the critical direction of the input wave). These assumed factors are required in order to investigate their seismic effect through the various cases in further numerical analyses.

2) The current numerical method lacks accuracy in the modeling of the mouth wall due to the simplified expression of the wall model. The modeling of the mouth wall is based on the reinforcing earth wall and will contribute to the damage mechanism of the mouth wall of precast arch culverts.

3) Bilinear spring elements were applied to express the interface of the arch members based on the concept of Penalty method with high compressive spring constant. However, in reality, it seems

that repeated collisions are taking place between the arch members which causes an insufficient evaluation of the stress state of the arch members. Therefore, contact-impact problem of the present numerical analysis method need to be improved to simulate the repeated collision problems for a more detailed inspection of the stress states of the arch members.